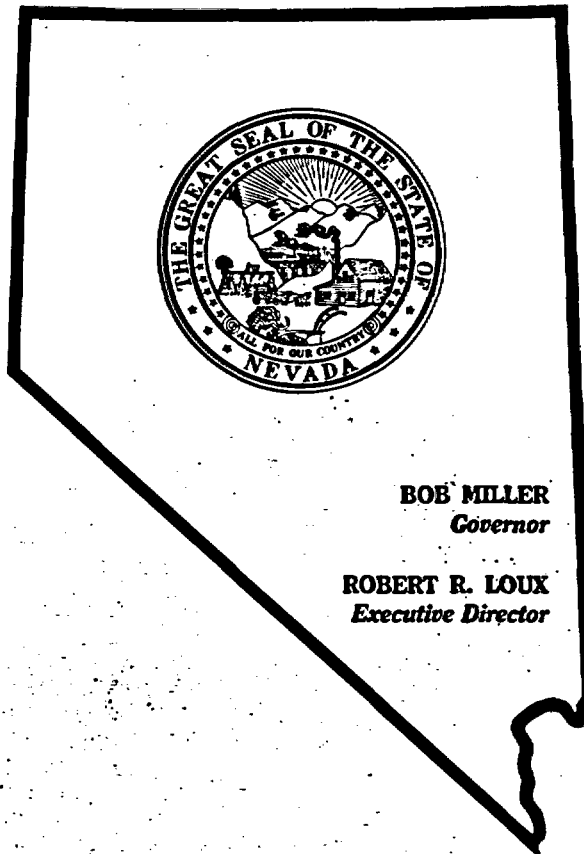
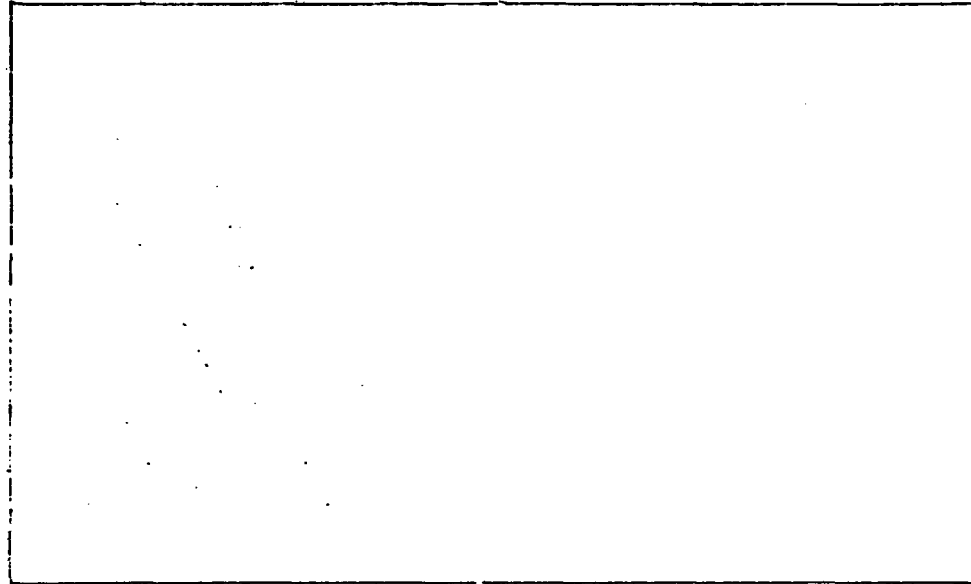


STATE OF NEVADA

**AGENCY FOR NUCLEAR PROJECTS/
NUCLEAR WASTE PROJECT OFFICE**



BOB MILLER
Governor

ROBERT R. LOUX
Executive Director

PRELIMINARY

**CENTER FOR VOLCANIC AND TECTONIC STUDIES¹
DEPARTMENT OF GEOSCIENCE**

**University of Nevada, Las Vegas
Las Vegas, Nevada 89154**

Report No. 69

**ANNUAL REPORT
1991-1992**

for the period October 1, 1991 to September 30, 1992
**submitted to the Nuclear Waste Project Office
State of Nevada**

December 15, 1992

**¹ EUGENE L. SMITH-PRINCIPAL INVESTIGATOR
TIM BRADSHAW-RESEARCH ASSOCIATE
SHIRLEY MORIKAWA-GRADUATE ASSISTANT
TRACY T. SWITZER-STUDENT ASSISTANT**

PRELIMINARY

**CENTER FOR VOLCANIC AND TECTONIC STUDIES¹
DEPARTMENT OF GEOSCIENCE**

**University of Nevada, Las Vegas
Las Vegas, Nevada 89154**

Report No. 69

**ANNUAL REPORT
1991-1992**

for the period October 1, 1991 to September 30, 1992
**submitted to the Nuclear Waste Project Office
State of Nevada**

December 15, 1992

¹ **EUGENE L. SMITH-PRINCIPAL INVESTIGATOR
TIM BRADSHAW-RESEARCH ASSOCIATE
SHIRLEY MORIKAWA-GRADUATE ASSISTANT
TRACY T. SWITZER-STUDENT ASSISTANT**

INTRODUCTION

The annual report of the Center for Volcanic and Tectonic Studies (CVTS) contains a series of papers, maps, and reprints that review the progress made by the CVTS between October 1, 1991 and December 31, 1992. During this period CVTS staff focused on several topics that had direct relevance to volcanic hazards related to the proposed high-level nuclear waste repository at Yucca Mountain, Nevada. These topics included:

- (1) The role of the mantle during regional extension.
- (2) The structural controls and emplacement mechanisms of Pliocene/Quaternary basaltic centers and dikes.
- (3) The detailed geochemistry of individual volcanic centers in Crater Flat, Nevada.
- (4) Estimating the probability of disruption of the proposed repository by volcanic eruption (this topic is being studied by Dr. C-H. Ho at UNLV).

Activities

CVTS staff presented papers at several professional meetings including:

- (a) Geological Society of America Annual Meeting in San Diego, California: October 21-24, 1991.
- (b) Geological Society of America Annual Meeting in Cincinnati, Ohio: October 26-29, 1992.
- (c) The international conference of volcanism and risk assessment in Colima, Mexico: January 22-26, 1992.
- (d) The American Geophysical Union Fall Meeting in San Francisco, California; December 12-17, 1992.

In addition CVTS staff participated in several technical exchanges and field trips with NRC, State of Nevada and NWTRB panels. These include presentations to:

- (1) U.S. Nuclear Regulatory Commission's Advisory Committee on Nuclear Waste meeting on the "Geological Dating of Quaternary Volcanic Features and Materials" on November 19, 1991 in Washington, D.C.
- (2) U.S. Technical Review Board's Panel on Structural Geology and Geoengineering on September 14-15, 1992 in Las Vegas.

(3) State of Nevada Commission on Nuclear Projects on April 10, 1992.

CVTS staff also presented invited talks, seminars and field trips to the public about volcanism and the proposed nuclear waste repository. CVTS staff feel that part of their responsibility is to provide the public with unbiased and alternative views of the issues related to the proposed high-level nuclear waste repository at Yucca Mountain. Invited talks and lectures to public meetings and civic groups as well as large enrollment classes at UNLV provide the community with a source of information regarding the geology and geologic hazards related to the project.

CVTS Staff

This year was a period of transition for CVTS staff. During the year four geologists served as research associates. During the period October 1, 1991 to December 30, 1992, CVTS staff included Eugene I. Smith (PI), Terry Naumann (October 1, 1991 to December 1, 1991), Jim Mills (February 1, 1992 to June 1, 1992), Mark Martin (February 1, 1992-October 1, 1992) and Tim Bradshaw (October 1, 1992 to present) as research associates and Tracy T. Switzer (student assistant). In addition, one graduate student (Shirley Morikawa) was partially funded to complete a Master's Thesis in geology. Mark Reagan and Dan Feuerbach (University of Iowa) received partial funding to do U-series dating of the Lathrop Wells cone. J.D. Walker (University of Kansas) continued to do isotopic analyses in cooperation with CVTS staff .

Organization of the Annual Report

This report includes the following contributions:

- (1) "The role of the mantle during crustal extension: constraints from geochemistry of volcanic rocks in the Lake Mead area, Nevada and Arizona" by D.L. Feuerbach (University of Iowa), E.I. Smith (CVTS-UNLV), J.D. Walker (University of Kansas) and Jean Tangeman (University of Michigan). This paper is in review by the Geological Society of America (Bulletin).
- (2) "Tertiary geology of the Reveille quadrangle, northern Reveille Range, Nye County, Nevada: Implications for shallow crustal structural control of Pliocene basaltic volcanism." by Mark Martin (CVTS-UNLV).
- (3) Activities of Tim Bradshaw; October 1, 1992 to December 30, 1992.
- (4) Copies of abstracts submitted by CVTS staff during the year of funding.

These include:

- (a) "New insights on structural controls and emplacement mechanisms of Pliocene/Quaternary basaltic dikes, southern Nevada and northwestern Arizona." by

Faulds, Feuerbach and Smith. Presented at the Geological Society of America National Meeting in San Diego.

(b) "Intermediate and mafic volcanic rocks of the northern White Hills, Arizona: implications for the production of intermediate composition volcanic rocks during regional extension" by Cascadden and Smith. Presented at the Geological Society of America National Meeting in San Diego.

(c) "Hornblende geobarometry from mid-Miocene plutons: implications regarding uplift and block rotation during Basin and Range extension" by Metcalf (UNLV) and Smith. Presented at the Geological Society of America National Meeting in San Diego.

(d) "Volcanic risk assessment studies for the proposed high-level radioactive waste repository at Yucca Mountain, Nevada, U.S.A. by Smith, Feuerbach (University of Iowa) Naumann, and Ho. Presented at the international conference of volcanism and risk assessment in Colima, Mexico

(e) "The Mt. Perkins Pluton: shallow-level magma mixing and mingling during Miocene extension" by Metcalf (UNLV), Smith, Nall (UNLV) and Reed (UNLV). Presented at the Geological Society of America National Meeting in Cincinnati.

(f) "Geochemical fingerprinting of progressive extension in the Colorado River extensional corridor, U.S.A.: a preliminary report" by Feuerbach (University of Iowa), Smith, Reagan and Faulds (University of Iowa) and Walker (University of Kansas). Presented at the American Geophysical Union Fall meeting in San Francisco.

(5) A paper entitled "Eruptive probability calculation for the Yucca Mountain site, U.S.A.: statistical estimation of recurrence rates" published in *The Bulletin of Volcanology* by Ho, Smith, Feuerbach (University of Iowa) and Naumann describing the cooperative study between CVTS staff and Dr. C.-H Ho regarding risk assessment studies.

**THE ROLE OF THE MANTLE DURING CRUSTAL EXTENSION: CONSTRAINTS
FROM GEOCHEMISTRY OF VOLCANIC ROCKS IN THE LAKE MEAD AREA,
NEVADA AND ARIZONA**

by

D.L. Feuerbach¹, E.I. Smith

Center for Volcanic and Tectonic Studies

Department of Geoscience

University of Nevada, Las Vegas

Las Vegas, Nevada 89154

J.D. Walker, J.A. Tangeman²

Isotope Geochemistry Laboratory

Department of Geology

University of Kansas

Lawrence, Kansas 66045

¹Now at Department of Geology, University of Iowa, Iowa City IA 52242

²Now at Department of Geological Sciences, University of Michigan, Ann Arbor MI 48109

ABSTRACT

One of the fundamental questions in areas of large-magnitude extension and magmatism is the role of the mantle in the extension process. The Lake Mead area is ideally suited for developing models that link crustal and mantle processes because it contains both mantle and crustal boundaries and it was the site of large-magnitude crustal extension and magmatism during Miocene time. In the Lake Mead area, the boundary between the amagmatic zone and the northern Colorado River extensional corridor (NCREC) parallels the Lake Mead fault system (LMFS) and is situated just to the north of Lake Mead. This boundary formed between 11 and 6 Ma during and just following the peak of extension, and corresponds to a contact between two mantle domains. There is circumstantial evidence for a spatial and temporal correlation between upper crustal extension and the thinning of the lithospheric mantle (LM) in the NCREC. During extension in the NCREC, LM may have been thinned and replaced by asthenosphere progressively to the west. During thinning and replacement of the LM in the NCREC, the LM in the amagmatic zone remained intact. Contrasting behavior to the north and south of this boundary may have produced the mantle domain boundary. The domain to the north of the boundary is characterized by mafic lavas with a LM isotopic and geochemical signature ($\epsilon Nd = -3$ to -9 ; $^{87}Sr/^{86}Sr = 0.706-0.707$). To the south of the boundary in the NCREC, lavas have an OIB-mantle signature and appear to have only a minor LM component in their source ($\epsilon Nd = 0$ to $+4$; $^{87}Sr/^{86}Sr = 0.703-0.705$). Mafic lavas of the NCREC represent the melting of a complex and variable mixture of asthenospheric mantle (AM), LM and crust. Pliocene alkali basalt magmas of the Fortification Hill field represent the melting of a source composed of a mixture of AM, HIMU-like mantle and LM. Depth of melting of alkali basalt magmas remained relatively constant from 12 to 6 Ma during and just after the peak of extension, but probably increased between 6 and 4.3 Ma following extension. Miocene and Pliocene low ϵNd and high $^{87}Sr/^{86}Sr$ magmas and tholeiites at Malpais Flattop were derived from a LM source and were contaminated as

they passed through the crust. The shift in isotopic values due to crustal interaction is no more than 4 units in ϵ Nd and 0.002 in $^{87}\text{Sr}/^{86}\text{Sr}$ and does not mask the character of the mantle source. The change in source of basalts from LM to AM with time, the OIB character of the mafic lavas and the HIMU-like mantle component in the source is compatible with the presence of rising asthenosphere, as an upwelling convective cell, or plume beneath the NCREC during extension. Passive rifting is probably more applicable to the NCREC than active rifting because OIB-type alkali basalt volcanism is concentrated in a restricted geographic area for nearly 5 m.y. The LMFS, a major crustal shear zone, parallels the mantle domain boundary. The LMFS may represent the crustal manifestation of differential thinning of the LM or the rejuvenation of an older lithospheric structure.

INTRODUCTION

In areas of large-scale extension there are fundamental questions regarding the role of the mantle in the extension process, the identification and age of mantle boundaries, and the relation between mantle and crustal boundaries. We use the Lake Mead area of southern Nevada and northwestern Arizona to address these questions. The Lake Mead area is well suited for this purpose because it contains both mantle and crustal boundaries and it was the site of large-magnitude crustal extension and magmatism during Miocene time.

The Lake Mead area contains the boundary between the Western Great Basin and Basin-Range mantle provinces (Figure 1) (Menzies et al., 1983; Fitton et al., 1991) and the contact between asthenospheric (OIB) and lithospheric (EM2) mantle domains (Menzies, 1989). Mafic volcanic rocks in the Basin-Range mantle province have ϵ Nd between +5 and +8 and initial $^{87}\text{Sr}/^{86}\text{Sr} = 0.703$ (Perry et al., 1987; Menzies et al., 1983; Farmer et al., 1989). In contrast, the Western Great Basin province is distinguished by $^{87}\text{Sr}/^{86}\text{Sr} > 0.706$ and ϵ Nd between 0 and -11 (Menzies et al., 1983; Fitton et al., 1988; Fitton et al., 1991). Mafic volcanic rocks of the Sierra Nevada mantle province (Figure 1)

(Leeman, 1970; Menzies et al., 1983; Fitton et al., 1988) are isotopically identical to those of the Western Great Basin province. Basalts with high $^{87}\text{Sr}/^{86}\text{Sr}$ and low ϵNd described by Farmer et al. (1989) in southern Nevada lie within the Western Great Basin province.

Several important crustal structures pass through the Lake Mead area (Figure 2a). Among these are the Lake Mead fault system (LMFS) (Anderson, 1973; Bohannon, 1984), a northeast trending set of left-lateral strike-slip faults, and the Las Vegas Valley shear zone (LVVSZ), a northwest striking set of right-lateral strike-slip faults (Longwell, 1960; Longwell et al., 1965; Duebendorfer and Wallin, 1991). The LMFS separates thick sections of Paleozoic and Mesozoic sedimentary rocks to the north from an area to the south nearly devoid of these sections (Longwell et al., 1965; Anderson, 1971). Segments of the LMFS define the boundary between the amagmatic zone and the Northern Colorado River extensional corridor (NCREC) (Faulds et al., 1990) (Figure 2a). The LMFS also separates two regions that have undergone different amounts of extension. To the south of the LMFS, in the NCREC, crust was extended by a factor of 3 to 4. To the north, in the amagmatic zone, crust was extended by a factor of 2 (Wernicke et al., 1988). The amagmatic zone is a region between 36° and 37° north latitude of minor igneous activity that separates the Great Basin from the Colorado River sections of the Basin-and-Range province. This zone corresponds to a regional southerly topographic slope and a gravity gradient with an amplitude of about 100 mgals (Eaton, 1982; Eaton et al., 1978). The zone also represents a boundary between contrasting migration directions of magmatism and extension (Taylor and Bartley, 1988; Glazner and Supplee, 1982; Reynolds et al., 1986). In addition to these structures, a major lithospheric boundary defined by Nd mapping of Proterozoic basement rocks trends north-south just to the east of the Colorado River (Bennett and DePaolo, 1989). To the west of the boundary in the Lake Mead area, Proterozoic rocks are characterized by model ages of 2.0-2.3 Ga. To the east of the boundary older basement rocks are 1.8 to 2.0 Ga.

The relation between the LMFS and the LVVSZ is hotly debated (e.g.,

Duebendorfer and Wallin, 1991). The LVVSZ crosses the amagmatic zone and does not serve as a boundary between the NCREC and the amagmatic zone. Recently Duebendorfer and Wallin (1991) suggested that the LVVSZ projects eastward to the north of Lake Mead and serves as the northern boundary of the Saddle Island detachment terrane. It is possible that the proposed eastward projection of the LVVSZ together with the LMFS forms the northern boundary of the NCREC.

Volcanism is rare in the amagmatic zone and is limited to low-volume Pliocene basalt centers at Black Point and in the Las Vegas Range and moderate volume basaltic-andesite volcanoes on Callville Mesa (Feuerbach et al., 1991) (Figure 2b). In the eastern part of the Lake Mead area at Gold Butte, and in the Grand Wash trough are numerous late-Cenozoic alkali basalt centers (Cole, 1989) (Figure 2a). Adjacent to and within the LMFS is the middle- to late-Miocene Hamblin-Cleopatra volcano (Thompson, 1985; Barker and Thompson, 1989), the Boulder Wash volcanic section (Naumann, 1987), and flows of late-Miocene basalt interbedded with Tertiary sediments near Government Wash north of Lake Mead (Figure 2b). The area south of the LMFS contains numerous Miocene and Pliocene volcanic centers (Figure 2b). The most notable of the Miocene centers are in the River Mountains (Smith, 1982), McCullough Range (Smith et al., 1988), Eldorado Mountains (Anderson, 1971), Black Mountains (Faulds et al., 1990), Hoover Dam (Mills, 1985); at Malpais Flattop (Faulds et al., 1991), and in the White Hills (Cascadden, 1991) (Figure 2a). Pliocene centers comprise the Fortification Hill volcanic field that extends discontinuously from near Willow Beach, Arizona to Lake Mead (Figure 2b). In the Lake Mead area, for the most part, volcanism preceeded block tilting related to regional extension (9 to 12 Ma; Duebendorfer and Wallin, 1991). Calc-alkaline intermediate lavas were erupted between 18.5 and about 11 Ma. Low-volume basaltic andesite (10.3 to 8.5 Ma), tholeiitic basalt (9.7 to 10.6 Ma), and alkalic basalt (4.3 to 6 Ma) mainly postdate extension (Smith et al., 1990).

This paper focuses on Miocene and Pliocene mafic volcanoes ($\text{SiO}_2 < 55\%$)

between 16.4 and 4.7 Ma in the anmagmatic zone and the NCREC. First, we present new geochemical data and infer the source of the mafic magmas. Next we show that crustal interaction (contamination and commingling) with mafic magmas occurred, but that the isotopic values of the lavas are not shifted enough to mask the character of their mantle source. Lastly, we use the mafic volcanic rocks that span the boundary between the anmagmatic zone and the NCREC as "a probe" into the mantle to determine (1) isotopic differences across the boundary, (2) the age of the boundary, and (3) any link between crustal and mantle processes.

INSTRUMENTAL TECHNIQUES

Whole rock major element concentrations were determined by Inductively Coupled Plasma techniques (ICP) at Chemex Labs, Inc. (Sparks, NV). Rare-earth elements and Cr, V, Sc, Co, Ta, Hf, Th were analyzed by Instrumental Neutron Activation Analysis (INAA) at the Phoenix Memorial Laboratory, University of Michigan. The multi-element standards G-2, GSP-1, BHVO-1, and RGM-1 were used as internal standards. Ba, Rb, Ni and Sr were determined by atomic absorption and Nb and Sr were analyzed by X-ray Fluorescence (XRF) at Chemex Labs, Inc. Rb and Sr were determined by isotope dilution for samples which were analyzed for Nd, Sr and Pb isotope concentrations. Ni, Nb, Rb, Sr, Zr, Y, Ba for Fortification Hill basalt were analyzed by XRF at the U.S. Geological Survey's analytical laboratory in Menlo Park, California. This study includes 27 new isotopic analyses from 11 volcanic sections which represent all major volcanic centers and a fairly complete sample of mafic volcanic rocks in the Lake Mead area.

Samples for isotopic analysis were dissolved at about 180°C in a sealed bomb using a HF/HNO₃ mixture. Samples were total-spiked for Rb, Sr, Nd and Sm. Separation of Rb, Sr, and REE group elements was done using standard cation exchange techniques. The HDEHP-on-Teflon method of White and Patchet (1984) was used for separation of Sm and Nd. The HBr and HNO₃ methods were used for separation of Pb and U,

respectively, on aliquots from the whole rock solution. All isotopic analyses were done on a VG Sector 54 mass spectrometer at the University of Kansas. Analyses of Sr and Nd were done in dynamic multicollector mode with $^{88}\text{Sr}=4\text{V}$ and $^{144}\text{Nd}=1\text{V}$; Rb and Sm were analyzed in static multicollector mode with $^{87}\text{Rb}=200\text{mV}$ and $^{147}\text{Sm}=500\text{mV}$. Analyses for Sr and Sm were done on single Ta filaments; Rb was run on single Re filaments. Nd was run both as NdO^+ and Nd^+ . Analytical blanks were less than 100pg for all elements. Strontium isotopic compositions are normalized for $^{86}\text{Sr}/^{88}\text{Sr}=0.1194$ and referenced to NBS-987 $^{87}\text{Sr}/^{86}\text{Sr}=0.710250$. Reproducibility of Sr values during these runs was better than ± 0.000020 based on replicate runs of NBS 987. Neodymium isotopic compositions are normalized to $^{146}\text{Nd}/^{144}\text{Nd}=0.7219$ and referenced to LaJolla $^{143}\text{Nd}/^{144}\text{Nd}=0.511850$. Epsilon values for Nd at crystallization are calculated using $(^{143}\text{Nd}/^{144}\text{Nd})_{(\text{CHUR},0\text{Ma})}=0.512638$, and $^{147}\text{Sm}/^{144}\text{Nd}_{(\text{CHUR},0\text{Ma})}=0.1967$. Reproducibility of Nd values are about 0.25 epsilon values based on replicate analyses of LaJolla and in-house standards. Lead isotopic analyses are referenced to NBS 981 (common Pb) $^{207}\text{Pb}/^{206}\text{Pb}=0.91464$ and are corrected for 0.10%/amu fractionation. Fractionation uncertainty is $\pm 0.05\%$ /amu (e.g., ± 0.08 for $^{208}\text{Pb}/^{204}\text{Pb}$, ± 0.04 for $^{207}\text{Pb}/^{204}\text{Pb}$ and ± 0.04 for $^{206}\text{Pb}/^{204}\text{Pb}$). Isotope dilution data for Sr, Rb, and Nd are reported in Table 1.

VOLCANOLOGY

Volcanic Rocks of the Northern Colorado River Extensional Corridor

Fortification Hill Field Fortification Hill basalt (FH) crops out in a 50 km long by 30 km wide north-northeast elongate area that extends from Lava Cascade, Arizona to Lake Mead (Figure 2). Volcanic centers occur near north-northwest trending high-angle normal faults. We divide the Fortification Hill basalts into older and younger alkalic basalts (OAB and YAB respectively) based on $\text{Na}_2\text{O}+\text{K}_2\text{O}$ (Figure 3a), light rare-earth element (REE) enrichment (Figure 3b) and modal mineralogy. OAB are mildly alkalic hypersthene (OAB-

hy) or nepheline-normative (OAB-ne) olivine-basalts with Ce/Yb mainly between 18-46 (Figure 3b). These rocks are dated between 5.88 to 4.73 Ma (Feuerbach et al., 1991). Several OAB have higher Ce/Yb and fall outside the limits of the OAB field depicted in Figure 3. Also, nepheline normative alkali basalts from Black Point have Ce/Yb between 7 and about 17 and are surrounded by a dotted line on Figure 3b. OAB lavas erupted from north-northwest aligned cinder cones on Fortification Hill and from cinder cones at Lava Cascade and in Petroglyph Wash (Figure 2). OAB lavas contain porphyritic iddingsitized olivine phenocrysts in a trachytic to pilotaxitic groundmass of olivine, andesine, labradorite, diopsidic-augite and iron oxide. Coarse-grained plugs of OAB in volcanic centers consist of olivine phenocrysts in a coarse-grained interstitial groundmass of andesine, labradorite, diopsidic-augite and olivine.

YAB are xenolith-bearing nepheline-normative alkali-olivine basalts with elevated Ce/Yb (37-68) (Figure 3b). These rocks range in age from 4.64 to 4.3 Ma (Feuerbach et al., 1991; Anderson et al., 1972) YAB occurs in three locations: a diatreme at Petroglyph Wash, en-echelon dikes and a vent along U.S. highway 93, about 10 km south of Hoover Dam, and south of Saddle Island between the North Shore road and Lake Mead (Figure 2) (Smith, 1984). The matrix of YAB ranges from glassy to interstitial or pilotaxitic and contains microlites of plagioclase, altered olivine, altered diopsidic-augite and magnetite. Olivine is the primary phenocryst phase. Ubiquitous to YAB are ultramafic inclusions and megacrysts of augite and kaersutite (Nielson, manuscript in preparation; Campbell and Schenk, 1950). Rare xenoliths of plagioclase-hornblende diorite also occur in YAB. Except for the presence of diorite inclusions in YAB, there is no petrographic evidence of crustal contamination in Fortification Hill lavas.

River Mountains In the River Mountains (Figure 2) an andesite-dacite stratovolcano is surrounded by a field of dacite domes (Smith, 1982; Smith et al., 1990). Volcanism occurred in four pulses. The first three are characterized by the eruption of calc-alkaline andesite and dacite flows and the last by rhyolite and alkali basalt. The first episode is

associated with the emplacement of a quartz monzonite stock (The River Mountain stock) dated at 13.4 ± 0.5 to 12.8 ± 0.5 Ma (K-Ar biotite dates; Armstrong, 1966, 1970). Anderson et al. (1972) reported a K-Ar whole rock date of 12.1 ± 0.5 Ma for a basaltic-andesite of the third pulse. In addition, Koski et al. (1991) dated pyroclastic deposits at the Three Kids Mine in the northern River Mountains between 14.0 ± 0.3 and 12.4 ± 0.5 Ma by the fission track technique (sphene) and concluded that tuff deposition was contemporaneous with volcanism in the River Mountains.

Boulder Wash Boulder Wash in the northern Black Mountains (Figure 2) contains a 700-m-thick section of calc-alkaline dacite flows and flow breccias interbedded with flows of pyroxene-olivine andesite containing abundant xenocrysts of quartz and orthoclase (Naumann and Smith, 1987; Naumann, 1987; Smith et al., 1990). Petrographic and textural evidence of magma commingling is well developed in the volcanic section and associated plutonic rocks. Smith et al. (1990) and Naumann (1987) concluded that various mixing ratios of alkali olivine basalt and rhyolite end members are responsible for the textural variations. A dacite flow in the eastern part of the volcanic field was dated at 14.2 Ma (K-Ar whole rock date; Thompson, 1985).

Malpais Flattop Malpais Flattop near Willow Beach, Arizona (Figure 2) contains a 100 m thick stack of hypersthene normative tholeiitic basalt flows (TH) that erupted from at least two centers now expressed as wide (40 m) dikes and plugs on the west side of the Malpais Flattop mesa (Faulds et al., 1991). Tholeiitic lavas have lower $\text{Na}_2\text{O} + \text{K}_2\text{O}$ than alkali basalts with comparable SiO_2 content (Figure 3a), lower Ce/Yb than most OAB (Figure 3b) and are hypersthene normative (Table 1). TH contain olivine and clinopyroxene phenocrysts; orthopyroxene is a common groundmass constituent. $^{40}\text{Ar}/^{39}\text{Ar}$ whole rock dates of 9.7 ± 0.5 and 10.6 ± 0.5 Ma were obtained for flows near the top and at the base of the flow stack respectively (Faulds and Gans, unpublished data). These dates contrast with a 6 Ma age reported by Anderson et al. (1972) and indicate that eruptions at Malpais mesa occurred 4 m.y. earlier than the production of Fortification Hill

basalts.

Eldorado Mountains A sequence of mafic to felsic volcanic rocks erupted between 18.5 and about 12 Ma in the Eldorado Mountains (Anderson, 1971; Darvall et al., 1991) (Figure 2). The sequence is divided into a lower section of basaltic-andesite (predominant) and rhyolite lavas (Patsy Mine volcanics; Anderson, 1971); and an upper section of basaltic andesite, dacite and rhyolite (Mt. Davis volcanics; Anderson, 1971). Mafic lavas lack petrographic and field textures characteristic of crustal contamination or magma commingling. A similar section of mafic lavas in the White Hills, Arizona (Figure 2a) formed by partial melting of mantle peridotite without significant crustal interaction (Cascadden and Smith, 1991; Cascadden, 1991). In the Eldorado Range, lavas and associated plutonic rocks span the period of most rapid extension. Patsy Mine and the lower parts of the Mt. Davis section are tilted nearly 90 degrees. Younger units are rotated less in the same structural blocks (Anderson, 1971).

Hamblin-Cleopatra Volcano The Hamblin-Cleopatra volcano (14.2-11.5 Ma) (Anderson, 1973; Thompson, 1985) which lies along the north shore of Lake Mead (Figure 2), is a 60 km³ stratovolcano comprised of shoshonite, latite, trachydacite and trachyte lava (Barker and Thompson, 1989). In addition, tephra, epiclastic sediments, intrusions and a well developed radial dike system form the volcano. The volcano was dissected into three segments by left-lateral strike-slip faulting associated with the LMFS (Anderson, 1973; Thompson, 1985; Barker and Thompson, 1989).

Volcanic Rocks in the Amagmatic Zone

Callville Mesa. Olivine-clinopyroxene bearing basaltic-andesite erupted from compound cinder cones on Callville Mesa and in West End Wash between 10.46 and 8.49 Ma (Feuerbach et al., 1991) (Figure 2). The vent on Callville Mesa sits on the footwall of an east-west striking, down-to-the-south normal fault (Figure 2). Flows on Callville Mesa are offset from 5 to 20 m by south-dipping west-southwest striking high-angle normal faults. Basaltic andesite contains abundant quartz and alkali-feldspar xenocrysts that are rimmed

by glass and acicular clinopyroxene (diopsidic-augite).

Because, the presence of a Paleozoic and/or Mesozoic sedimentary section is in general characteristic of the amagmatic zone but not of the NCREC, the presence or absence of these rocks is our main field criterion for assigning a volcano to a specific province. The volcanic center at Callville Mesa sits on the boundary between the two provinces within the LMFS and just to the south of the proposed eastward projection of the LVVSZ. The Bitter Spring Valley fault passes just to the north and the Hamblin Bay fault projects just to the south. It is unclear whether Mesozoic and Paleozoic sedimentary rocks lie beneath the volcanic centers on Callville Mesa since volcanoes sit on a thick section of Tertiary sediments. However just to the northeast of Callville Mesa, flows of basaltic andesite rest on Tertiary sediments which in turn sit unconformably on steeply tilted Triassic and Jurassic sedimentary section. This relationship is the basis for the assignment of the Callville Mesa volcano to the amagmatic zone.

Black Point At Black Point on the west shore of the Overton Arm of Lake Mead (Figure 2), thin flows of alkali basalt (6.02 Ma; Feuerbach et al., 1991) associated with north-striking en-echelon dikes overlie gypsiferous sediments of the Tertiary Horse Spring Formation. Total outcrop area is about 12 km². Basalts at Black Point are nepheline-normative alkali basalts (OAB-ne) that contain iddingsitized olivine, labradorite and diopsidic-augite phenocrysts within either a trachytic or ophitic groundmass.

Las Vegas Range The Las Vegas Range locality is composed of thin flows of alkali basalt in a fault bounded basin just to the west of U.S. highway 93 (Figure 2). Flows (2 km²) are mostly covered by Quaternary fanglomerate and alluvium and as a result no source area was discovered. Basalt in the Las Vegas Range is dated at 16.4±0.6 Ma (K-Ar whole rock date; Smith, unpublished data).

Basalt of Government Wash Olivine-phyric basalt crops out near Government Wash just north of Lake Mead. An 60-80-m-thick section of flows and agglomerates are interbedded with the Lovell Wash member of the Tertiary Horse Spring Formation (Duebendorfer,

personal communication, 1991). Basalt of Government Wash is dated at 12.0 Ma (K-Ar plagioclase date) (Duebendorfer et al., 1991a).

Volcanic Rocks at Gold Butte and in the Grand Wash Trough

The Grand Wash trough and the Gold Butte area (Figure 2) contain flows, dikes and plugs of olivine-phyric alkali basalt that locally contain mantle xenoliths (Cole, 1989). Basalt in the Grand Wash trough is dated at 3.99 to 6.9 Ma (K-Ar plagioclase) and is younger than alkali basalt to the west in the Gold Butte area (K-Ar plagioclase dates of 9.15 to 9.46 Ma ; Cole, 1989) (Figure 2). Cole (1989) suggested that the alkali basalt formed by partial melting of spinel peridotite. Low ϵ Nd values (0 to +3.5) suggest that lavas may have been contaminated by mafic crust or LM.

SOURCE OF MAFIC LAVAS

Introduction

In this section we argue that the isotopic variation of alkali basalt in the NCREC is primarily due to differences in the mantle source not to crustal contamination. Crustal contamination is less of a factor for alkalic than tholeiitic rocks since they are lower in volume and less likely to reside in upper crustal chambers where open system processes occur. Also, high Sr and light rare-earth element concentrations of alkalic magmas tend to overwhelm any effects of crustal contamination. Furthermore, alkalic magmas commonly contain mantle xenoliths and apparently rose quickly through the crust with little or no contamination (e.g., Glazner and Farmer, 1992). Crustal contamination was an important factor in the production of intermediate lavas of the River Mountains, mafic lavas at Callville Mesa, hypersthene-normative alkali basalts (OAB-hy) of the Fortification Hill field, and tholeiitic basalts at Malpais Flattop. Although these magmas were contaminated by crust, we will show that the isotopic shift due to crustal interaction is small when compared to the overall isotopic variation. Therefore, the isotopic composition of these

contaminated mafic magmas is not shifted enough by crustal interaction to mask the character of their mantle source. They are still useful for the mapping of mantle domains.

Mantle Source and Crustal Contamination

OAB, YAB and Grand Wash Trough

YAB and OAB of the Fortification Hill field and alkali basalts of Grand Wash trough have $^{87}\text{Sr}/^{86}\text{Sr} = 0.703\text{-}0.706$, $\epsilon \text{Nd} = -1$ to $+6.7$, $^{206}\text{Pb}/^{204}\text{Pb} = 17.8\text{-}18.7$ and $^{208}\text{Pb}/^{204}\text{Pb} = 38\text{-}38.5$ (Table 1). These alkali-basalts have Nd and Sr isotopic compositions and trace-element distributions that are similar to those of modern-day asthenosphere-derived ocean island basalts (OIB) (Zindler and Hart, 1986; Fitton et al., 1991) (Figures 4). We suggest that YAB originated from a source dominated by asthenospheric mantle (AM), and as discussed below OAB melted a mixed AM-LM source dominated by AM (Table 2).

When compared to typical OIB and the alkali-basalts of the Grand Wash trough, OAB and YAB appear to contain an additional component. YAB and OAB plot between LM and higher values of ϵNd and $^{206}\text{Pb}/^{204}\text{Pb}$ (Figures 5) rather than lower Pb and higher ϵNd as do Grand Wash trough basalts. We suggest that the trend toward higher rather than lower Pb is due to the presence of HIMU-like mantle ($\epsilon \text{Nd} = 3.5$, $^{206}\text{Pb}/^{204}\text{Pb} > 20$) in the source of OAB and YAB. HIMU-like mantle may reside in either the LM or upper asthenosphere (Zindler and Hart, 1986; Hart, 1988; Hart et al., 1992) or as detached oceanic slabs deep within the mantle (Weaver, 1991b). Weaver (1991b) and Hart et al. (1992) suggest that the source of HIMU-mantle is in the asthenosphere and that it is incorporated into the OIB source by rising plumes or mantle diapirs. We infer that the presence of this component in OAB and in xenolith bearing YAB and its higher abundance in xenolith bearing alkali basalts is more compatible with its residence in AM than LM.

OAB containing normative hypersthene (OAB-hy) are the oldest mafic lavas of

the Fortification Hill field and have higher $^{87}\text{Sr}/^{86}\text{Sr}$ (0.7055-0.7057) and lower ϵNd (-0.68 to -0.9) than the nepheline normative basalts of this group (Figure 4). Both crustal contamination and the presence of a LM component in the source must be considered as explanations for the lower ϵNd and higher $^{87}\text{Sr}/^{86}\text{Sr}$ of the OAB-hy lavas. Glazner and Farmer (1992) demonstrated that xenolith bearing alkali basalts from the Mojave Desert, California have Sr and Nd isotopic compositions similar to typical OIB, and xenolith-free basalts have a range of compositions that trend from OIB toward values more typical of continental lithosphere. They suggest that these isotopic compositions can be explained if xenolith-bearing magmas passed through the crust quickly without interaction and xenolith-free magmas stopped in the crust long enough for xenoliths to drop or be digested and for crustal interaction to occur. In detail, alkali basalts in the Mojave Desert display a trend toward higher $^{87}\text{Sr}/^{86}\text{Sr}$ and lower ϵNd with time (Glazner and Farmer, 1992). They attributed this trend to the hybridization of asthenospherically derived partial melts by commingling with partial melts of Late Jurassic gabbro and Proterozoic diabase. By this mechanism, ϵNd can be changed by as much as 3 units without appreciably changing major or trace element chemistry. Two observations suggest that the Glazner and Farmer (1992) model does *not* explain the isotopic composition of OAB-hy. First, in the NCREC, a probable mafic crustal contaminant is Proterozoic (1.7 Ga) amphibolite that crops out in the footwall of the Saddle Island detachment (Duebendorfer et al., 1990). Isotopically, the amphibolite has low $^{87}\text{Sr}/^{86}\text{Sr}_{\text{T=6 Ma}}$ (0.7029) and high $\epsilon \text{Nd}_{\text{T=6 Ma}}$ (3.18). Therefore, contamination of asthenospherically derived magmas by this type of crust *will probably not* produce OAB-hy or other xenolith-free mafic lavas. Second, OAB-hy are temporally separated from other magma types in the NCREC. This temporal distribution is circumstantial evidence that OAB-hy magmas may sample a different mixture of mantle than OAB-ne or YAB. Therefore, we suggest that OAB-hy and some OAB-ne represent a mixture of AM and LM (Figure 5), not cryptic contamination of mafic magmas by crust.

The trend toward higher ϵNd , lower $^{87}\text{Sr}/^{86}\text{Sr}$ and higher $^{206}\text{Pb}/^{204}\text{Pb}$ between

6 and 4.3 Ma (Figures 4 and 5) suggests that if the source for OAB is a mixture of AM and LM then the ratio of LM to AM is decreasing in the source with time. This relation implies that the source of OAB was near the boundary between AM and LM and *either* this boundary rose through the source area due to extension-related lithospheric thinning, or that the depth of melting increased between 6 and 4.74 Ma. Since, little upper crustal extension occurred between 6 and 4.74 Ma (Feuerbach et al., 1991), we prefer the latter model. Alkali basalts are generated from mantle peridotite at pressures between 15 and 20 Kb corresponding to a depth of about 45 to 60 km (Takahashi and Kushiro, 1983). The boundary between LM and AM beneath the NCREC was probably in this depth range during the Pliocene. Our depth estimate is consistent with the depth of the LM-depleted mantle (asthenosphere) boundary estimated by Daley and DePaolo (1992; Figure 1) for the same time interval and geographic area.

Low ϵ Nd Basalts

Low ϵ Nd alkali basalts occur as pre-11 Ma lavas in the River Mountains, Eldorado Range, Boulder Wash area, Hamblin-Cleopatra volcano, and in the Las Vegas Range, and as post-11 Ma lavas at Callville Mesa and Black Point ($^{87}\text{Sr}/^{86}\text{Sr} = 0.705\text{--}0.710$ and $\epsilon \text{ Nd} = -4$ to -12) (Figures 4).

Andesite and dacite in the River Mountains show abundant field and petrographic evidence of assimilation and magma commingling (Smith et al., 1990). Alkali basalt lacks evidence of contamination and was considered by Smith et al. (1990) to have been generated by partial melting of mantle peridotite. Intermediate lavas in the River Mountains may represent hybrid compositions formed by the commingling of mafic and felsic end-members. This interpretation is supported by a positive correlation between $^{87}\text{Sr}/^{86}\text{Sr}$ and SiO_2 and a negative correlation between $\epsilon \text{ Nd}$ and SiO_2 (Figure 6). The isotopic compositions of basalt and rhyolite end members of the mixing sequence provide a quantitative estimate of the magnitude of isotopic shift due to magma commingling (Figure 4). This shift is no more than 4 units in $\epsilon \text{ Nd}$ and 0.002 in $^{87}\text{Sr}/^{86}\text{Sr}$.

Callville Mesa lavas have $^{87}\text{Sr}/^{86}\text{Sr} = 0.708\text{-}0.709$ and $\epsilon \text{Nd} = -8$ to -10 and are similar in isotopic composition and trace-element chemistry (high Ba, K, and Sr and low Nb and Ti) to mafic lavas derived from LM in the western United States (Fitton et al., 1991; Farmer et al., 1989). However, Callville Mesa lavas differ by having lower Pb ratios ($^{207}\text{Pb}/^{204}\text{Pb} = 15.45\text{-}15.5$; $^{208}\text{Pb}/^{204}\text{Pb} = 37.7\text{-}38$; $^{206}\text{Pb}/^{204}\text{Pb} = 17.2\text{-}17.4$) than typical lithospheric-mantle derived basalts ($^{207}\text{Pb}/^{204}\text{Pb} = 15.6$; $^{208}\text{Pb}/^{204}\text{Pb} = 38.7$; $^{206}\text{Pb}/^{204}\text{Pb} = 18.3$) (Figure 5), having trends on Rb/Sr, Th/Nb and La/Nb vs. SiO_2 plots that project toward crustal compositions (Figure 7a,b and c), and by displaying ample evidence of crustal contamination. These geochemical and petrographic features suggest that Callville magmas were contaminated by the crustal lithosphere. The crustal component has $^{87}\text{Sr}/^{86}\text{Sr} > 0.710$, low Pb isotope ratios, and $\epsilon \text{Nd} < -10$ (Figure 5). We suggest that the crustal contaminant is similar in chemistry to Proterozoic rocks of the Mojave crustal province which extends into the Lake Mead area (Wooden and Miller, 1990). Although, rocks of the Mojave province display a wide range of Pb isotope values, low ratios ($^{207}\text{Pb}/^{204}\text{Pb} < 15.5$; $^{208}\text{Pb}/^{204}\text{Pb} < 38$; $^{206}\text{Pb}/^{204}\text{Pb} < 17.4$) are common. Because of the common occurrence of quartz and alkali feldspar xenocrysts in Callville Mesa lavas, the contaminant is assumed to be a felsic rock. Uncontaminated magma at Callville Mesa is similar in major and trace element composition to OAB. A normative nepheline bearing alkali basalt (sample 24-100; Table 1), the oldest flow recognized from the Callville Mesa center, plots in the field of OAB in terms of $\text{Na}_2\text{O} + \text{K}_2\text{O}$ (Figure 3a), Ce/Yb (Figure 3b) and trace element ratios (Figure 7).

Tholeiitic Basalt

Tholeiitic basalts at Malpais Flattop have high Sr ($^{87}\text{Sr}/^{86}\text{Sr} = 0.7075$), low ϵNd (-8.33) and increasing Rb/Nb, Th/Nb and La/Nb (Figure 8a,b and c). These lavas may have been contaminated as they passed through the crust. It is generally accepted that tholeiitic basalts equilibrate at shallower depths in the mantle than alkali basalts (24 to 45 km; Takahashi and Kushiro, 1983). If OAB were generated near the LM-AM boundary as

suggested above, it is reasonable to assume that the tholeiitic basalts were produced by melting of LM. Tholeiitic basalts in the western United States are generally assumed to have been affected by small amounts of crustal contamination as well as fractional crystallization (Dungan, 1992). The close spatial and temporal association of alkali and tholeiitic basalts, lack of mantle xenoliths together with isotopic and chemical signatures support the contamination hypothesis (for example: Perry et al., 1987; Glazner and Farmer, 1992). To estimate the changes in isotopic composition of lithospherically derived magmas due to contamination, we compared tholeiitic basalts to alkali basalt derived in the LM (e.g., Las Vegas Range alkali basalt to Malpais Flattop tholeiite). Tholeiitic basalts have higher $^{87}\text{Sr}/^{86}\text{Sr}$ and lower $\epsilon \text{ Nd}$ than alkali basalts ($^{87}\text{Sr}/^{86}\text{Sr}=0.0007$ higher, $\epsilon \text{ Nd}= 1.13$ lower). Other investigators noted similar isotopic changes due to crustal contamination. For example, Glazner and Farmer (1992) noted a shift in $\epsilon \text{ Nd}$ by as much as 3 units as the result of contamination of mafic magmas by mafic crust. Daley and DePaolo (1992) estimated that $\epsilon \text{ Nd}$ may be lowered by 2 to 3 units by crustal contamination. Crowley (1984) demonstrated a shift in $^{87}\text{Sr}/^{86}\text{Sr}$ by up to 0.001 when comparing tholeiites and alkali basalts derived from the LM. Based on our data and the work of others, we conclude that the isotopic compositions of tholeiitic basalt reflect the melting of enriched mantle (LM) and that the changes in $\epsilon \text{ Nd}$ (1 to 3 units) and $^{87}\text{Sr}/^{86}\text{Sr}$ (0.001) due to crustal contamination are small when compared to overall variations of $\epsilon \text{ Nd}$ and $^{87}\text{Sr}/^{86}\text{Sr}$.

Summary

Mafic lavas of the NCREC represent the melting of a complex and variable mixture of AM, LM and crust (Table 2). YAB represent the melting of a source composed mainly of a mixture of AM and HIMU-like mantle. The source of OAB-hy and OAB-ne is a mixture of AM and LM dominated by AM. Low $\epsilon \text{ Nd}$ and high $^{87}\text{Sr}/^{86}\text{Sr}$ magmas and tholeiites were derived from a LM source and were contaminated as they passed through the crust. This shift in isotopic values due to crustal interaction (commingling and

contamination) is no more than 4 units in ϵ Nd and 0.002 in $^{87}\text{Sr}/^{86}\text{Sr}$ and does not mask the character of the mantle source.

MANTLE AND CRUSTAL BOUNDARIES

In this section, we argue that (1) the boundary between two *crustal* provinces, the NCREC and the amagmatic zone, corresponds in general to a *mantle* boundary between AM beneath the NCREC and LM beneath the amagmatic zone, (2) the mantle boundary formed between about 11 and 6 Ma during and just after the main phase of Tertiary extension in the western Lake Mead area (9 to 12 Ma), (3) the LMFS may be the upper crustal expression of the mantle boundary, and (4) during the peak of extension passive rifting resulted in upwelling AM beneath the NCREC.

Our arguments below are based on the premise that depth of generation of alkali basalt magma in the study area remains relatively constant with time from 16 to 9 Ma (the period of peak extension regionally; see below). This assumption is based on the work of Takahashi and Kushiro (1983). Tholeiitic basalts are generated by partial melting of mantle peridotite with the mineral assemblage clinopyroxene, olivine, orthopyroxene at pressures of 8 to 15 Kb corresponding to depths of 24 to 45 km. Alkali basalts are produced from a similar source at pressures between 15 and 20 Kb corresponding to a depth of about 45 to 60 km. Crustal extension is accompanied by the rise of the geotherm to higher levels of the lithosphere. Therefore the expected relationship between extension and volcanism is the production of tholeiitic basalts during extension when isotherms are elevated and alkali basalts late when isotherms relax. In the Lake Mead area, however, the most compositionally primitive basalts in any given area are generally alkalic regardless of age and relation to extension. An exception is the tholeiitic basalt at Malpais Flattop. Therefore, depth of melting appears to remain relatively constant with time and variations in chemical and isotopic compositions are due to the rise of the LM-asthenosphere boundary rather than significant changes in the depth of melting.

In our discussion below, we divide the mafic volcanic rocks into those that erupted during and prior to the major phase of upper crust extension and those that erupted during a period of reduced upper crust extension. The time of peak upper crustal extension varies across the region (Wernicke et al., 1988; Fitzgerald et al., 1992), however in the Las Vegas area it occurred between 12 and 9 Ma (Duebendorfer and Wallin, 1991). To the south in the Eldorado and Black Mountains and to the east in the Gold Butte and Virgin Mountains, extension began at about 16 Ma (Anderson, 1971; Wernicke et al., 1988; Faulds et al., 1990). Wernicke estimated that in the Las Vegas region 75% of extension occurred between 16 and 10 Ma and 25% between 10 and 5 Ma. Structural information from the Lake Mead region suggests that 9 Ma is a more precise date for the termination of peak extension (Duebendorfer and Wallin, 1991). Therefore we use 9 Ma to separate mafic lavas produced during the peak of extension from those that erupted during waning extension.

The Mantle Boundary

Isotopic data for post-9 Ma mafic lavas show regional differences which we infer to be a boundary in the lava's source region in the mantle. Contours ($^{87}\text{Sr}/^{86}\text{Sr} = 0.706$ and $\epsilon \text{Nd} = -1$) separating lavas with a dominant LM component ($^{87}\text{Sr}/^{86}\text{Sr} > 0.706$, $\epsilon \text{Nd} < -1$) from those with an AM ($^{87}\text{Sr}/^{86}\text{Sr} < 0.706$, $\epsilon \text{Nd} > -1$) component define a boundary that extends from just north of the River Mountains into the Grand Wash trough (Figure 8). The boundary parallels the LMFS along most of its length and is also roughly coincident with the boundary between the NCREC and the amagmatic zone. Post-9 Ma magmas tap mantle dominated by AM to the south of the boundary and LM to the north. Because sample locations in some areas are separated by considerable distance, placement of these contours is somewhat arbitrary, however they do define the general area of isotopic change. We suggest that this boundary formed during and just after the period of peak extension. Pre-9 Ma basalts throughout the region have uniform ϵNd and $^{87}\text{Sr}/^{86}\text{Sr}$ and were derived by melting of LM (Figure 9). Also, trace element compositions of pre-9

Ma mafic lavas are similar to those basalts of the Western Great Basin province derived from LM (Fitton et al., 1991) (Figure 10a). Therefore, prior to about 9 Ma, LM extended beneath the entire Lake Mead area. Post 9-Ma basalts in the NCREC to the south of the boundary display a dramatic shift in $^{87}\text{Sr}/^{86}\text{Sr}$ and ϵNd . $^{87}\text{Sr}/^{86}\text{Sr}$ changes from about 0.707 to 0.703-0.705 and ϵNd from about -9 to higher values (-1 to +6.7) (Figure 8). Chemically, mafic volcanic rocks acquire the signature of OIB lavas of the Transition Zone (Figure 10b). In the amagmatic zone to the north of the boundary, post-9 Ma mafic lavas at Black Point and at Callville Mesa retain the isotopic signature of pre-9 Ma lavas (Figure 8) and may represent the easternmost limit of the southern Nevada basalt field of Farmer et al. (1989). Our interpretation of this data is that between 11 and about 6 Ma, the source of mafic lavas in the NCREC changed from LM to AM. The source of lavas in the amagmatic zone remained in the LM. Apparently, the LM was thinned or removed from beneath the NCREC but remained intact beneath the amagmatic zone. Therefore, we infer that the mantle boundary between LM (north) and AM (south) formed between about 11 and 6 Ma.

Daley and DePaolo (1992) concluded on the basis of an isotopic study that the lithosphere in the Las Vegas area thinned by about 50% less than would be predicted by the amount of upper crustal extension. This statement is partially based on isotopic values for tholeiitic basalt at Malpais Flattop and a 5.8 Ma K-Ar age for these lavas reported by Anderson et al. (1972). The isotopic data and geochronology suggest that near the end of the major phase of upper crustal extension (10 to 6 Ma), the lithosphere had not thinned enough to bring AM into the depth range of tholeiitic magmas. However, recent $^{40}\text{Ar}/^{39}\text{Ar}$ dating shows that Malpais Flattop is between 9.7 Ma and 10.6 m.y. old, not 5.8 Ma (Faulds and Gans, unpublished data). Although, the conclusion of Daley and DePaolo (1992) is permissible considering the new dates, their estimates of the magnitude of lithospheric extension can no longer be as tightly constrained.

Mantle Plumes?

The change in source of basalts from LM to AM with time, the OIB character of the mafic lavas and the presence of a HIMU-type mantle component are compatible with the presence of a rising asthenospheric plume beneath the NCREC. Mechanisms to account for lithospheric extension and OIB type volcanism commonly call for an upwelling mantle plume (active rifting) (e.g., Eaton, 1982; Fitton et al., 1991). However, the persistence of volcanism with OIB character for nearly 5 m.y. argues against such a mechanism, because plumes or convecting cells are not coupled to the lithosphere. The lithosphere drifts over the heat source resulting in a volcanic chain. Mantle heat sources (plumes) apparently drift, but not necessarily at the same rate or in the same direction as the lithospheric plates.

Unusually hot asthenosphere may not be required to induce lithospheric extension and volcanism (Buck, 1986; Perry et al., 1987; White, 1987; White et al., 1988). Mantle upwelling may be passive and caused by stretching and thinning of the lithosphere. The mantle rises to compensate for thinning crust. Melting results from the decompression of asthenospheric mantle as it rises passively beneath the stretched and thinned lithosphere. Small increases in temperature are sufficient to generate large volumes of melt during decompression. An increase of 100° C doubles the amount of melt; 200° C can quadruple melt volume (White and McKenzie, 1989). Melt produced by passive mantle upwelling are thought to underplate the thinned lithosphere where they form a gabbroic layer. After a sufficient volume of magma is generated, small batches of mafic magma rise into the upper crust. Only about 10% of the magma generated in the mantle eventually reaches the surface (White and McKenzie, 1989). During passive mantle upwelling, isotopically enriched lithosphere may be thermally but not chemically converted to asthenosphere and may convectively mix with isotopically depleted asthenospheric mantle (Perry et al., 1987). OIB basalts may result from the partial melting of this two component mantle. Hence, a deep mantle source for OIB is not required.

Passive rifting models infer that mantle convection is coupled to the lithosphere and OIB type volcanism may occur for long periods of time in a restricted geographic area. Perry et al. (1987, 1988) applied a passive rifting model to the Rio Grande rift in central New Mexico and suggested that volcanism in the Colorado Plateau-Basin-Range transition zone may be explained by passive rifting. Recently, Bradshaw (1991) suggested a modified passive rifting model. Plate tectonics, rather than deep seated mantle plumes may provide the ultimate driving force for extension and magmatism. According to Bradshaw, melting of LM in the NCREC was initiated by heat input from warmer asthenosphere as it rose to fill a slab window left by the northward migration of the Farallon Plate.

Passive rifting is probably more applicable to the NCREC than active rifting for two reasons. First, OIB-type alkali basalt volcanism is concentrated in a restricted geographic area for nearly 5 m.y. Volcanic chains with orientations explainable by lithospheric plate motion are not present. Second, alkali basalt magmas in the NCREC result from melting a three component source composed of LM, AM and HIMU-mantle. LM was an important component in the source of older OAB-hy and low ϵ Nd alkali basalts but becomes less important with time. This geochemical pattern is compatible with the model of passive rifting and lithospheric erosion as described by Perry et al. (1987) for the Rio Grande Rift.

Passive rifting may have been preceded by active rifting in the NCREC. Faulds et al. (1990) suggested that upwelling was active in the NCREC during mid-Miocene extension. Faulds et al. (1990) developed a kinematic model that infers that extension (spreading) occurred about discrete axes and that highly extended areas lie directly above areas of divergent flow in the asthenosphere. Alternatively, passive rifting between 11 and 6 Ma may be a continuation of an earlier more intense passive rifting event related to the opening of a slab window left by the northward migration of the Farallon Plate (Bradshaw, 1991).

Does LM Thin Progressively to the West?

During the peak of extension, most mafic lavas in the NCREC were derived by melting LM. An exception is 9.4 Ma basalt at Gold Butte that displays a different isotopic signature ($\epsilon \text{Nd} = -0.9$ and $^{87}\text{Sr}/^{86}\text{Sr} = 0.705$). The higher ϵNd and lower $^{87}\text{Sr}/^{86}\text{Sr}$ may be explained by the presence of AM in the source. If this assumption is correct, then Basalt at Gold Butte has a substantial AM component about 3 m.y. earlier than alkali basalt in the NCREC to the west (Figures 9 and 11). We interpret this relationship as circumstantial evidence for westward thinning of LM with time in the Lake Mead area. In the NCREC (Wernicke et al., 1988; Smith et al., 1990) and Gold Butte area (Fitzgerald et al., 1991) upper crustal extension may have migrated from east to west between 16 Ma and about 9 Ma. The postulated westward thinning of the mantle lithosphere may mirror spatially and temporally (?) westward migrating upper crustal extension. Directional thinning of the LM will be difficult to test further because of a lack of alkali basalt lavas of a suitable age along an east-west transect across the NCREC.

Links Between Mantle and Crust

$^{87}\text{Sr}/^{86}\text{Sr} = 0.706$ and $\epsilon \text{Nd} = -1$ contours trend east-northeast and are colinear with the LMFS (Figure 8). The LMFS is a set of northeast striking left-lateral faults with 65 km of accumulated slip that occurred between 17 and 10 Ma (Anderson, 1973; Bohannon 1979, 1984). Weber and Smith (1987) considered the LMFS and the Saddle Island detachment (Smith, 1982; Duebendorfer et al., 1991a) to be a kinematically coordinated system of faults. If the Weber and Smith (1987) model is correct, then the LMFS is a shallow crustal structure. Recently, Smith et al. (1991) suggested that the Saddle Island fault originated as a steeply dipping normal fault and that the LMFS represents the northern boundary of the Saddle Island allochthon. In this case, the LMFS may extend into the middle to lower crust. Faulds et al. (1990) considered both the LMFS and the LVVSZ as the northern boundary of the NCREC and to correspond to

intracontinental transform faults separating en echelon axes of extension. We suggest that the similar trend and geographic location of the isotopic boundaries and the LMFS argues for a genetic relationship between the two features. The LMFS may represent the crustal manifestation of differential thinning of the LM or the rejuvenation of an older lithospheric structure. Whatever the connection, it appears that the LMFS reflects mantle processes and may be an important deeply penetrating (?) crustal structure.

SUMMARY

The formation of a mantle domain boundary is depicted on four diagrammatic north-south sections across the Lake Mead area (Figure 11). The sections display the interaction of mantle and crust during the early stage of extension in the Lake Mead area (16-12 Ma), the peak of extension (12-9 Ma), after the peak of extension during the eruption of Fortification Hill basalts (6 Ma) and after extension during the eruption of xenolith bearing alkali basalts (4.3 Ma).

Early Stage of Extension (Figure 11a). Crustal extension was initiated about 16 Ma in the Lake Mead-Gold Butte area by either active mantle convection (Fitton et al., 1991) or the opening of a slab window (Bradshaw, 1991). Mafic magmas were generated in LM and locally rose to the surface without being significantly contaminated (e.g., Las Vegas Range, alkali basalt in River Mountains). Mafic magma stalled in the crust at "ductile barriers" and commingled with crustal magma to form calc-intermediate volcanoes and plutons (Smith et al., 1990; Bradshaw, 1991).

Peak of Extension (Figure 11b). Upper crustal extension occurred in the NCREC between 12 and 9 Ma but was not accompanied by significant magmatism. During extension in the NCREC, LM may have been thinned and replaced by asthenosphere progressively to the west. During thinning and replacement of the LM in the NCREC, the LM in the amagmatic zone remained intact. Contrasting behavior to the north and south of this boundary produced the mantle domain boundary. The LMFS is spatially and temporally

related to the mantle boundary. The LMFS may be the crustal manifestation of differential thinning of the LM. Mantle convection between 12 and 9 Ma is probably passive and is driven by crustal thinning.

After the Peak of Extension (Figure 11c). After the peak of extension, volcanism in the NCREC originates in the asthenosphere near the boundary with the LM at a depth of 45 to 60 km. In the amagmatic zone mafic volcanic rocks at Black Point originate in the LM. Isotopic compositions of alkali basalts define two mantle domains. The domain to the north is characterized by LM ($\epsilon Nd = -3$ to -9 ; $^{87}Sr/^{86}Sr = 0.706-0.707$). To the south mafic lavas have an OIB-mantle signature and appear to have only a minor LM component in their source ($\epsilon Nd = 0$ to $+4$; $^{87}Sr/^{86}Sr = 0.703-0.705$). The change in source of basalts from LM to AM with time, the OIB character of the mafic lavas and the presence of a HIMU-like mantle component is compatible with the presence of rising asthenosphere, as an upwelling convective cell, or plume beneath the NCREC at 6 Ma after the peak of extension. Passive rifting is probably more applicable to the NCREC than active rifting because OIB-type alkali basalt volcanism is focused in a small geographic area for at least 5 Ma.

After Extension (Figure 11d). Low volume xenolith bearing alkali basalts formed in the NCREC by melting asthenosphere mixed with a HIMU-like component. Since, lithospheric thinning is unlikely at 4.3 Ma, the lower proportion of LM in the source of alkali basalts and the higher proportion of HIMU-like mantle suggests that the depth of melting increased between 6 and 4.3 Ma. Passive rifting may have continued as late as 4.3 Ma as evidenced by the presence of the HIMU-like mantle component in mafic lavas of this age.

ACKNOWLEDGMENTS

This research was supported by a grant from the Nevada Nuclear Waste Project Office. We thank Ernest Duebendorfer, James Faulds and Terry Naumann for informative

discussions and for reading early versions of this paper and Nathan F. Stout for drafting several of the figures. We thank the staff of the Phoenix Memorial Laboratory, University of Michigan for completing the REE analyses and Dave Nealey (USGS) for arranging for XRF analyses of selected samples. Partial laboratory support at the University of Kansas was provided by National Science Foundation grant EAR-8904007 awarded to Walker. We thank Randy Van Schmus and Drew Coleman for helpful discussions concerning the collection of the isotopic data.

REFERENCES

- Anderson, R.E., 1971, Thin skin distension in Tertiary rocks of southeastern Nevada: *Geological Society of America Bulletin*, v. 82, p. 42-58.
- Anderson, R.E., 1973, Large-magnitude late Tertiary strike-slip faulting north of Lake Mead, Nevada: *U.S. Geological Survey Professional Paper 794*, 18p.
- Anderson, R.E., Longwell, C.R., Armstrong, R.L., and Marvin, R.F., 1972, Significance of K-Ar ages of Tertiary rocks from the Lake Mead region, Nevada-Arizona: *Geological Society of America Bulletin*, v. 83, p. 273-288.
- Armstrong, R.L., 1966, K-Ar dating using neutron activation for Ar analysis: *Geochimica et Cosmochimica Acta.*, v. 30, p. 565-600.
- Armstrong, R.L., 1970, Geochronology of Tertiary igneous rocks, eastern Basin and Range province, western Utah, eastern Nevada, and vicinity, U.S.A.: *Geochimica et Cosmochimica Acta*, v. 34, 203-232.
- Barker, D.S., and Thompson, K.G., 1989, Hamblin-Cleopatra volcano, Nevada: genesis of a shoshonite-latitude-trachydacite-trachyte suite: in *Continental Magmatism abstracts*, IAVCEI, New Mexico Institute of Mining and Geology Bulletin 131, p. 17.
- Bennett, V.C. and DePaolo, D.J., 1987, Proterozoic crustal history of the western United States as determined by Nd isotopic mapping: *Geological Society of America*

Bulletin, v. 99, p. 674-685.

- Bohannon, R.G., 1979, Strike-slip faults of the Lake Mead region of southern Nevada: in Armentrout, J.M., Cole, M.R., and Terbest, H., eds., *Cenozoic paleogeography of the western United States*, Pacific Section, Society of Economic Paleontologists and Mineralogists Pacific Coast Paleogeography Symposium 3, p. 129-139.
- Bohannon, R.G., 1984, Nonmarine sedimentary rocks of Tertiary age in the Lake Mead region: U.S. Geological Survey Professional Paper 1259, 72p.
- Bradshaw, T.K., 1991, Tectonics and magmatism in the Basin and Range Province of the Western United States: The Open University (GB), Ph.D. dissertation, 247 pp.
- Buck, W.R., 1986, Small-scale convection induced by passive rifting: the cause for uplift of rift shoulders: *Earth and Planetary Sciences Letters*, v. 77, p. 362-372.
- Campbell, I., and Schenk, E.T., 1950, Camptonite dikes near Boulder Dam, Arizona: *American Mineralogist*, v. 35, p. 671-692.
- Cascadden, T.E and Smith, E.L., 1991, Intermediate and mafic volcanic rocks of the northern White Hills, Arizona: Implications for the production of intermediate composition volcanic rocks during regional extension: *Geological Society of America, Abstracts with Programs*, v. 23, no. 5, p. 390.
- Cascadden, T.E., 1991, Style of volcanism and extensional tectonics in the eastern Basin and Range province: northern Mohave County, Arizona: M.S. thesis, University of Nevada, Las Vegas, 156 pp.
- Cole, E.D., 1989, Petrogenesis of late Cenozoic alkalic basalt near the eastern boundary of the Basin-and-Range: upper Grand Wash trough, Arizona and Gold Butte, Nevada: M.S. Thesis, University of Nevada, Las Vegas, 68 pp.
- Cooper, J.L., and Hart, W.K., 1990, Mantle sources in the Arizona transition zone and global mantle heterogeneity: *Geology*, v. 18, p. 1146-1149.
- Crowley, J.C., 1984, Strontium isotope and rare earth element analysis of Rio Grande rift basalts: implications for magmagenesis in continental rifts: Ph.D. dissertation,

- Brown University, Providence, 116 pp.
- Daley, E.E., and DePaolo, D.J., 1992, Isotopic evidence for lithospheric thinning during extension: southeastern Great Basin: *Geology*, v. 20, p. 104-108.
- Darvall, P., Gans, P.B., and Lister, G.S., 1991, Normal faulting in the Eldorado Mountains, southeastern Nevada: *Geological Society of America, Abstracts with Programs*, v. 23, no. 2, p. 17.
- Duebendorfer, E.M., Shafiquallah, M., Damon, P.E., 1991a, The Las Vegas Valley Shear Zone: A middle to late Miocene extensional transfer fault: *Geological Society of America Abstracts with Programs*, v. 23, no. 5, p. A188.
- Duebendorfer, E.M., Sewall, A.J., and Smith, E.L., 1991b, The Saddle Island Detachment fault, an evolving shear zone in the Lake Mead area of southern Nevada: *in* Wernicke, B., ed., *Mid-Tertiary extension at the latitude of Las Vegas: Geological Society of America Memoir 176*, p. 77-97.
- Duebendorfer, E.M., and Wallin, E.T., 1991, Basin development and syntectonic sedimentation associated with kinematically coupled strike-slip and detachment faulting, southeastern Nevada: *Geology*, v. 19, p. 87-90.
- Dungan, M.A., 1992, Interpretation of elemental and isotopic signatures of extension-related basalts: implications of Northern Rio Grande Rift volcanism (abs.): *Transactions , American Geophysical Union*, v. 73, no. 10, p. 334.
- Eaton, G.P., 1982, The Basin and Range province: Origin and tectonic significance: *Annual Review of Earth and Planetary Sciences*: v. 10, p. 409-440.
- Eaton, G.P., Wahl, R.R., Prostka, H.J., Mabey, D.R., and Kleinkopf, M.D., 1978, Regional gravity and tectonic patterns: Their relation to late Cenozoic epeirogeny and lateral spreading in the western Cordillera: *in* R.B Smith and Eaton, G.P., eds., *Cenozoic Tectonics and Regional Geophysics of the Western Cordillera*, *Geological Society of America Memoir 152*, p. 51-93.
- Farmer, G.L., Perry, F.V., Semken, S., Crowe, B., Curtis, D., and DePaolo, D.J., 1989,

- Isotopic evidence of the structure and origin of subcontinental LM in southern Nevada: *Journal of Geophysical Research*, v. 94, p. 7885-7898.
- Faulds, J.E., Geissman, J.W., and Mawer, C.K., 1990, Structural development of a major extensional accommodation zone in the Basin and Range province, northwestern Arizona and southern Nevada; implications for kinematic models of continental extension: in Wernicke, B.P., ed., *Basin and Range extensional tectonics near the latitude of Las Vegas, Nevada: Geological Society of America Memoir 176*, p.37-76.
- Faulds, J.E., Feuerbach, D.L., and Smith, E.L., 1991, New insights on structural controls and emplacement mechanisms of Pliocene/Quaternary basaltic dikes, southern Nevada and northwestern Arizona: *Geological Society of America Abstracts with Programs*, v. 23, no. 5, p. 118.
- Feuerbach, D.L., Smith, E.L., Shafiqullah, M., and Damon, P.E., 1991, New K-Ar dates for late-Miocene to early Pliocene mafic volcanic rocks in the Lake Mead area, Nevada and Arizona: *Isochron West*, no. 57, p. 17-20.
- Fitton, J.G., James, D., Kempton, P.D., Ormerod, D.S., and Leeman, W.P., 1988, The role of LM in the generation of Late Cenozoic basic magmas in the western United States: *Journal of Petrology, Special Lithosphere Issue*, p. 331-349.
- Fitton, J.G., James, D., and Leeman, W.P., 1991, Basic magmatism associated with Late Cenozoic extension in the western United States: compositional variations in space and time, *Journal of Geophysical Research*, v. 96, no. B8, p. 13,693-13,711.
- Fitzgerald, P.G., Fryxell, J.E., and Wernicke, B.P., 1991, Miocene crustal extension and uplift in southeastern Nevada: constraints from fission track analysis: *Geology*, v. 19, p. 1013-1016.
- Glazner, A.F. and Farmer, G.L., 1991, Production of isotopic variability in basalts by cryptic mafic contamination: *Transactions of the American Geophysical Union*, v. 72, p. 267.

- Glazner, A.F., and Farmer, G.L., 1992, Production of isotopic variability in continental basalts as cryptic crustal contamination: *Science*, v. 255, p. 72-74.
- Glazner, A.F., and Supplee, J.A., 1982, Migration of Tertiary volcanism in the southwestern United States and subduction of the Mendocino fracture zone: *Earth and Planetary Science Letters*, v. 60, p. 429-436.
- Hart, W.K., 1985, Chemical and isotopic evidence for mixing between depleted and enriched mantle, northwestern U.S.A.: *Geochemica and Cosmochemica Acta*, v. 49, p. 131-144.
- Hart, S.R., 1988: *Earth and Planetary Science Letters*, v. 90, p. 273-
- Hart, S.R., Hauri, E.H., Oschmann, L.A., Whitehead, J.A., 1992, Mantle plumes and entrainment: isotopic evidence: *Science*, v. 256, p. 517-520.
- Koski, R.J., 1991, New K-Ar dates from the Three Kids Mine, Clark County, Nevada: *Isochron West*, no. 56, p.
- Leat, P.T., Thompson, R.N., Dicken, A.P., Morrison, M.A., and Hendry, G.L., 1989, Quaternary volcanism in northwestern Colorado: implications for the roles of asthenosphere and lithosphere in the genesis of continental basalts: *Journal of Volcanology and Geothermal Research*, v. 37, p. 291-310.
- Leat, P.T., Thompson, R.N., Morrison, M.A., Hendry, G.L., and Dicken, A.P., 1991, Alkaline hybrid mafic magmas of the Yampa area, NW Colorado, and their relationship to the Yellowstone mantle plume and LM domains: *Contributions to Mineralogy and Petrology*, v. 107, p. 310-327.
- Leeman, W.P., 1970, Late Cenozoic alkali-olivine basalts of the Basin-Range province, USA: *Contributions to Mineralogy and Petrology*, v. 25, p. 1-24.
- Longwell, C.R., 1960, Possible explanation of diverse structural patterns in southern Nevada: *American Journal of Science*, v. 258-A (Bradley Volume), p. 192-203.
- Longwell, C.R., Pampeyan, E.H., Bower, B., and Roberts, R.J., 1965, Geology and mineral deposits of Clark County, Nevada: Nevada Bureau of Mines and Geology

Bulletin 62, 218 pp.

- Menzies, M.A., 1989, Cratonic, circumcratonic and oceanic mantle domains beneath the western United States: *Journal of Geophysical Research*, v. 94, p. 7899-7915.
- Menzies, M.A., Leeman, W.P., and Hawkesworth, C.J., 1983, Isotope geochemistry of Cenozoic volcanic rocks reveals mantle heterogeneity below western U.S.A.: *Nature*, v. 303, 9. 205-209.
- Mills, J.G., 1985, The geology and geochemistry of volcanic and plutonic rocks in the Hoover Dam 7.5 minute quadrangle, Clark County, Nevada and Mojave County, Arizona: M.S. thesis, University of Nevada, Las Vegas, 119 pp.
- Naumann, T.R., 1987, Geology of the central Boulder Canyon quadrangle, Clark County, Nevada: M.S. thesis, University of Nevada, Las Vegas, 68 pp.
- Naumann, T.R. and Smith, E.L., 1987, Evidence for magma mixing in Mid-Tertiary rocks, Lake Mead region, southern Nevada: *Geological Society of America Abstracts with Programs*, v. 19, p. 435-436.
- Perry, F.V., Baldrige, W.S., and DePaolo, D.J., 1987, Role of asthenosphere and lithosphere in the genesis of late Cenozoic basaltic rocks from the Rio Grande Rift and adjacent areas of the southwestern United States: *Journal of Geophysical Research*, v. 92, p. 9193-9213.
- Reynolds, S.J., Florence, F.P., Welty, J.W., Roddy, M.S., Currier, D.A., Anderson, B.V., and Keith, S.B., 1986, Compilation of radiometric age determinations in Arizona: *Arizona Bureau of Geology and Mineral Technology Bulletin* 197, 258 p.
- Smith, E.L., Feuerbach, D.L., Naumann, T.R., and Mills, J.G., 1990, Geochemistry and evolution of mid-Miocene igneous rocks in the Lake Mead area of Nevada and Arizona, in Anderson, J.L. ed, *Cordilleran Magmatism: Geological Society of America Memoir* 176, p. 169-194.
- Smith, E.L., Feuerbach, D.L., and Duebendorfer, E.M., 1991, Magmatism, extensional tectonics and sedimentation in the Lake Mead area of Nevada and Arizona: A new

- model: Geological Society of America Abstracts with Programs, v. 23, p. 63.
- Smith, E.I., 1982, Geology and geochemistry of the volcanic rocks in the River Mountains, Clark County, Nevada and comparisons with volcanic rocks in nearby areas: in Mesozoic-Cenozoic Tectonic Evolution of the Colorado River Region, California, Arizona, and Nevada, edited by E.G. Frost, and D.L. Martin, Cordilleran Publishers, San Diego, California, p. 41-54.
- Smith, E.I., 1984, Geological map of the Boulder Beach Quadrangle, Nevada: Nevada Bureau of Mines and Geology Map 81, scale 1:24,000.
- Smith, E.I., Schmidt, C.S., and Mills, J.G., 1988, Mid-Tertiary volcanoes of the Lake Mead area of southern Nevada and Northwestern Arizona: in Weide, D.L., and Faber, M.L., This Extended Land, Geological Journeys in the southern Basin and Range, Geological Society of America, Cordilleran Section Field Trip Guidebook; UNLV Department of Geoscience, Special Publication No. 2, p. 107-122.
- Takahashi, E., and Kushiro, I., 1983, Melting of dry peridotite at high pressures and basalt magma genesis: American Mineralogist, v. 68, p. 859-879.
- Taylor, W.J., and Bartley, J. M., 1988, Prevolcanic extensional breakaway zone, east-central Nevada: Geological Society of America Abstracts with Programs, v. 19, p. 457.
- Thompson, K.G., 1985, Stratigraphy and petrology of the Hamblin-Cleopatra volcano, Clark County, Nevada: M.S. Thesis, University of Texas, Austin, 306 pp.
- Walker, J.D. and Coleman, D.S., 1991, Geochemical constraints on mode of extension in the Death Valley region: Geology, v. 19, no. 10, p. 971-974.
- Weaver, B.L., 1991a, The origin of ocean island basalt end-member compositions: trace element and isotopic constraints: Earth and Planetary Science Letters, v. 104, p. 381-397.
- Weaver, B.L., 1991b, Trace element evidence for the origin of ocean-island basalts: Geology, v. 19, p. 123-126.

- Weaver, B.L., Wood, D.A., Tarney, J., and Joron, J.L., 1986, Role of subducted sediment in the genesis of ocean island basalts: Geochemical evidence from South Atlantic Ocean Islands: *Geology*, v. 14, p. 275-278.
- Weber, M.E. and Smith, E.I., 1987, Structural and geochemical constraints on the reassembly of disrupted mid-Miocene volcanoes in the Lake Mead-Eldorado Valley area of southern Nevada: *Geology*, v. 15, p. 553-556.
- Wernicke, B., and Axen, G.J., 1988, On the role of isostasy in the evolution of normal fault systems: *Geology*, v. 16, p. 848-861.
- White, W.M., and Patchet, P.J., 1984, Hf-Nd-Sr isotopes and incompatible element abundances in island arcs: implications for magma origins and crust-mantle evolution: *Earth and Planetary Science Letters*, v. 67, p. 167-185.
- White, R.S. and McKenzie, D.P., 1989, Magmatism at rift zones: the generation of volcanic continental margins and flood basalts: *Journal of Geophysical Research*, v. 94, p. 7685-7730.
- White, R.S., 1987, The earth's crust and lithosphere: *Journal of Petrology*, Special Lithosphere Issue, p. 1-10.
- White, R.S., Spence, G.D., Fowler, S.R., McKenzie, D.P., Westbrook, G.K., and Bowen, A.D., 1988, Magmatism at rifted continental margins: *Nature*, v. 330, p. 439-444.
- Wooden, J.L. and Miller, D.M., 1990, Chronologic and Isotopic framework for early Proterozoic crustal evolution in the eastern Mohave Desert region, SE California: *Journal of Geophysical Research*, v. 95, B12, p. 20,133-20,146.
- Zindler, A., and Hart, S.R., 1986, Chemical geodynamics: *Annual Review of Earth and Planetary Science Letters*, v. 14, p. 493-571.

FIGURES:

1. Major mantle and crustal provinces in the southern Basin and Range. The boundaries of the Western Great Basin province are from Fitton et al. (1991). Mafic lavas in the Sierran province (Menzies et al., 1983) are identical in isotopic signature to those in the Western Great Basin province. Boundary between EM2 and OIB-mantle is from Menzies (1989) and the extent of the amagmatic zone from Eaton (1982) and Eaton et al. (1978). Other geologic boundaries are from Fitton et al. (1991). The NCREC was originally defined by Faulds et al. (1990). Rectangle indicates area represented in Figure 2a.

2a. Index map of southern Nevada showing geologic features and sample stations. Rectangle indicates the area of Figure 2b. Patterned area is Lake Mead. LVVFZ-Las Vegas Valley fault zone, LMFS-Lake Mead fault system, LVR-Las Vegas Range. BP-Black Point, RM-River Mountains, McR-McCullough Range, BM-Black Mountains, WH-White Hills, GB-Gold Butte, GWT-Grand Wash trough, EM-Eldorado Mountains, NCREC-Northern Colorado River extensional corridor.

2b. Detailed index map of Lake Mead area and Northern Colorado River extensional corridor showing geologic features mentioned in the text and the location of sample stations (numbers in boxes correspond to first two digits of sample numbers on Table 1). CM-Callville Mesa, BW-Boulder Wash, HC-Hamblin Cleopatra volcano, PW-Petroglyph Wash, FH-Fortification Hill, SI-Saddle Island, LC-Lava Cascade, HD-Hoover Dam, WB-Willow Beach, MFT-Malpais Flattop, Gov W-Government Wash, US-93-exposures of alkali basalt along US route 93.

3a. Plot of total alkalis ($\text{Na}_2\text{O}+\text{K}_2\text{O}$) vs. SiO_2 for volcanic rocks of the Fortification Hill volcanic field, Callville Mesa, Black Point and Malpais Flattop. Open circles-Young alkali

basalts (YAB) of the Fortification Hill field, Filled circles-Older alkali basalts (OAB) of the Fortification Hill field, Open triangles-Hypersthene normative alkali basalts (OAB-hy) of the Fortification Hill field, Filled triangles-Tholeiitic basalts (TH) from Malpais Flattop, Open boxes-mafic lavas of Callville Mesa (CM).

3b. Plot of Ce/Yb vs. SiO₂ for volcanic rocks of the Fortification Hill volcanic field, Callville Mesa, Black Point and Malpais Flattop. Symbols are defined in the caption of Figure 3a. Solid circles surrounded by dotted line are mafic lavas at Black Point.

4. Post 9-Ma alkali basalts in the northern Colorado River extensional corridor are similar to ocean island basalts (OIB) in terms of ϵ Nd and $^{87}\text{Sr}/^{86}\text{Sr}$. Pre 9-Ma mafic lavas region wide and post 9-Ma basalts in the anagmatic zone originated in the LM. LM in the Lake Mead area has a wider range of isotopic compositions than LM reported by Farmer et al. (1989) for southern Nevada basalts. In the River Mountains, magma commingling resulted in a change of ϵ Nd of about 4 units and $^{87}\text{Sr}/^{86}\text{Sr}$ of about 0.002 (indicated by brackets). DM-depleted mantle (MORB), HIMU-a mantle component with high μ ($^{238}\text{U}/^{204}\text{Pb}$). OIB-ocean island basalt.

5. Mafic lavas of the Fortification Hill field appear to contain a HIMU-like component in their source. Fortification Hill basalts define a trend that extends from lithospheric mantle toward HIMU-like mantle. Mafic lavas of the Grand Wash trough lack this component and trend toward typical asthenospheric mantle. Callville Mesa lavas are low in Pb and show the affect of contamination by Mojave-type crust (lower to middle crust). Mafic volcanic rocks in the River Mountains commingled with felsic upper crust and trend toward higher $^{206}\text{Pb}/^{204}\text{Pb}$. Symbols defined on Figure 4.

6. Three-dimensional plot of ϵ Nd vs. $^{87}\text{Sr}/^{86}\text{Sr}$ vs. SiO_2 for volcanic rocks of the River Mountains. The positive correlation between SiO_2 and $^{87}\text{Sr}/^{86}\text{Sr}$ and the negative correlation between SiO_2 and ϵ Nd suggest that rhyolite and basalt are end-members of a mixing sequence. Intermediate compositions represent the mixing of the end-member compositions in various proportions.

7. Trace-element ratio vs. SiO_2 plots for volcanic rocks of the Fortification Hill volcanic field, Callville Mesa and Malpais Flattop. Symbols defined in caption to Figure 3a. OAB and YAB have ratios typical of ocean island basalts (OIB). Callville Mesa and tholeiitic lavas trend from the OIB field toward crust. Boxes indicate the field of ocean island basalts.

7a. Rb/Sr vs. SiO_2 .

7b. Th/Rb vs. SiO_2 .

7c. La/Nb vs. SiO_2 . TH-indicates hidden data point for tholeiitic basalt.

8. Map showing $^{87}\text{Sr}/^{86}\text{Sr}$ and ϵ Nd for pre-9 Ma mafic lavas in the Lake Mead area. The magmatic zone lies to the north of the Lake Mead fault system (LMFS), the northern Colorado River extensional corridor is to the south. Prior to 9 Ma isotopic values were relatively constant across the Lake Mead region and indicate that mafic volcanoes are tapping lithospheric mantle.

9. Map showing $^{87}\text{Sr}/^{86}\text{Sr}$ and ϵ Nd for post-9 Ma mafic lavas in the Lake Mead area. Contours separate areas where mafic volcanoes are tapping asthenospheric mantle (ϵ Nd > -1, $^{87}\text{Sr}/^{86}\text{Sr}$ < 0.704) from those areas where volcanoes are tapping lithospheric

mantle (LM). Note that the LMFS is colinear with the isotopic contours and that AM is mainly present to the south in the NCREC. Values in italics are OAB-hy.

10a. Spider plot of incompatible elements vs. abundance normalized to OIB average of Fitton et al. (1991). Post 9-Ma mafic lavas in the NCREC (open triangles) are similar in trace element abundance and pattern to lavas in the Colorado Plateau-Basin and Range Transition Zone derived by melting AM (solid circles) (Fitton et al., 1991).

10b. Mafic volcanic rocks in the Lake Mead area erupted prior to 9 Ma (open triangles) are similar to lavas of the Western Great Basin province (solid circles) produced by melting LM (Fitton et al., 1991).

11. Summary of mantle evolution and magmatism in the Lake Mead area. Sections are diagrammatic and are roughly drawn in a north-south direction. Mantle currents and crustal extension are in an east-west direction. LMFS-Lake Mead Fault system, NCREC-northern Colorado River extensional corridor.

a. Crustal extension was initiated about 16 Ma in the Lake Mead-Gold Butte area by either active extension (Fitton et al., 1991) or the opening of a slab window (Bradshaw, 1992). Mafic magmas are generated in LM and locally rise to the surface without being significantly contaminated (e.g., Las Vegas Range, alkali basalt in River Mountains). A large volume of mafic magma is stalled in the crust at "ductile barriers" (Smith et al., 1990; Bradshaw, 1992) and commingles with crustal magma to form calc-intermediate volcanoes and plutons.

b. Upper crustal extension occurred in the NCREC between 12 and 9 Ma but was not accompanied by significant magmatism. During extension in the NCREC, LM may have

been thinned and replaced by asthenosphere progressively to the west. During thinning and replacement of the LM in the NCREC, the LM in the anmagmatic zone remained intact. Contrasting behavior to the north and south of this boundary produced the mantle domain boundary. The domain to the north is characterized by LM ($\epsilon \text{Nd} = -3$ to -9 ; $^{87}\text{Sr}/^{86}\text{Sr} = 0.706-0.707$). To the south mafic lavas have an OIB-mantle signature and appear to have only a minor LM component in their source ($\epsilon \text{Nd} = 0$ to $+4$; $^{87}\text{Sr}/^{86}\text{Sr} = 0.703-0.705$).

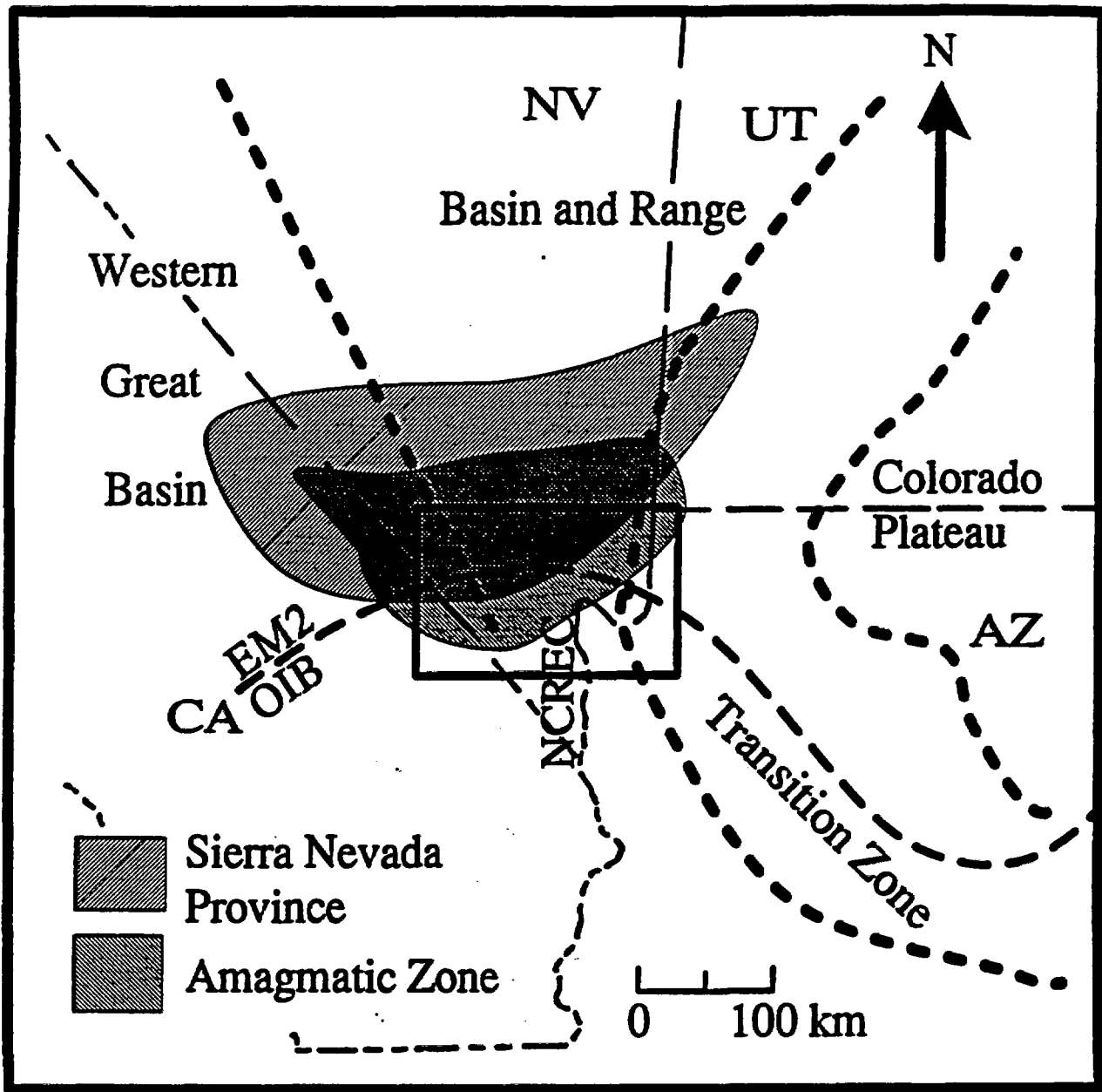


Figure 1.

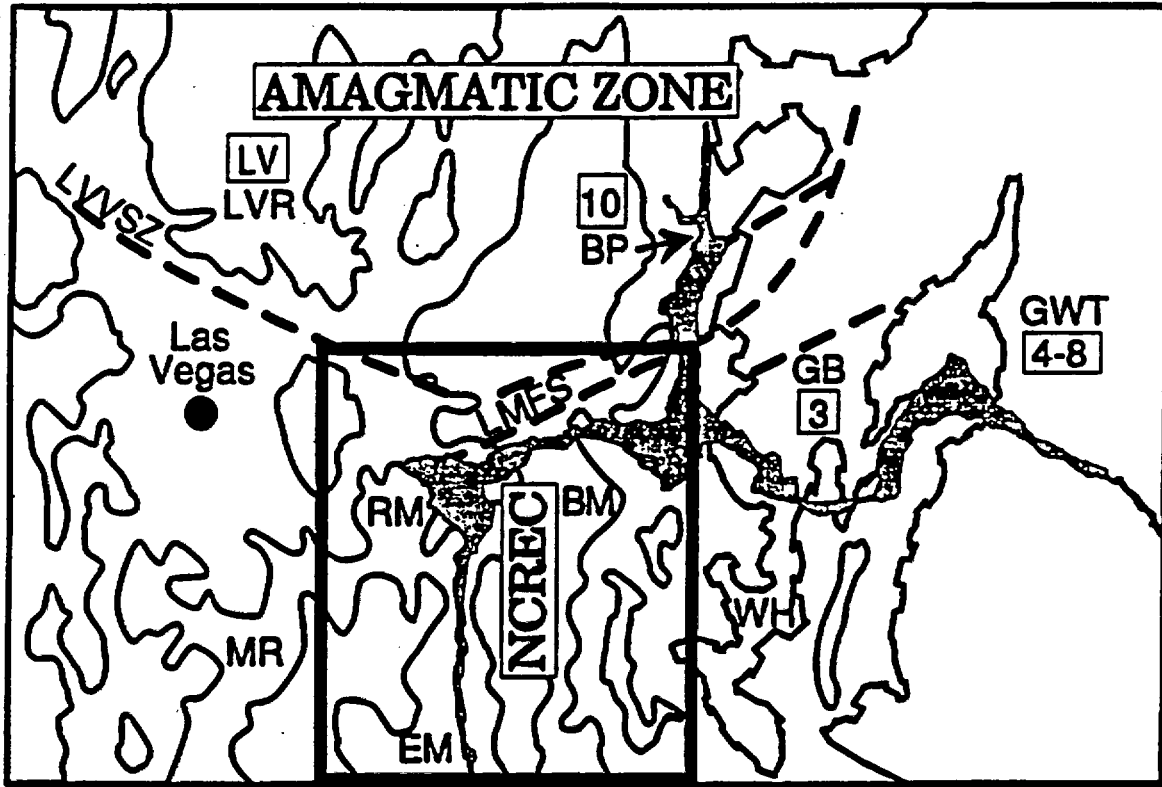


Figure 2a.

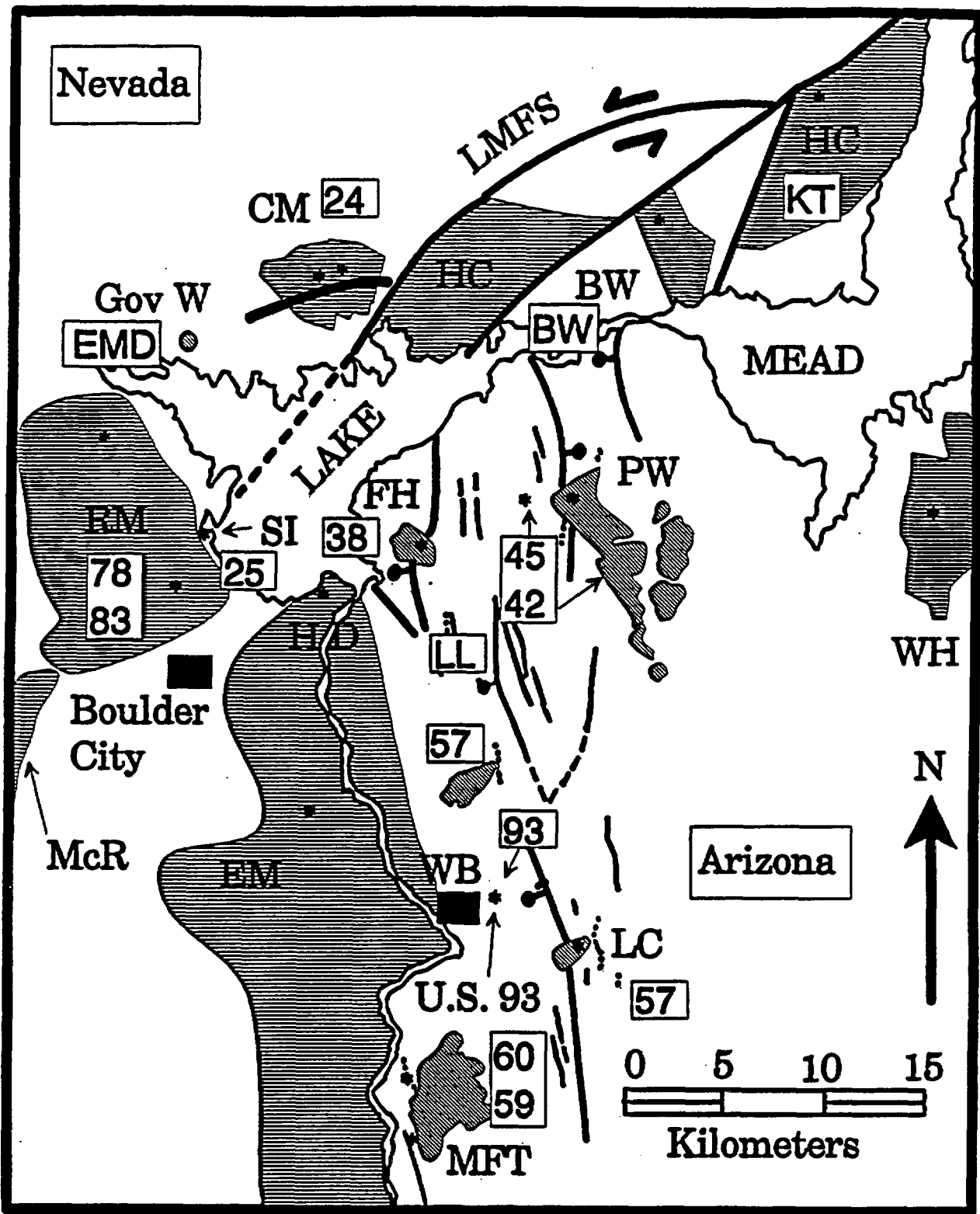


Figure 2b.

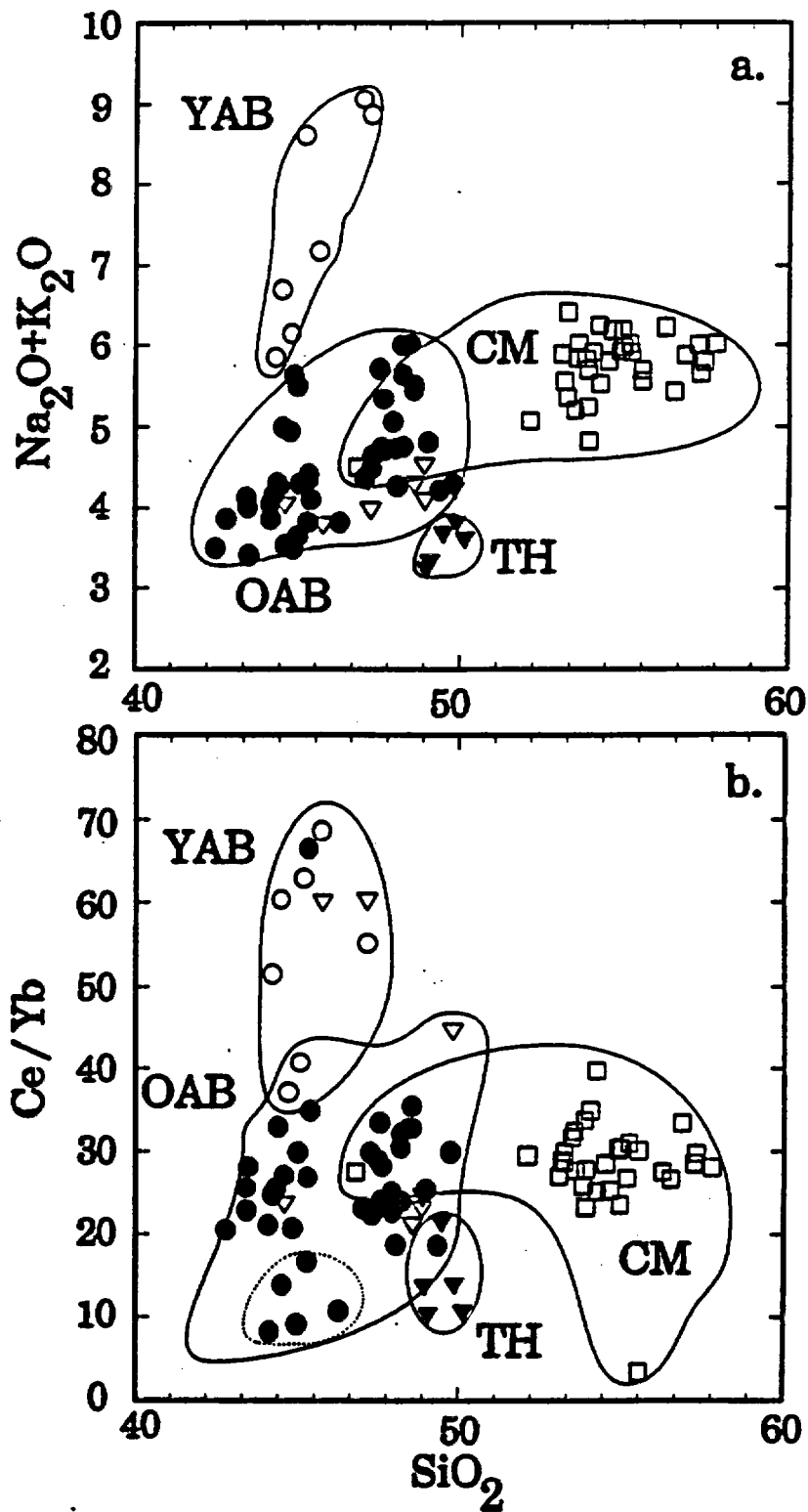


Figure 3.

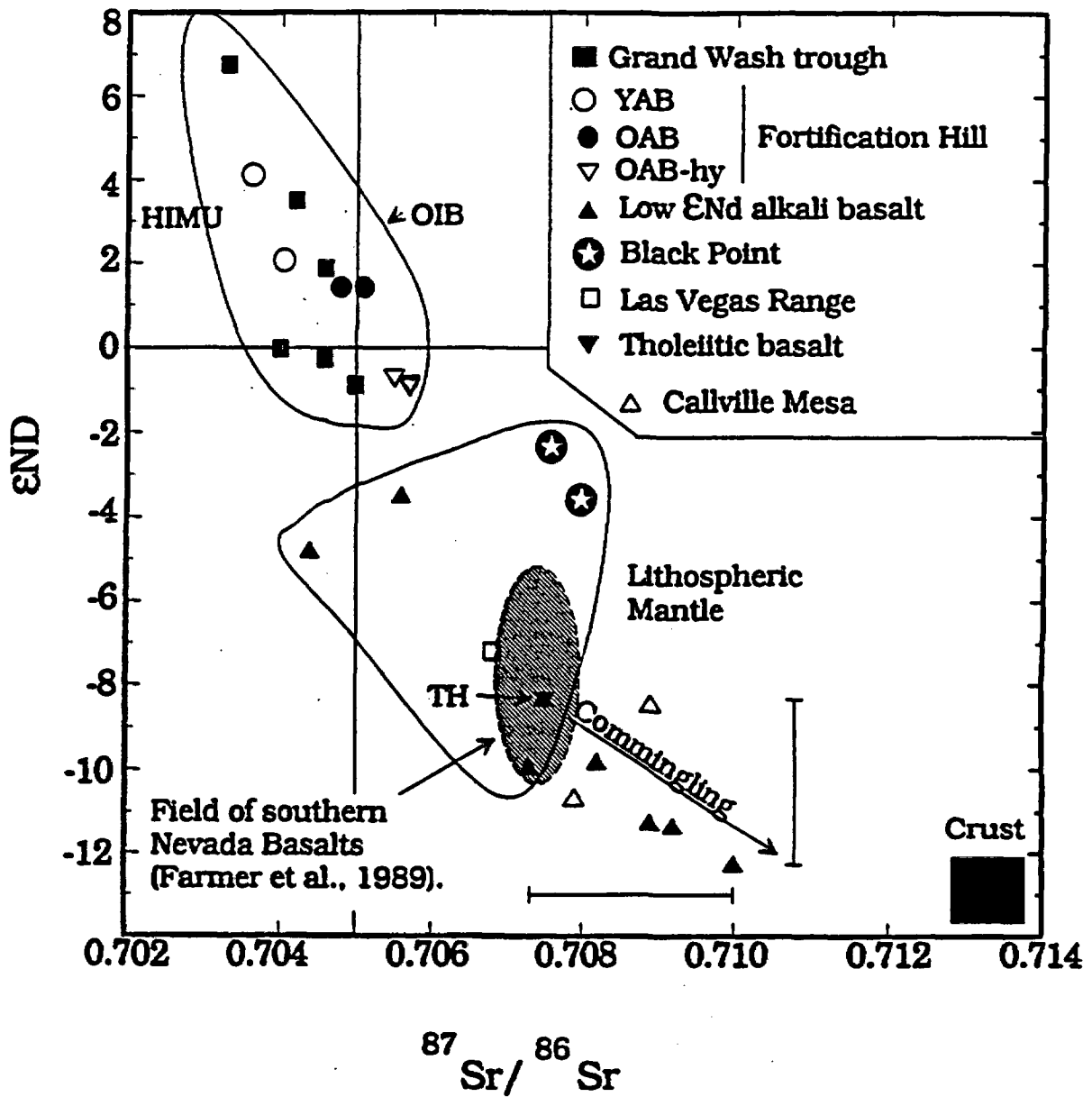


Figure 4.

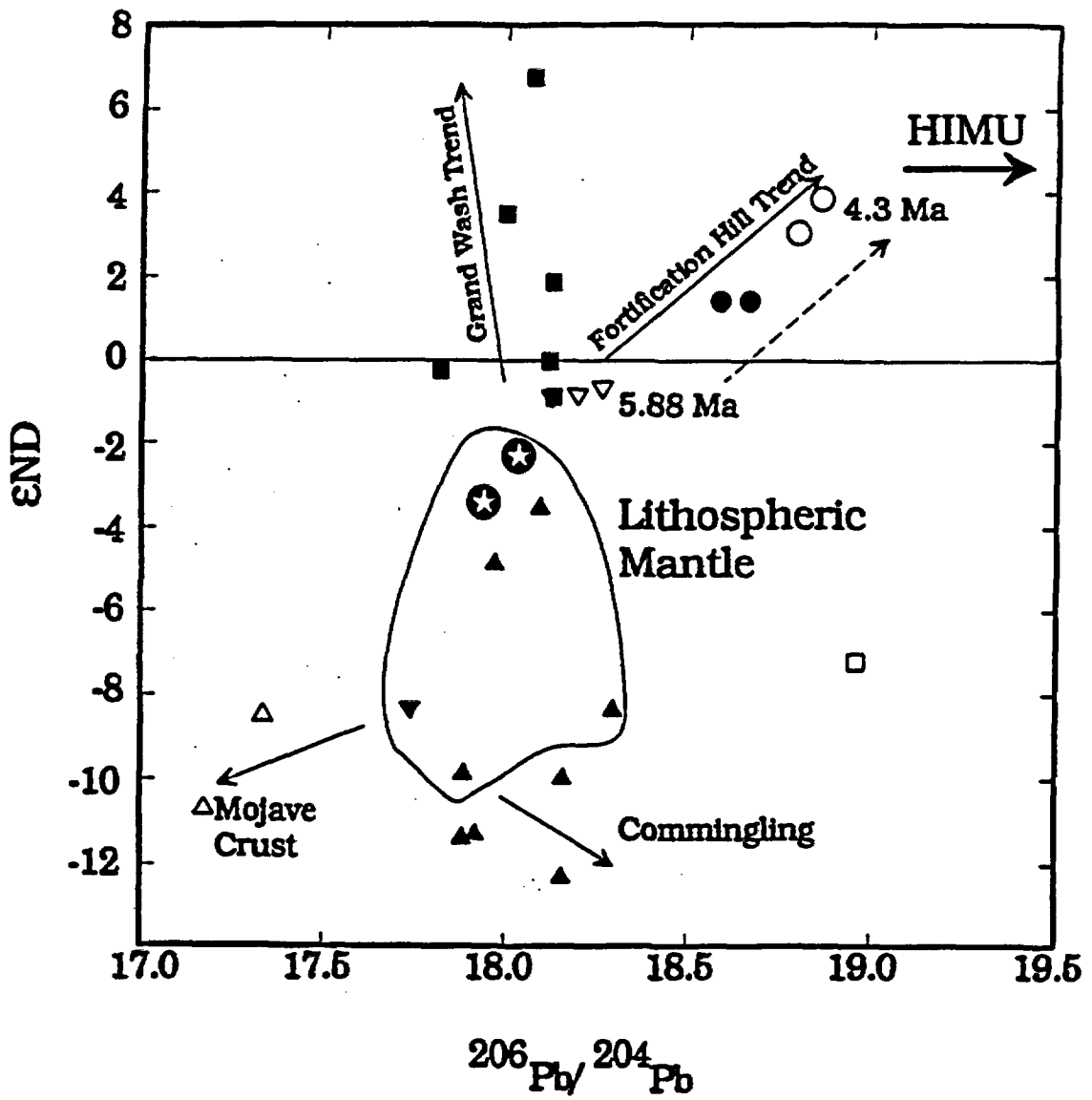


Figure 5.

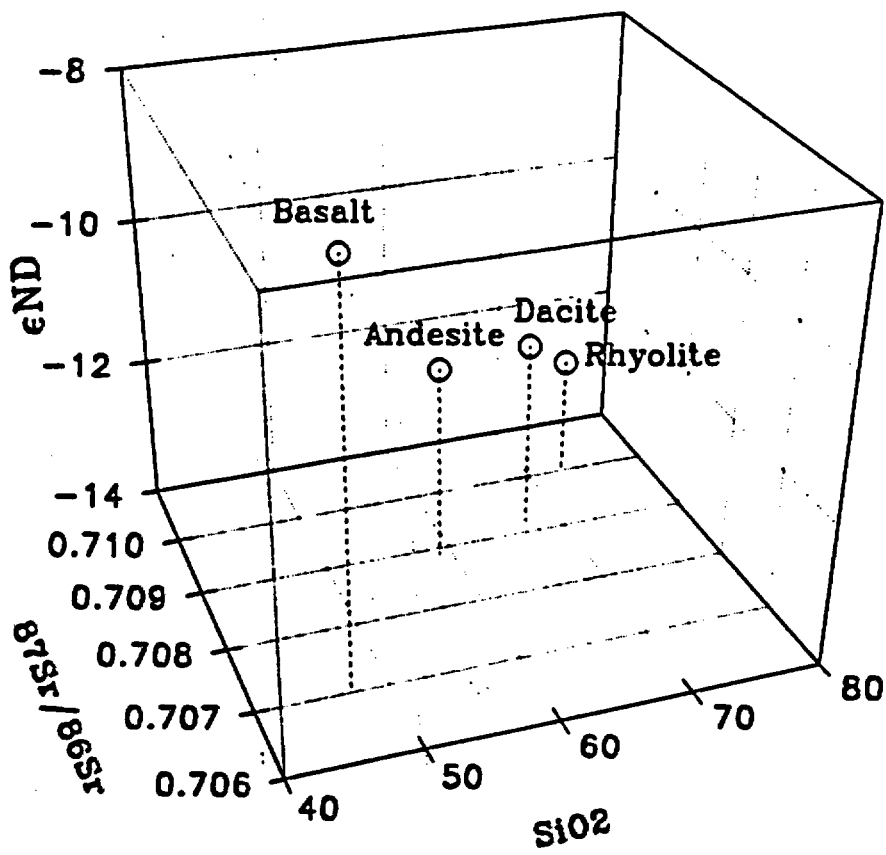
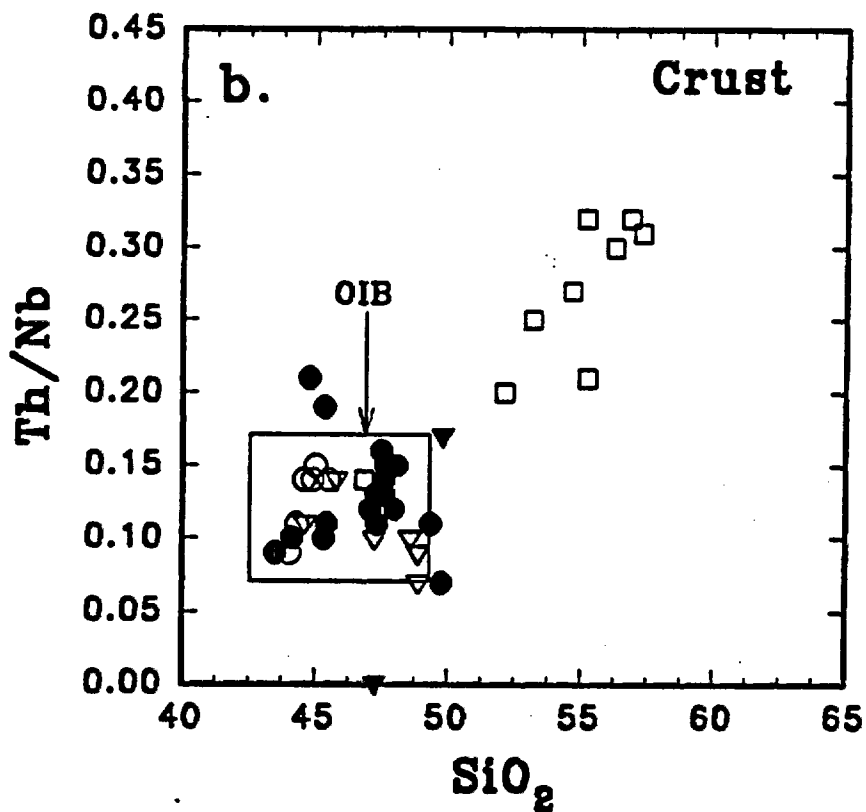
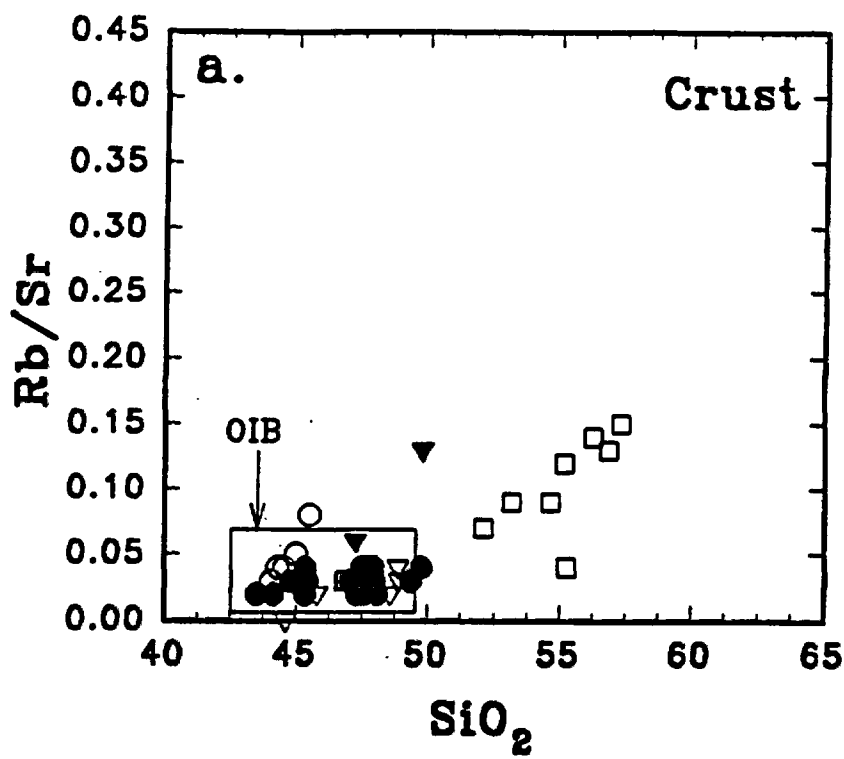


Figure 6.



Figures 7a and 7b.

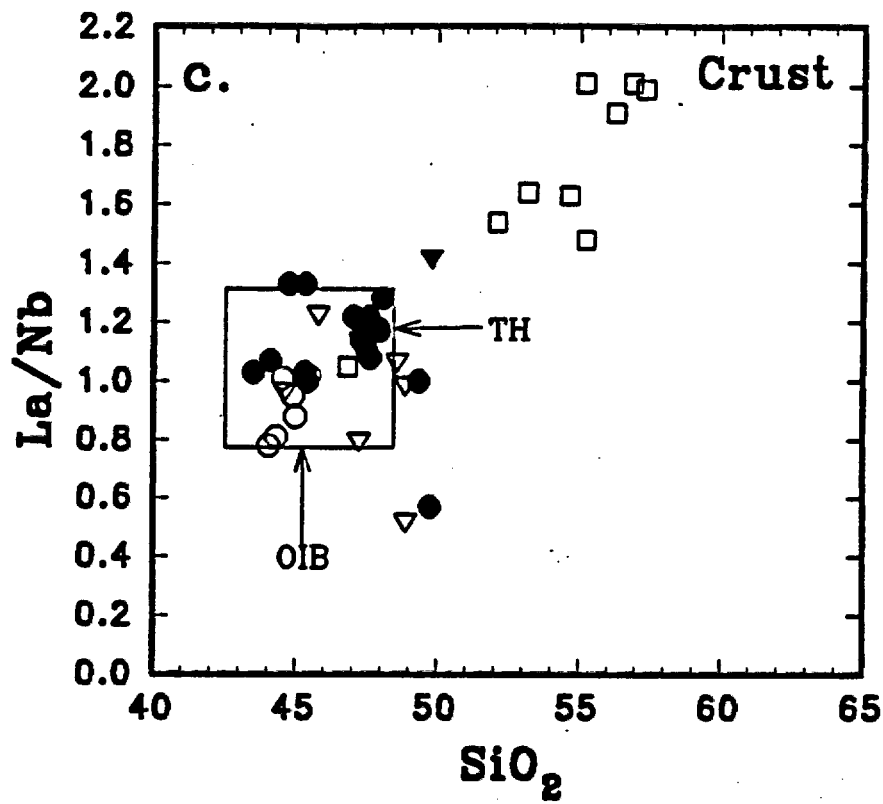


Figure 7c.

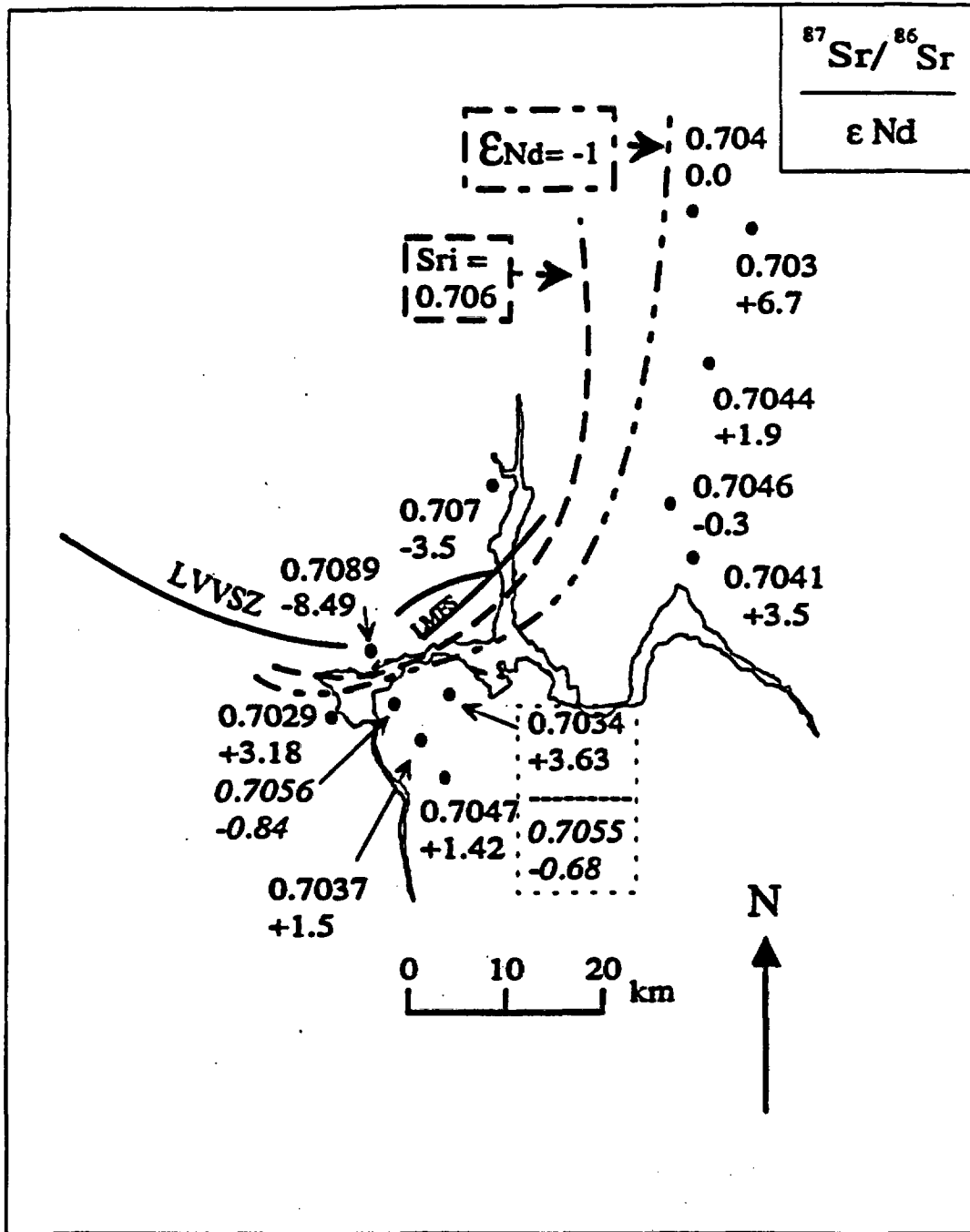


Figure 8.

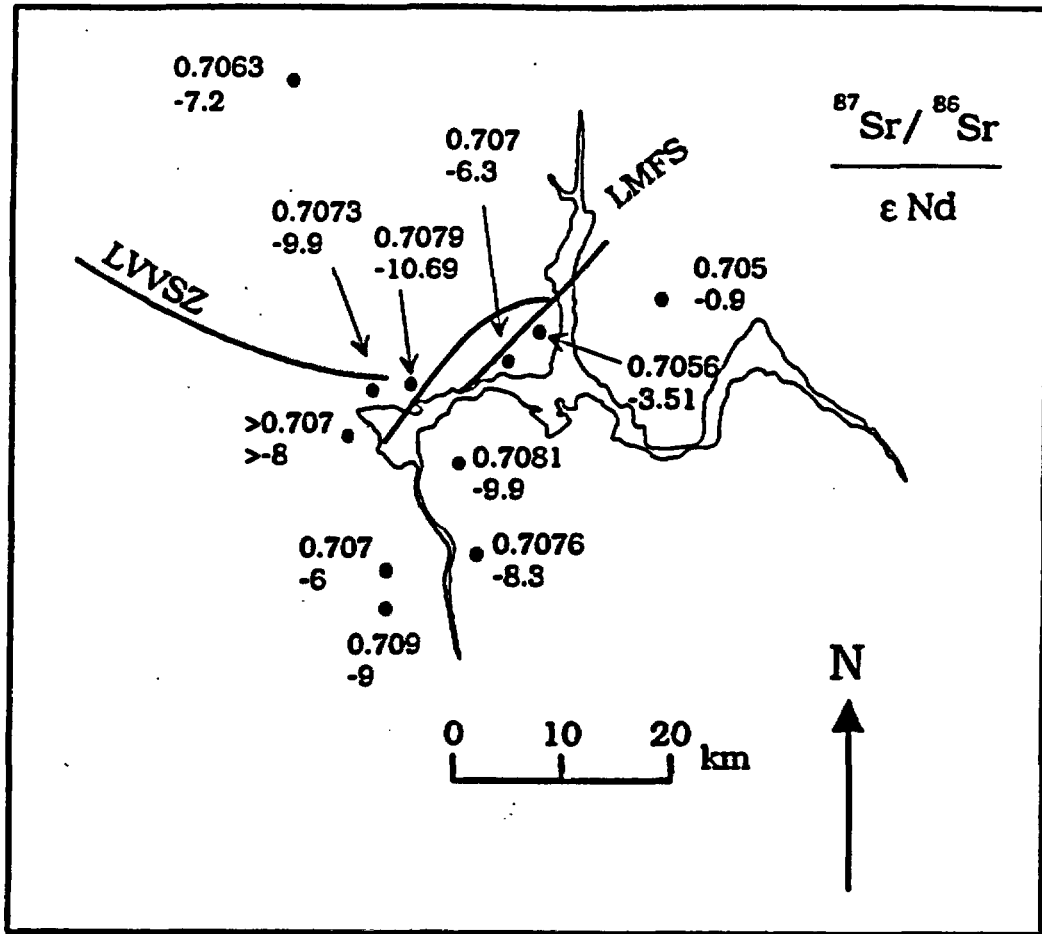


Figure 9.

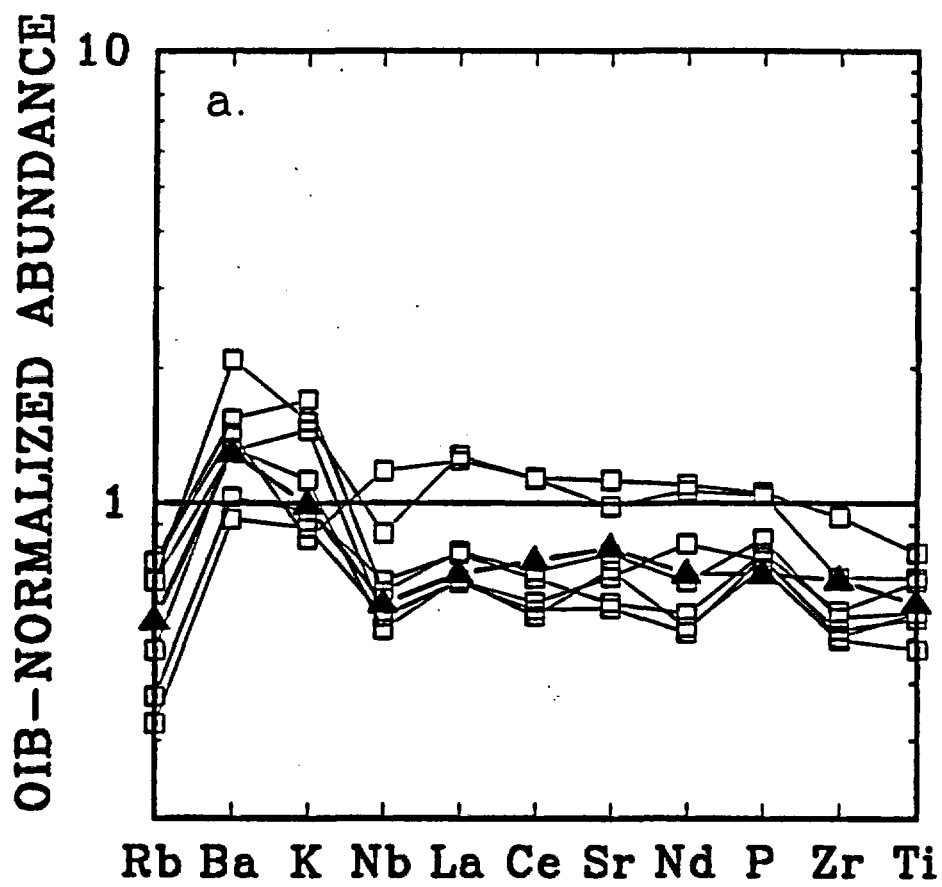


Figure 10a.

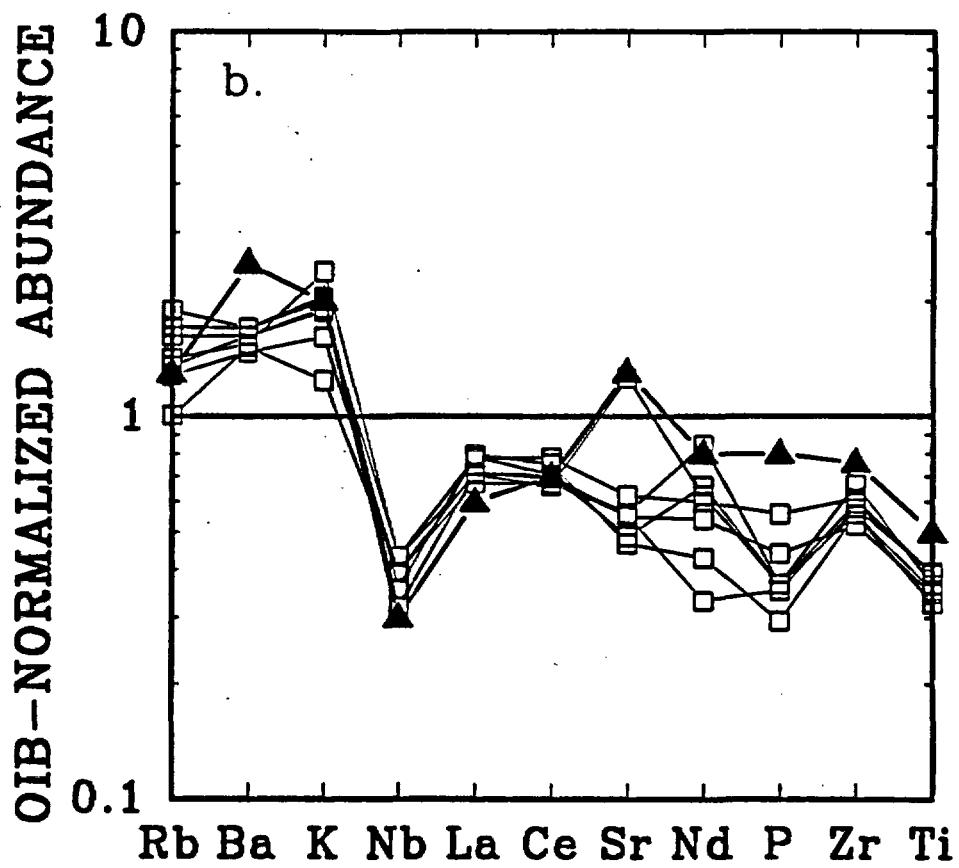


Figure 10b.

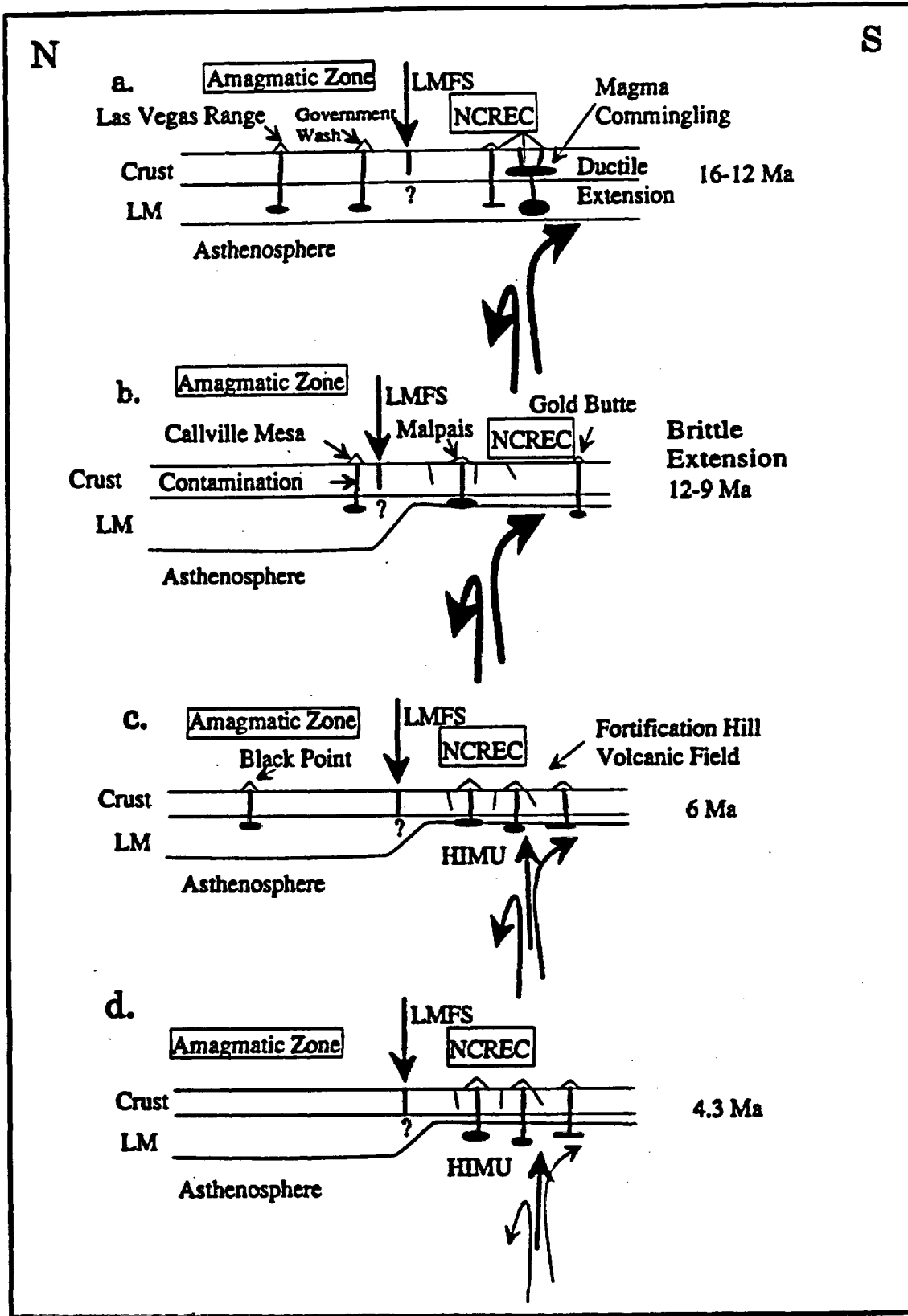


Figure 11.

TABLE 1. Selected Isotopic and Geochemical Data From the Volcanic Rocks in the Lake Mead Area.

Sample	Fortification Hill Volcanic Field												
	U.S. 93			Petroglyph Wash			Malpais Flattop			Fortificatio			
	YAB	YAB	YAB	YAB	YAB	YAB	YAB	YAB	TH	TH	TH	TH	TH
93-96	93-94	93-93	45-124	42-76	25-2	25-1	60-5	60-3	60-06	60-04	59-103	84-60	
SiO ₂	44.05	47.01	44.31	45.50	45.00	44.90	44.57	47.64	46.99	47.87	47.28	49.81	48.87
Al ₂ O ₃	15.52	16.77	15.87	16.89	16.79	16.53	16.34	16.31	0.00	14.67	14.95	15.75	15.25
FeO	10.46	10.57	9.80	10.04	10.88	11.14	10.44	11.07	13.19	13.34	12.38	10.05	10.11
CaO	9.07	7.31	8.34	8.53	8.78	7.68	8.77	7.24	8.38	9.29	8.90	7.48	9.52
MgO	5.88	4.12	3.26	5.94	6.21	5.73	5.52	7.91	8.75	6.95	6.82	8.04	7.15
Na ₂ O	3.08	4.85	3.89	4.78	4.94	4.73	4.15	3.16	2.72	2.80	2.92	3.10	3.19
K ₂ O	2.80	4.18	2.85	2.20	3.70	1.04	1.94	1.02	0.81	1.21	1.07	1.08	1.23
TiO ₂	3.02	2.82	2.77	2.52	2.54	2.40	2.46	1.40	1.18	1.53	1.40	1.46	1.53
MnO	0.15	0.15	0.14	0.19	0.18	0.16	0.19	0.17	0.19	0.20	0.19	0.23	0.17
P ₂ O ₅	0.78	0.87	0.82	0.77	0.88	0.72	0.68	0.16	0.22	0.25	0.24	0.25	0.37
LOI	6.48	2.53	9.43	1.12	0.60	2.93	4.28	0.92	1.44	0.59	0.77	1.33	
Total	101.40	101.30	101.55	98.48	100.65	98.06	99.50	97.07	98.34	98.76	96.98	98.58	97.41

Trace and Rare-Earth Elements in ppm (instrumental neutron activation analysis [INAA], isotope dilution [ID], atomic absorption [AA], x-ray fluorescence spectrometry [XRF]).

Cr(INAA)	103	99	76		113	139	151	254	337	227	242	269	221
Co(INAA)	25	23	23	28	30	29	28	40	52	42	41	43	24
Sc(INAA)	15.2	13.1	12.7	17.4	18.6	18.0	18.9	36.4	25.6	33.0	30.0	38.8	28.3
V (INAA)		153	142	192	216	186	179	226	214	247	221		
Hf(INAA)	7.16	7.80	7.33	6.98	7.22	6.45	6.73	3.93	2.71	3.21	3.57	7.14	2.94
Tb(INAA)	6.08	7.38	7.28	12.05	12.40	8.51	8.50	1.90	1.90	2.45		1.82	2.49
Ta(INAA)	4.81	5.48	5.01	5.68	0.00	4.02	3.50					0.70	1.49
La(INAA)	53.1	58.9	55.8	85.5	75.1	59.9	60.6	15.6	13.2	15.5	14.9	15.6	27.8
Ce(INAA)	107.0	124.0	118.0	140.9	151.0	116.3	116.2	33.2	34.8	29.9	35.7	32.4	39.7
Sm(INAA)	8.5	8.4	7.9	8.9	8.6	8.8	9.0	4.4	3.6	4.0	3.9	4.2	4.6
Eu(INAA)	2.3	2.4	2.4	2.4	2.3	2.4	2.4	1.4	1.3	1.3	1.1	0.0	1.6
Yb(INAA)	2.1	2.3	2.0	2.1	2.4	2.8	3.2	3.2	2.5	2.8	2.6	1.5	1.7
Lu(INAA)	0.3	0.3	0.3	0.4	0.2	0.3		0.4	0.3	0.4	0.3	0.5	0.3
Sr(AA)	1020		1400	820	874	870	1000				274	280	485
Rb(AA)	34		52	64	42	22	36				16	36	18
Ba(AA)	880		704	880	0	744	792				280	264	600
Ni(AA)	66		46	70	68	64	70				84	118	80
Nb(XRF)	68		69	84	85	63	60				13	11	28
Zr(XRF)	285		300		300	260	250				105		124
Sr(ID)					873.59	999.69					297.25		
Rb(ID)					43.4	20.24					16.69		
Nd(ID)					49.48	46.29					16.72		

Selected Normative Minerals

Nepheline	6	7	7	12	21	7	9	0	0	0	0	0	0
Hypersthene	0	0	0	0	0	0	0	10	8	16	6	19	4

Isotopic analysis by Mass Spectrometry

¹⁴³ Nd/ ¹⁴⁴ Nd	0.512824	0.512801	0.512211
Epsilon Nd	3.63	3.18	-8.33
(⁸⁷ Sr/ ⁸⁶ Sr) _i	0.70347	0.70433	0.70758
²⁰⁶ Pb/ ²⁰⁴ Pb	18.741	18.718	17.742
²⁰⁷ Pb/ ²⁰⁴ Pb	15.523	15.564	15.531
²⁰⁸ Pb/ ²⁰⁴ Pb	38.476	38.639	38.830

Sample	n Hill				Lava Cascade								
	OAB-by 84-59	OAB-by 38-15	OAB-by 38-138	OAB-by 38-13	OAB-by 57-101	OAB 57-132	OAB 57-113	OAB 57-112	OAB 57-111	OAB 57-109	OAB 57-108	OAB 57-107	OAB 57-106
SiO2	48.58	44.62	48.89	45.79	47.24	45.43	44.15	44.28	44.41	42.84	45.06	45.35	44.46
Al2O3	15.80	14.29	16.73	14.50	15.18	15.67	15.22	15.20	15.81	15.09	16.25	16.71	16.64
FeO	10.40	11.93	10.44	12.80	12.07	13.96	13.38	13.78	13.42	12.90	12.68	13.81	13.01
CaO	10.30	7.92	10.87	8.38	10.12	10.87	10.69	10.54	10.89	10.96	10.92	11.13	10.77
MgO	6.41	8.55	5.47	8.78	8.16	8.59	8.06	8.33	6.79	7.17	5.57	5.54	5.52
Na2O	3.12	2.81	3.30	2.86	2.87	2.98	2.88	3.01	3.12	2.74	3.20	3.15	3.08
K2O	1.09	1.10	0.80	0.84	1.15	1.20	1.10	1.10	1.10	1.00	1.00	1.20	1.10
TiO2	1.60	1.29	1.51	1.41	1.89	1.81	1.76	1.78	1.90	1.73	1.99	2.07	1.95
MnO	0.17	0.15	0.16	0.16	0.23	0.19	0.18	0.19	0.18	0.17	0.18	0.19	0.18
P2O5	0.44	0.28	0.49	0.28	0.46	0.53	0.52	0.53	0.52	0.49	0.54	0.53	0.53
LOI		3.45	1.42	1.48	1.38	0.65	0.52	0.20	0.05	1.84	0.60	0.59	1.06
Total	97.93	96.45	100.08	97.34	100.75	101.88	98.46	98.94	98.19	96.93	97.99	100.27	98.30

Cr(INAA)	186	322	162	361	257	296	268	301	187	258	96	80	81
Co(INAA)	24	44		53	44	44	43	46	41	42	36	35	34
Sc(INAA)	30.8	23.1	27.4	26.5	31.9	29.7	30.2	30.0	31.8	30.8	28.9	0.0	27.4
V (INAA)		209	234	213		244	229	230	282	234	239	245	232
Hf(INAA)	2.87	2.56	3.46	3.38	5.56	3.50	3.26	3.26	3.96	3.69	3.60	4.51	2.88
Th(INAA)	2.71	2.73	4.19	2.87	2.95	3.31	3.15	3.13	3.64	3.34	3.91	3.66	3.98
Ta(INAA)	1.42	1.80	1.65	1.69	1.58	1.17	1.66	1.54	1.73	1.69	2.39	2.07	1.97
La(INAA)	30.0	23.3	29.0	24.6	24.9	29.0	32.1	32.2	32.9	30.2	34.2	37.2	36.5
Ce(INAA)	40.5	45.7	50.3	52.4	43.5	51.6	59.2	54.7	64.6	56.2	64.9	69.7	67.3
Sm(INAA)	5.4	4.5	5.3	4.8	4.7	5.1	5.3	5.5	5.6	5.5	5.8	6.0	5.9
Eu(INAA)	1.6	1.4	1.5	1.6	1.6	1.5	1.5	1.5	1.6	1.5	1.7	1.6	1.6
Yb(INAA)	1.9	1.9	2.1	2.2	0.7	1.5	2.8	2.2	2.5	2.7	2.2	2.6	2.0
Lu(INAA)	0.4		0.4		0.2	0.4	0.3	0.2	0.2	0.3	0.3	0.4	0.4
Sr(AA)	490	380	470	455	600	410	451					464	
Rb(AA)	12		14	10	12	12	10					11	
Ba(AA)	590	400	680	475	456	432	480					536	
Ni(AA)	46	230		166	110	134	126					42	
Nb(XRF)	28	24	56	28	31	29	30					36	
Zr(XRF)	130	108	141	116	145	140	140					160	
Sr(ID)				434.24			451.23					463.93	
Rb(ID)				14.31			9.68					11.09	
Nd(ID)							24.77					27.26	

Nepheline	0	0	0	0	0	6	6	6	6	5	4	5	5
Hyperssthene	4	1	2	4	1	0	0	0	0	0	0	0	0

143Nd/144Nd				0.512595			0.512711					0.512711	
Epsilon Nd				-0.84			2.2					1.42	
(87Sr/86Sr)i				0.70565			0.70479					0.70479	
206Pb/204Pb				18.194			18.670					18.991	
207Pb/204Pb				15.523			15.570					15.555	
208Pb/204Pb				38.309			38.612					38.535	

Sample	Petroglyph Wash													
	OAB	OAB	OAB	OAB	OAB	OAB	OAB	OAB	OAB	OAB	OAB	OAB	OAB	OAB
	57-105	57-10	57-09	42-84	42-83	42-82	42-81	42-78	42-77	42-75	42-74	42-73	42-128	42-127
SiO2	43.34	43.48	43.47	47.66	48.24	47.52	48.58	48.22	48.46	44.90	45.02	44.79	47.95	45.36
Al2O3	15.10	15.24	15.15	16.70	16.76	16.61	17.00	16.24	16.69	17.57	17.59	17.42	16.41	14.34
FeO	13.10	12.70	12.53	11.45	10.50	10.56	10.58	11.70	10.54	11.68	12.28	12.23	11.33	11.56
CaO	10.57	10.46	11.06	10.07	9.92	9.79	9.73	9.72	9.73	10.68	10.76	10.86	10.02	9.34
MgO	8.71	9.14	8.64	6.10	5.38	5.35	5.00	5.93	5.37	6.28	6.53	6.36	4.78	9.41
Na2O	2.39	2.76	2.84	3.57	3.56	3.57	3.61	3.49	3.56	3.42	3.32	3.11	3.39	2.90
K2O	1.00	1.16	1.20	1.81	2.12	2.11	1.93	2.58	2.54	2.27	2.25	1.89	1.60	1.40
TiO2	1.71	1.75	1.76	1.71	1.72	1.76	1.79	1.89	1.69	1.97	2.01	2.11	1.61	1.28
MnO	0.18	0.18	0.18	0.17	0.16	0.16	0.16	0.17	0.15	0.18	0.18	0.19	0.16	0.16
P2O5	0.49	0.30	0.33	0.51	0.58	0.57	0.57	0.57	0.60	0.75	0.76	0.71	0.55	0.53
LOI	2.58	0.81	0.81	0.94	1.72	1.42	1.47	0.46	1.76	1.12	0.46	1.38	0.78	1.16
Total	99.37	98.06	98.07	100.75	100.75	99.50	100.50	101.05	101.15	100.95	101.30	101.20	98.58	97.44

Cr(INAA)	325	308	313	138	60	50	48	62	50	49	49	47	63	454
Co(INAA)	46	45	47	33	33	32	33	34	33	35	37	36	31	44
Sc(INAA)	30.1	31.3	31.2	26.8	26.2	25.0	26.7	26.9	27.0	26.6	26.9	26.6	24.9	27.8
V (INAA)	258	263	297	238	232	281	233	251	251	259	278	308	197	198
Hf(INAA)	3.55	4.02	3.65	3.61	4.44	4.00	4.33	4.48	4.85	4.83	5.11	4.73	3.27	3.10
Tb(INAA)	2.65	3.52	3.80	4.52	5.16	5.28	5.72	5.54	5.98	9.96	10.20	9.62	5.10	6.77
Ta(INAA)	1.68	1.53	1.57	1.76	1.95	1.87	1.92	2.43	2.01	2.78	2.74	3.13	1.97	2.05
La(INAA)	28.9	23.3	27.2	32.4	37.2	37.7	37.4	38.1	39.4	65.6	65.8	61.4	40.0	48.1
Ce(INAA)	52.9	52.7	55.6	61.7	74.9	72.3	78.7	77.1	82.0	124.0	124.0	116.0	78.5	83.9
Sm(INAA)	4.9	4.6	5.1	5.3	6.1	6.2	6.2	6.3	6.5	7.7	7.7	7.1	6.3	6.0
Eu(INAA)	1.4	1.4	1.6	1.4	1.7	1.6	1.9	1.7	1.8	1.9	2.0	1.8	1.6	1.4
Yb(INAA)	1.9	2.3	2.2	2.2	2.5	2.5	2.2	2.4	2.5	2.7	2.7	2.9	3.1	1.3
Lu(INAA)	0.3	0.3	0.2	0.3	0.4	0.4	0.3	0.3	0.4	0.4	0.4	0.4	0.2	0.3
Sr(AA)	490			530		598						760	570	550
Rb(AA)	10			20		22						20	24	20
Ba(AA)	424			680		800						1080	720	736
Ni(AA)	138			54		30						24	34	200
Nb(XRF)	28			30		34						46	34	36
Zr(XRF)	130			145		155						190	155	140
Sr(ID)						597.57								
Rb(ID)						22.13								
Nd(ID)						32.25								

Nepheline	3	3	8	3	5	5	3	6	6	11	10	8	2	4
Hypersthene	0	0	0	0	0	0	0	0	0	0	0	0	0	0

143Nd/144Nd	0.512603
Epsilon Nd	-0.69
(87Sr/86Sr)i	0.70555
206Pb/204Pb	18.263
207Pb/204Pb	15.548
208Pb/204Pb	38.397

Sample	Fortification Hill					Black Point			Las Vegas Range	Callville Mesa			
	OAB	OAB	OAB	OAB	OAB	OAB	OAB	OAB	LV-104	CM	CM	CM	CM
	38-144	38-143	38-14	38-136	38-135	38-133	10-121	10-120		24-91	24-70	24-69	24-68
SiO2	47.34	47.97	47.62	48.25	47.60	47.29	44.38	46.32	42.49	54.05	57.32	53.61	55.18
Al2O3	15.87	16.05	15.28	15.96	15.70	15.58	14.35	15.30	10.76	16.51	15.87	15.91	15.84
FeO	11.66	11.87	11.73	12.26	12.57	12.54	13.82	13.39	12.79	10.21	8.80	8.89	8.49
CaO	10.24	10.16	8.94	10.27	9.98	10.07	6.55	7.93	9.78	6.47	6.74	7.15	6.64
MgO	5.84	5.32	7.78	5.82	5.84	6.03	8.76	8.92	13.45	3.22	4.15	4.99	4.33
Na2O	3.18	3.26	3.39	3.34	3.30	3.14	4.17	2.97	2.39	4.21	3.51	3.36	3.52
K2O	1.40	1.40	1.29	1.40	1.40	1.30	0.70	0.90	1.00	2.01	2.48	2.33	2.54
TiO2	1.41	1.46	1.39	1.53	1.61	1.63	1.10	1.16	1.69	1.81	1.09	1.06	1.07
MnO	0.16	0.17	0.17	0.18	0.18	0.17	0.19	0.19	0.16	0.14	0.13	0.11	0.10
P2O5	0.48	0.49	0.27	0.48	0.49	0.49	0.30	0.34	0.67	0.50	0.25	0.31	0.30
LOI	1.12	0.49	1.54	0.21	0.71	0.82	3.14	4.11	1.79	0.17	0.44	2.83	2.17
Total	98.70	98.64	99.51	99.70	99.38	99.06	97.66	101.53	96.97	99.30	100.90	100.65	100.25
Cr(INAA)	173	70	270	117	112	176	271	326	816	23	115	156	134
Co(INAA)	34	33	40	35	37	35	56	54	58	25	25	27	28
Sc(INAA)	27.3	26.3	24.5	28.8	28.7	27.8	24.5	24.7	22.2	15.8	17.3	17.5	18.2
V(INAA)	205	236	227	244	239	255	194	177	234	182	143	151	153
Hf(INAA)	2.72	4.18	3.11	3.45	3.55	3.60	1.70	2.83	5.22	4.67	4.77	3.91	4.29
Tb(INAA)	2.86	3.23	2.75	3.34	3.72	3.33		1.16	5.20	7.53	5.90	4.96	5.46
Ta(INAA)	1.60	1.31	1.18	1.69	1.22	1.31	0.95		0.71	1.67	1.12	1.03	0.96
La(INAA)	29.5	32.7	23.8	33.1	31.7	31.2	12.6	11.8	46.0	42.9	37.9	31.8	34.2
Ce(INAA)	54.2	57.5	52.3	56.0	58.6	62.2	24.3	24.7	92.0	87.5	72.4	65.1	72.1
Sm(INAA)	5.1	5.5	4.8	5.6	5.4	5.3	3.1	3.1	10.2	6.2	5.5	4.9	5.2
Eu(INAA)	1.4	1.5	1.5	1.6	1.5	1.4	0.9	1.1	2.3	1.6	1.2	1.2	1.4
Yb(INAA)	2.4	2.5	2.2	2.3	1.8	2.1	1.8	2.3	1.7	2.2	2.4	2.2	2.6
Lu(INAA)	0.2	0.4	0.3	0.3	0.3	0.4	0.3	0.2	0.1	0.3	0.3	0.3	0.3
Sr(AA)	500	550			490	495	246	260			376		424
Rb(AA)	12	14			12	14	9	13			56		51
Ba(AA)	570	690			640	600	176	190			880		880
Ni(AA)	60	24	118		40	42	206				52		60
Nb(XRF)	26	28	22		26	26	13	10			19		17
Zr(XRF)	122	138	116		126	126	77	90			155		145
Sr(ID)		491.11					246.12	306.35	795.58				423.51
Rb(ID)		14.86					8.98	14.45	48.27				50.94
Nd(ID)		25.45						11.09	55.76				25.97
Nepheline	2	3.31	2	2	2	1	7.34	1.3	5	0	0	0	0
Hypersthene	0	0	0	0	0	0	0	0	0	12	14	16	14
143Nd/144Nd		0.512592					0.512456	0.512520	0.512269				0.512090
Epsilon Nd		-0.9					-3.55	-2.3	-7.2				-10.69
(87Sr/86Sr)i		0.70567					0.70793	0.70753	0.70632				0.70792
206Pb/204Pb		18.123					17.947	18.033	18.963				17.173
207Pb/204Pb		15.541					15.499	15.581	15.642				15.433
208Pb/204Pb		38.156					38.291	38.9	38.845				37.814

Sample	CM 24-66	CM 24-65	CM 24-64	CM 24-63	CM 24-62	CM 24-61	CM 24-60	CM 24-59	CM 24-58	CM 24-57	CM 24-56	CM 24-55
SiO2	53.84	56.53	53.50	54.52	56.27	55.73	55.56	57.80	57.25	55.00	54.96	54.26
Al2O3	16.16	15.99	16.13	16.22	15.88	15.84	15.91	15.78	15.97	16.30	16.29	15.59
FeO	8.55	9.17	9.55	8.68	8.88	9.09	8.66	8.47	8.72	9.42	9.32	8.99
CaO	7.13	6.53	7.17	7.23	6.77	6.88	6.91	6.28	6.46	7.34	7.31	6.75
MgO	4.64	4.44	4.92	4.43	4.33	4.24	4.40	4.07	4.31	4.74	4.28	5.06
Na2O	3.56	3.57	3.58	3.48	3.62	3.54	3.38	3.57	3.56	3.57	3.68	3.55
K2O	1.99	2.30	1.80	1.72	2.24	2.74	2.35	2.49	2.49	2.46	2.55	2.03
TiO2	1.11	1.08	1.20	1.12	1.06	1.13	1.06	1.02	1.04	1.19	1.25	1.05
MnO	0.11	0.13	0.14	0.12	0.12	0.12	0.11	0.12	0.12	0.14	0.14	0.12
P2O5	0.33	0.30	0.32	0.29	0.28	0.30	0.28	0.26	0.28	0.35	0.35	0.27
LOI	2.30	0.39	0.65	2.01	1.33	0.87	1.88	0.60	0.25	0.16	0.31	3.11
Total	99.81	100.55	99.05	99.92	100.90	100.60	100.60	100.55	100.55	100.75	100.55	100.85

Cr(INAA)	160	112	135	121	124	113	115	116	113	107	107	150
Co(INAA)	29	25	30	27	25	25	24	25	24	28	28	27
Sc(INAA)	19.5	17.2	20.5	19.0	17.6	17.6	17.3	17.0	16.4	20.9	21.9	16.8
V (INAA)	155	146	153	162	139	163	141	144	146	177	175	141
Hf(INAA)	4.60	4.43	4.46	4.79	4.51	4.18	4.21	4.67	4.31	4.50	5.32	3.85
Tb(INAA)	5.57	5.69	5.24	5.65	5.79	5.14	5.61	6.39	5.92	5.95	6.31	4.71
Ta(INAA)	1.12	1.32	1.16	1.10	0.88	0.87	0.96	1.13	1.07	1.30	1.78	1.11
La(INAA)	35.9	35.3	33.3	35.4	36.2	36.3	35.5	38.2	38.6	36.9	39.1	32.0
Ce(INAA)	74.8	69.9	68.4	73.9	71.2	64.0	7.5	75.4	71.0	74.4	77.7	63.5
Sm(INAA)	5.4	5.3	5.3	5.5	5.3	5.6	5.3	5.3	5.6	5.7	5.8	4.9
Eu(INAA)	1.4	1.4	1.4	1.6	1.4	1.2	1.3	1.3	1.3	1.5	1.6	1.2
Yb(INAA)	2.5	2.7	2.6	2.3	2.5	2.3	2.2	2.7	2.5	2.4	3.3	2.5
Lu(INAA)	0.3	0.3	0.4	0.3	0.3	0.3	0.3	0.3	0.4	0.4	0.3	0.3
Sr(AA)					416							
Rb(AA)					60							
Ba(AA)					880							
Ni(AA)					50							
Nb(XRF)					19							
Zr(XRF)					150							
Sr(ID)												
Rb(ID)												
Nd(ID)												

Nepheline	0	0	0	0	0	0	0	0	0	0	0	0
Hypersthene	15	16	17	15	15	14	14	14	15	16	14	17

143Nd/144Nd
Epsilon Nd
(87Sr/86Sr)_i
206Pb/204Pb
207Pb/204Pb
208Pb/204Pb

Sample	Gold Burn				Grand Wash Trough				River Mountains			
	CM 24-53	CM 24-50	CM 24-49	CM 24-100	3-6	4-13	5-14	6-39	7-33	8-62	78-218	78-222
SiO2	53.92	56.87	55.24	46.83	46.3	47.58	48.81	48.44	47.85	47.31	47.1	59
Al2O3	16.35	15.49	15.98	14.78	14.64	14.4	14.95	14.57	14.53	15.99	14.5	16.6
FeO	10.06	8.61	8.97	11.34	12.59	14.53	11.73	12.75	13.83	11.37	10.9	6.9
CaO	7.63	6.32	6.90	9.03	7.98	8.74	8.64	9.88	7.41	10.43	11.2	5.5
MgO	5.28	4.27	4.10	6.25	9.16	8.55	7.14	8.42	7.86	4.73	6.3	2.6
Na2O	3.40	3.48	3.55	3.45	3.16	3	3.22	3.1	4.32	3.49	2.8	3.9
K2O	1.46	2.37	2.33	1.19	1.59	1.55	1.57	1.92	2.42	1.72	1.8	0.9
TiO2	1.49	1.01	1.13	2.18	1.19	1.25	1.54	0.91	1.85	2.29	1.2	2.3
MnO	0.15	0.15	0.14	0.13	0.18	0.19	0.16	0.17	0.17	0.16	0.1	0.1
P2O5	0.29	0.20	0.25	0.45	0.27	0.26	0.43	0.29	0.59	0.18	1	0.6
LOI	0.75	0.28	0.40	2.57	1.06	0.19	1.09	0.01	0.01	1.63	2.3	1
Total	100.90	99.24	99.17	98.20	98.12	100.24	99.28	100.46	100.75	99.3	99.2	99.4
Cr(INAA)	130	106	145	312	253	326	256	459	189	223		
Co(INAA)	30	24	29	38	46.68	50.49	39.52	47.2	47	34.3		
Sc(INAA)	23.2	17.3	19.6	24.1	23.73	27	23.91	26.7	15.4	0.4	29.6	11.2
V(INAA)	189	127	171	226	216	242	215	208	182	255		
Hf(INAA)	3.97	4.20	3.86	4.45	3.63	3.14	3.24	3.59	6.42	3.84	8.1	7.3
Tb(INAA)	5.06	6.11	4.89	3.61	2.72		2.78	3.21	3.62	2.25	13.2	14.9
Ta(INAA)	1.42	0.97	0.97	1.68					3.16	1.35	1.5	1
La(INAA)	35.1	38.3	34.0	27.3	23.86	9.04	19.21	20.9	34.6	18.9	107.6	81.7
Ce(INAA)	70.1	77.3	67.6	59.8	46.11	21.87	44.26	44.8	71	39.1	242.4	167.9
Sm(INAA)	5.4	5.8	5.3	5.9							15.5	8.7
Eu(INAA)	1.4	1.0	1.4	1.7	1.45	0.95	1.33	1.4	1.96	1.31	3.9	2
Yb(INAA)	3.0	2.3	2.2	1.8	2.47	1.96	2.28	0.16	1.55	2.11	2.1	2.3
Lu(INAA)	0.4	0.4	0.3	0.3	0.35	0.3	0.24	0.22	0.18	0.37	0.4	0.4
Sr(AA)		360	970	520								
Rb(AA)		48	40	14								
Ba(AA)		840	840	440								
Ni(AA)		46	36	128								
Nb(XRF)		19	23	26								
Zr(XRF)		155	185	155								
Sr(ID)			970.19		421.14	321.83	378.36	419.48	723.94	447.64		959.65
Rb(ID)			40.1		14.88	7.47	8.06	12.45	22.94	10.04		83.62
Nd(ID)			29.96		22.47	14.35	17.89	20.52	29.65	16.21	98.57	54.9
Nepheline	0	0	0	2.71	5.22	4.34	1.27	6.76	11.38	6.99	3.72	0
Hypersthene	18	14	14	0	0	0	0	0	0	0	0	15.33
143Nd/144Nd			0.512203		0.512592	0.512295	0.512716	0.512636	0.512984	0.512817	0.512210	0.512060
Epsilon Nd			-8.49		-0.9	-0.27	1.87	-0.04	6.75	3.49	-8.34	-11.28
(87Sr/86Sr)i			0.70893		0.70502	0.7046	0.7044	0.70399	0.70332	0.70417	0.708954	0.7082
206Pb/204Pb			17.332		18.130	17.821	18.127	18.119	18.075	17.999	18.299	17.922
207Pb/204Pb			15.496		15.527	15.550	15.509	15.518	15.473	15.500	15.605	15.537
208Pb/204Pb			38.01		38.068	38.050	37.895	38.034	37.704	37.758	38.699	38.791

	Wilson Ridge		Government Wash	Hamblin-Cleopatra Volcano		Boulder Wash	
Sample	78-223	83-348	LL-88-41	EMD-209	KT82-15	KT82-183	BW-6
SiO ₂	67.2	72.9	54.1	51.9	56.43	55.89	50.2
Al ₂ O ₃	14.2	12.6	16.9	15.2	16.36	16.34	15.9
FeO	3.5	2.7	8.9	9.4	6.76	7.17	10.8
CaO	2.3	0.5	7.4	8.2	6.56	5.4	8.4
MgO	0.9	0.2	4.5	3.8	3.43	3.48	4.2
Na ₂ O	3.6	2.2	4.2	3.7	3.98	4.1	3.6
K ₂ O	0.4	0.2	1.5	1.8	1.31	1.39	2.7
TiO ₂	4.9	7.5	2.1	3.2	2.47	2.72	1.6
MnO	0.1		0.1	0.2	0.1	0.11	0.1
P ₂ O ₅	0.1		0.7	1.8	0.49	0.49	0.5
LOI	3	0.1	0.5	1.2	1.38	2.85	0.4
Total	100.2	98.9	100.9	100.4	99.27	99.94	98.4
Cr(INAA)					63	47	
Co(INAA)			20		20.65	22.76	
Sc(INAA)	3.8	1.5			14.06	14.11	23.4
V(INAA)			198		147	145	
Hi(INAA)	4.8	4.9	5.1		6.76	8.15	4.5
Tb(INAA)	17.6	31.2	12.4		10.46	13.53	5.1
Ta(INAA)	1.2	15.3	2.1		2.75	2.84	1.6
La(INAA)	52.4	55.6	123		65.23		50.2
Ce(INAA)	90.7	124.5	213		114.03	126.79	75.3
Sm(INAA)	4.2	3.7	10.9		7.75	8.29	
Eu(INAA)	1.2	1	2.6		1.89	1.99	2.1
Yb(INAA)	1.3	2.2	2.3		1.73	2.04	1.7
Lu(INAA)	0.2	0.3	0.3			0.26	0.4
Sr(AA)							
Rb(AA)							479
Ba(AA)							569
Ni(AA)							
Nb(XRF)							
Zr(XRF)							
Sr(ID)	467.99	79.76	1155.78	1299.65	432.85	588.44	692.48
Rb(ID)	129.26	198.08	42.05	75.97	45.83	47.52	46.3
Nd(ID)	28.2	22.84	76.018	74.18	45.08	45.27	42.57
Nepheline	0	0	0	0	0	0	3.17
Hypersthene	2.24	5.87	18.11	17.98	11.07	16.93	0
¹⁴³ Nd/ ¹⁴⁴ Nd	0.512055	0.512008	0.512133	0.512128	0.512390	0.512456	0.512316
Epsilon Nd	-11.57	-12.28	-9.86	-9.94	-4.84	-3.51	-6.23
(⁸⁷ Sr/ ⁸⁶ Sr) _i	0.709233	0.710015	0.70815	0.707337	0.70442	0.70562	0.70732
²⁰⁶ Pb/ ²⁰⁴ Pb	17.885	18.156	17.887	18.16	17.971	18.096	18.008
²⁰⁷ Pb/ ²⁰⁴ Pb	15.553	15.578	15.537	15.56	15.515	15.538	15.562
²⁰⁸ Pb/ ²⁰⁴ Pb	38.982	38.906	38.725	38.939	38.944	38.549	38.864

Explanation for Table 1

YAB-Young alkali basalts of the Fortification Hill field (6-4.3 Ma).

OAB-Older normative nepheline alkali basalts of the Fortification Hill field (6 Ma).

OAB-hy--Older normative hypersthene alkali basalts of the Fortification Hill field (6 Ma).

TH-Tholeiitic basalts from Malpais Flattop, Arizona (9.7-10.6 Ma).

Locality Descriptions

<i>Locality</i>	<i>Location Lat. Long.</i>	<i>Age Ma</i>	<i>Description</i>
YAB			
U.S. 93	36°00'00"N 114°45'00"W	4.64-4.3	Volcanic center with numerous dikes. Amphibole megacrysts numerous; mantle xenoliths rare.
Petroglyph Wash	36°04'37"N 114°35'44"W	4.3	Alkali basalt forms a small cylindrical vent. Amphibole megacrysts are common.
Saddle Island	36°02'30"N 114°48'0036° 04'37"N 114° 35'44"W"W	not dated	Flow interbedded with Tertiary gravel. Mantle xenoliths are rare.
TH			
Malpais Flattop	35°45'00"N 114°40'00"W	10.6-9.7 [⁴⁰ Ar/ ³⁹ Ar dates]	100 m thick stack of hypersthene normative tholeiitic basalt flows with wide dikes.
OAB			
Fortification Hill	36°03'45"N 114°40'56"W	5.89 to 5.42	Over 80 flows associated with cinder cones and shallow intrusions.
Lava Cascade	35°52'38"N 114°35'15"W	5.16 to 4.74	Flows and vent zone at summit of Black Mountains.
Petroglyph Wash	36°04'37"N 114°35'44"W	5.43 to 4.61	Stack of flows related to at least two vents.
Black Point	36°24'43"N 114°23'02"W	6.01	Flows and dikes. Flows interbedded with gypsiferous Tertiary sediments.

Las Vegas Range	36°30'19"N 115°02'30"W	16.4	One or two alkali basalt flows tilted about 20 degrees east extensively covered by Quaternary sediments.
Callville Mesa	36°10'19"N 114°42'30"W	10.46 and 8.49	Olivine-clinopyroxene bearing basaltic-andesite flows erupted from compound cinder cones.
Gold Butte	36°15'00"N 114°15'00"W	9.15 to 9.46	Flows of alkali basalt along the Gold Butte fault.
Grand Wash trough	36°15'00"N 113°50'00"W	3.99 to 6.9	Flows, dikes and plugs of olivine-phyric alkali basalt that locally contain mantle xenoliths.
River Mountains	36°05'00"N 114°50'00"W	13.4- 12.1	Andesite-dacite stratovolcano surrounded by a field of dacite domes and a basalt shield.
Wilson Ridge	36°06'21"N 114°37'30"W	13.4	Basalt dikes cutting Wilson Ridge pluton.
Government Wash	36°07'00"N 114°45'00"W	12	80-m-thick section of flows and agglomerates are interbedded with the Lovell Wash member of the Tertiary Horse Spring Formation.
Hamblin-Cleopatra	36°10'00"N 114°36'00"W	14.2- 11.5	60 km ³ stratovolcano comprised of shoshonite, latite, trachydacite and trachyte lava. Volcano is cut by a radial dike system.
Boulder Wash	36°07'00"N 114°37'00"W	14.2	700-m-thick section of calc-alkaline dacite flows and flow breccias interbedded with flows of pyroxene-olivine andesite. 36°04'37"N 114°35'44"W

Eldorado
Mountains
[Isotope data from
Daley and DePaolo,
1992]

35°45'00"N
114°42'00"W

18.5-12
[⁴⁰Ar/³⁹Ar
dates]

A lower section of basaltic-andesite (predominant) and rhyolite lavas and an upper section of basaltic andesite, dacite and rhyolite. The sections are separated by a dacite ash-flow tuff (tuff of Bridge Spring).

All dates are K-Ar except where noted.

Table 2. Source of Mafic Volcanic Rocks in the Lake Mead Area

Magma Type	YAB	OAB-ne	OAB-hy	TH	Low ϵ Nd Alkali Basalts
Components in source	AM + HIMU +LM	AM+HIMU+ LM	AM+LM+ HIMU	LM+crust [contamination]	LM+crust [commingling]

Notes: Size of text indicates relative contribution of each component. YAB-young alkali basalts of the Fortification Hill field, OAB-ne and OAB-hy, nepheline and hypersthene bearing alkali basalts of the Fortification Hill field, TH-tholeiitic basalts at Malpais Flattop, AM-asthenospheric mantle, LM-lithospheric mantle, HIMU-high uranium ($^{238}\text{U}/^{204}\text{Pb}$) mantle component.

**Tertiary geology of the Reville quadrangle, northern Reville Range, Nye
County, Nevada: Implications for shallow crustal structural control of Pliocene
basaltic volcanism.**

Mark W. Martin*

**Department of Geosciences, Center for Volcanic and Tectonic Studies, University of Nevada, Las
Vegas, Nevada 89154**

***Present address: Pecten International Company, P.O. Box 576, Houston, TX 77001-0576**

ABSTRACT

Detailed field study of the Reveille quadrangle indicates that this area experienced a protracted history of Tertiary deformation and volcanism. Tertiary [> 31.3 Ma (?)] east-trending normal faulting accompanied by coarse to fine grained clastic sedimentation preceded the onset of volcanic activity in this area. Volcanic units range from basalt to rhyolite and are Oligocene(?) to Pliocene in age. Paleotopography appears to have played an important role in controlling the distribution of the Tertiary volcanic units and in most instances is responsible for the geometry of the contacts between lithologic units. Paleotopography, as it affected Tertiary depositional patterns in the northern Reveille Range, was probably controlled by Mesozoic contractional deformation, pre-volcanic east-trending normal faulting, caldera formation, and range-bounding normal faults.

In the northern Reveille range Pliocene basaltic centers are spatially associated with older Tertiary volcanic rocks; however, basaltic centers in this area are not spatially associated with topographically higher Paleozoic marine sedimentary rocks. Several of the basaltic centers within the northern Reveille Range appear to be associated with preexisting shallow crustal structure, including caldera margins and tectonic joint sets.

INTRODUCTION

Ultimately, to understand whether or not preexisting shallow crustal structure influenced the emplacement and eruption of Pliocene basaltic volcanism in the northern Reveille Range, it is necessary to understand fully the preexisting stratigraphic succession and deformation history in the area. The Reveille Range is an excellent area in which to address this question because Pliocene basalts in this Range are associated with both Paleozoic miogeoclinal strata and pre-Pliocene Tertiary volcanic rocks. This unique relationship offers the opportunity to see deeper (relatively) structural and stratigraphic levels, and to view pre-Pliocene structures which controlled basalt emplacement and provides a glimpse of the vent geometry and the style and

mechanism of basaltic magma emplacement at shallow crustal levels in this part of the Basin and Range. This study bears directly on geologic and volcanic characterization of the proposed repository site at Yucca Mountain because recent basaltic volcanism is spatially and temporally associated with older Tertiary structure at the site location, and future basalt eruption cannot be excluded. Understanding the mechanism and style of Pliocene basaltic emplacement and eruption in the vicinity of Yucca Mountain has important implications for repository site characterization and feasibility.

Existing lithologic nomenclature proposed by Ekren et al. (1973) and later followed by Jones and Bullock (1985) for the northern Reveille range is used in the present study. However, based on more detailed mapping, this study presents a different stratigraphic succession than that devised by Ekren et al. (1973). In general, Ekren et al. (1973) interpreted many of the Tertiary lithologic contacts in the northern Reveille range as fault contacts. However, detailed mapping indicates that most of these contacts are not faults. Steep, geometrically non-planar depositional contacts were mapped as faults by Ekren et al. (1973). Although many lithologic contacts are not exposed because they are covered by alluvium, field relations indicate that within the northern Reveille range a significant amount of paleotopography was present during the deposition of Tertiary volcanic units. A least some of this paleotopography is related to the rims and walls of two Tertiary calderas in the northern Reveille Range.

This study presents field data accumulated from detailed mapping (1:24,000) in the Reveille quadrangle and the interpretation of these observations. This paper includes a revised Tertiary stratigraphic succession and deformation history, interpretation of the environment of deposition of Tertiary volcanic units, and an alternative interpretation for many of the lithologic contacts in the northern Reveille Range. These observations and interpretations are important to understanding the influence of preexisting shallow crustal structure has on the emplacement and eruption of subsequent Pliocene basaltic volcanoes.

STRATIGRAPHIC EVIDENCE FOR TOPOGRAPHY

The lithologic description of the stratigraphy in the northern Reveille Range was presented by Ekren et al. (1973). This stratigraphic nomenclature was generally followed and only slightly modified by Jones and Bullock (1985). The lithologic nomenclature used in this study is virtually identical to that of Ekren et al. (1973). However, this study presents a slightly different stratigraphic succession (Plate 1) than that put forth by Ekren et al. (1973). The main distinction between the results found in this study and that of Ekren et al. (1973) is that these authors inferred that most of the lithologic contacts in the northern Reveille Range were faults, whereas this study proposes that these contacts are depositional. The following section discusses the field observations that support this interpretation.

Oldest Tertiary sedimentary rocks

Ekren et al. (1973) identified a thrust fault that places Silurian-Devonian carbonates on conglomerates and fine grained clastic rocks presumed to be Pennsylvanian and Permian in age. Closer inspection of this relation indicates that there is no shallowly dipping thrust fault associated with this contact. There is evidence, however, that supports the existence of a sub-vertical east-striking fault cutting the Paleozoic section. In buttress unconformity on this fault and resting depositionally on the Paleozoic section is a Paleozoic clast conglomerate and interbedded carbonate sandstone, siltstone, and mudstone. In proximity to the fault, the fault, the Paleozoic strata and the clastic sequence are silicified. The conglomerate consists of very angular clasts of Paleozoic rocks near the fault. Away from the fault the clasts become more rounded. The conglomerate comprises only clasts from the Paleozoic section, all of which can be derived from the immediate vicinity. The clastic section also appears to contain large blocks (upto 2 m in diameter) of locally derived Paleozoic carbonate floating within it. In addition, an important observation is that this sequence contains no evidence for volcanic detritus.

The favored interpretation explaining these observations is that the conglomerates and interbedded fine-grained clastic rocks were shed southward off an east-trending fault scarp

(probably a normal fault with down-to-the-south throw). Faulting and deposition of the clastic sequence probably occurred simultaneously and fluids migrating along the fault were responsible for the silicification proximal to the fault. An occasional large block of carbonate was apparently shed off the up thrown block into the clastic basin.

The field relationships in the vicinity of the clastic sequence permit the interpretation that the oldest volcanic tuff (Windous Butte?, 31.3 Ma) in the range rest depositionally on this clastic sequence (PLATE 1). This, and the observation that the clastic sequence is composed solely of Paleozoic clasts and finer grained material with no evidence for any volcanic component suggest an Oligocene or Eocene age. In addition, a rhyolite dike of similar modal phenocryst composition to the oldest volcanic tuff (Windous Butte?) in the range intrudes the clastic section. If the above interpretation is correct, and this clastic section was being shed off an east-striking normal fault then a permissive conclusion of this data (in light of the poor timing constraints) is that some extension occurred in this region prior to Tertiary volcanism.

Windous Butte Tuff(?)

This unit was originally correlated with the tuff of William's Ridge and Morrey Peak(?) by Ekren et al. (1973). However, more recently Best et al. (1989) assigned this name to the intracaldera facies in the northern Pancake Range. The outflow equivalent of this unit is named the Windous Butte Tuff (Best et al., 1989). The Windous Butte Tuff is 31.3 Ma and this name has been adopted for this study.

The Windous Butte(?) was considered the oldest volcanic unit in the northern Reveille Range by Ekren et al. (1973). The largest exposure of Windous Butte in the Northern Reveille Range was inferred by Ekren et al. (1973) to be fault bounded. This study suggest an alternative interpretation for this exposure. Originally, Ekren et al. (1973) inferred that the main exposure of Windous Butte(?) was in fault contact with Paleozoic marine sediments. Jones and Bullock (1985) inferred that the Window Butte tuff (?) occupies an east-trending graben bound on both side by Paleozoic sedimentary rocks. However, field relations clearly indicate that the southern

contact of Windous Butte(?) on Paleozoic rocks is depositional. This contact is subvertical to moderately dipping and the compaction foliation in the Windous Butte(?) fans from subvertical to moderately dipping at the contact to subhorizontal away from it (Plate 1). The northern contact of Windous Butte(?) against Paleozoic rocks is never well exposed, but the compaction foliation also fans away from the Paleozoic rocks and along this contact there is no demonstrative evidence for a fault. Here it is suggested that the Windous Butte filled an east-trending paleovalley in the Paleozoic basement. In light of the evidence for east-trending normal faulting prior to deposition of the Windous Butte(?) discussed above, this paleovalley may have existed as a fault-bound graben.

Ekren et al. (1973) also infer that the overlying tuff of Goblin Knobs is juxtaposed with the Windous Butte(?) along a high-angle strike-slip fault. Although poorly exposed, this study found no satisfying field evidence for a fault along this contact. Where compaction foliation in these adjacent units was observed, orientations are nearly coplanar, and strong discordance of the foliation was not observed. With no demonstrative evidence for a fault between these two units, this contact is tentatively considered depositional.

Tuff of Arrowhead.

The tuff of Arrowhead is comprised of two or more outflow cooling units and is quite variable in composition and texture (Ekren et al., 1973; this study). Contrary to interpretations by Ekren et al. (1973), field studies document that the tuff of Arrowhead rests depositionally on the tuff of Goblin Knobs and, therefore, it is younger than the tuff of Goblin Knobs. Although the contact between the tuffs of Arrowhead and Goblin Knobs is very poorly exposed, in all locations the tuff of Arrowhead occupies a higher topographic level than the tuff of Goblin Knob. No field evidence was identified that suggests a shallow-angle fault along this contact as inferred by Ekren et al. (1973). East of the Arrowhead district, the tuff of Arrowhead rest depositionally on a thin lens (~2-3 m thick) of very well rounded cobble conglomerate that in turn lies above the tuff of Goblin Knob (Plate 1). These field relations support the interpretation that the tuff of Arrowhead

rests depositionally on the tuff of Goblin Knob. However, the tuff of Arrowhead everywhere rests on the lowest stratigraphic exposures of the tuff of Goblin Knobs. Continuous exposure in this region indicates that the highest exposed stratigraphic levels of the tuff of Goblin Knobs rest ~100 m above the stratigraphically highest exposure of the tuff of Arrowhead. Together, these data suggest that prior to deposition of the tuff of Arrowhead a significant amount of topography was present on the tuff of Goblin Knobs.

The relative age between the tuff of Northern Reville Range and the tuff of Arrowhead is presently unclear. However, in general the tuff of Arrowhead is more strongly hydrothermally altered than the tuff of Northern Reville Range. Although not conclusive evidence, this may suggest that the tuff of Arrowhead is older. Forth coming geochronology on these units should clarify their absolute ages.

Field Evidence for Calderas

Since the study by Ekren et al. (1973) a significant amount of new geological field data have been collected from the central Nevada region. Studies by numerous workers indicate that there are many Oligocene and Miocene calderas in central and south-central Nevada (Fig. 1; Best et al. 1989, and reference therein). The field relations described below indicate that the northern Reville Range also experienced this regional caldera formation event.

Tuff of Goblin Knobs

The tuff of Goblin Knobs covers most of the eastern half of the Reville quadrangle. This unit was originally considered equivalent to the Monotony tuff (27.1 Ma) by Ekren et al. (1973). The tuff of Goblin Knobs has since yielded a $^{40}\text{Ar}/^{39}\text{Ar}$ (single sanidine) age of 25.4 Ma (Best et al. , 1992). This unit consists of a thick sequence (700+ m) of welded tuff containing ubiquitous large pumice and lithic clasts (~60 cm). The thickness of the section, the lack of clearly defined cooling units, and the overall coarseness of pumice and lithic clasts suggests that it is an intracaldera facies.

Location of Oligocene and Miocene calderas

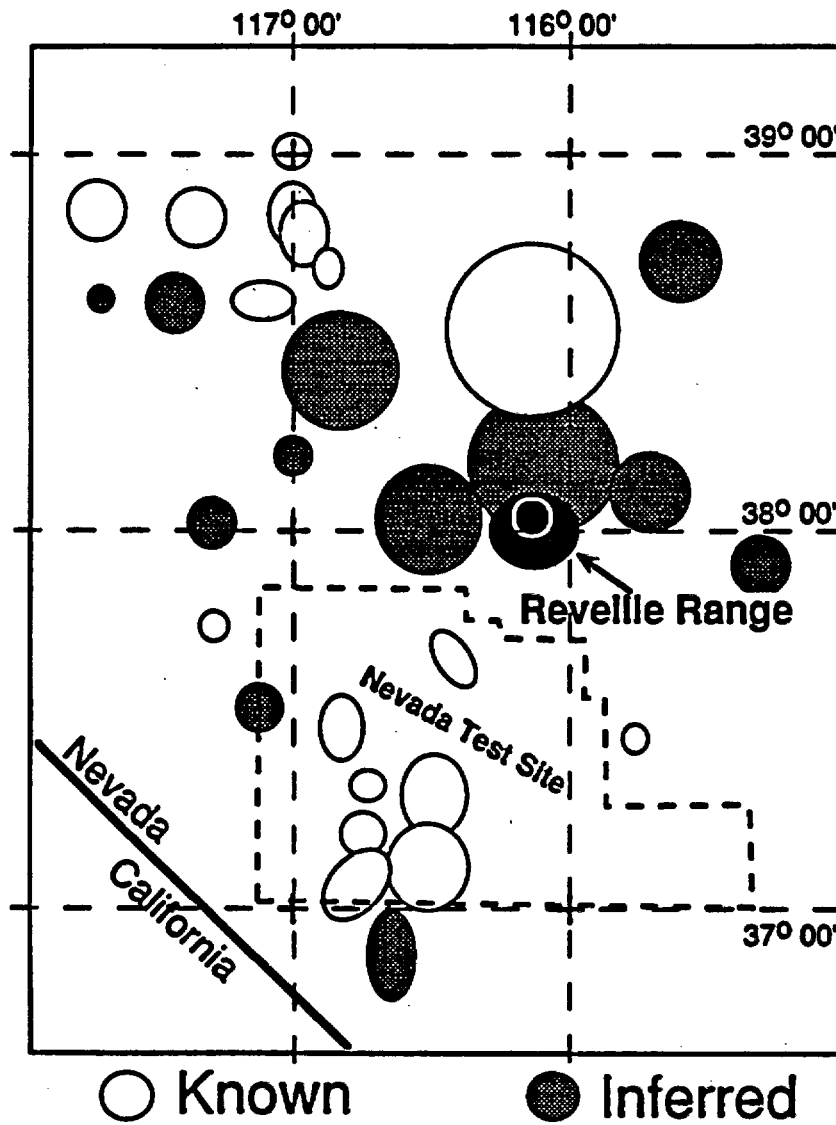


Figure 1. Modified from Best et al. (1989)

Simplified geologic map of the northern Reveille Range

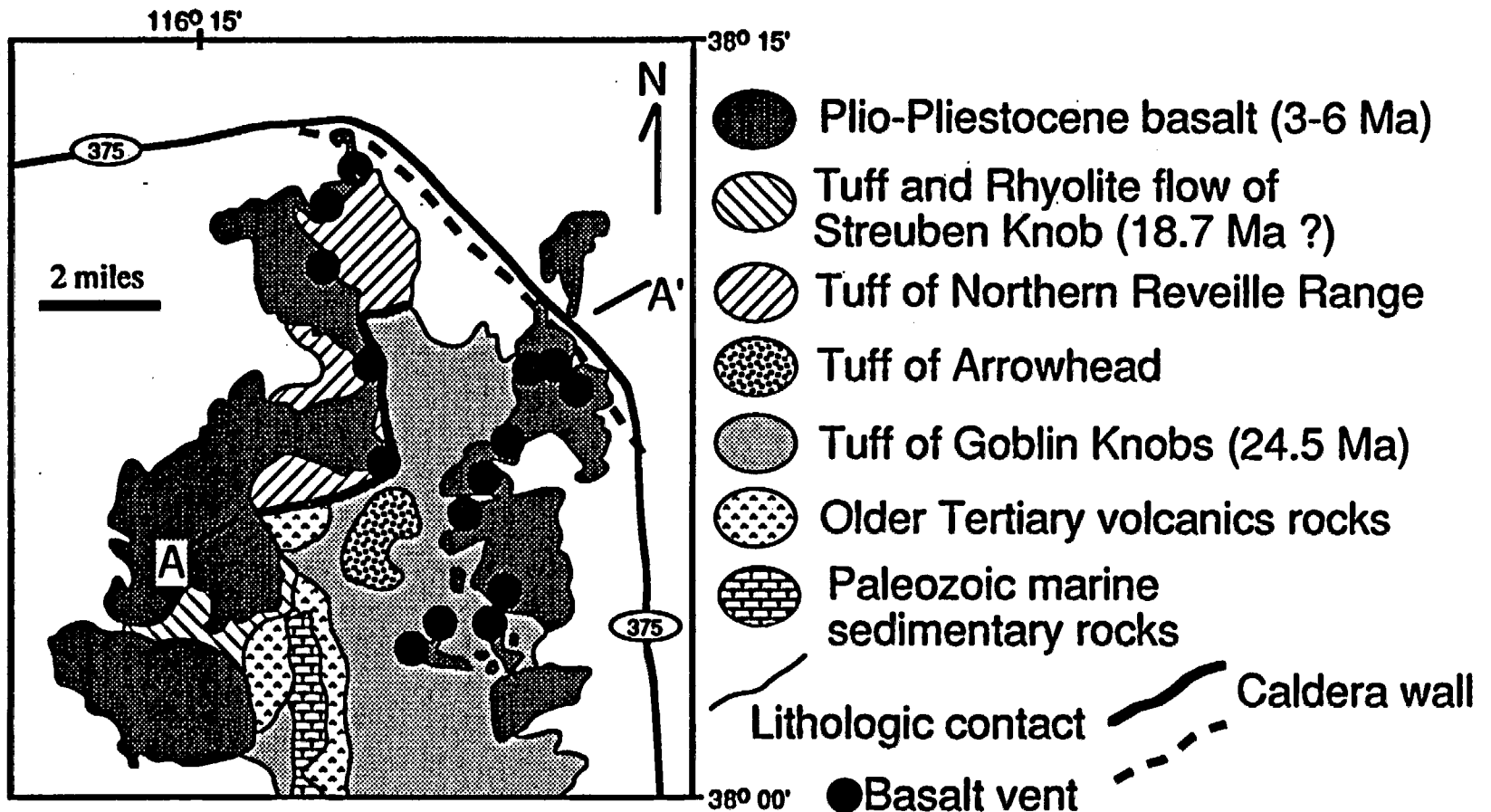
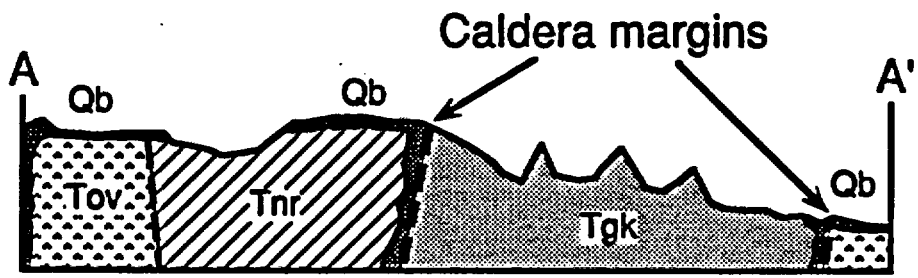


Figure 2

Generalized cross-section through the northern Reveille Range



-  Plio-Pliocene Basalt (3-6 Ma)
-  Tuff of Northern Reveille Range (18.7 Ma?)
-  Tuff of Goblin Knobs (24.5 Ma)
-  Older Tertiary volcanic rocks

Figure 3

A part of the northern caldera wall for the tuff of Goblin Knobs is well constrained by the geology in the southern Pancake Range and the northern Reveille Range (see Ekren et al., 1973; Figs. 2 & 3). Because of the distinctly different geology exposed north and south of the pass separating these two ranges and the interpretation by Ekren et al. (1973) that the tuff of Goblin Knobs and Monotony tuff are age equivalent, these authors inferred the existence of a left-lateral strike-slip fault separating the two areas. However, because the tuff of Goblin Knobs is younger than the Monotony Tuff, and there is no demonstrative field evidence for the left-lateral strike-slip fault inferred by Ekren et al. (1973), a caldera margin in this position appears a more reasonable interpretation of the field relationships. If this interpretation is correct, the breccia sheets mapped in the vicinity of the pass separating these two ranges (Ekren et al., 1973) probably were shed off the caldera margin, rather than shed off strike-slip fault scarps as envisioned by Ekren et al. (1973).

Tuff of the Northern Reveille Range

Field relations support the interpretation that a portion of the caldera that erupted the tuff of Northern Reveille Range was erupted from a caldera in the northwestern part of the Reveille quadrangle. The following section outlines the field evidence that supports this interpretation.

The tuff of Northern Reveille Range is greater than 300 m thick and contains abundant large lithic and pumice clasts (70 cm). No internal cooling units could be defined. However, in places the tuff contains a vertical basal vitrophyre (a minimum of 10-20 meters of relief is observed along strike of this vertical vitrophyre) that contains glassy pumice and granitic clasts. Where exposed, this vitrophyre is in sharp angular discordance with older volcanic rocks. In these localities, overlying welded pumice tuff contain a vertical foliation that fans to sub-horizontal.

In the north-central part of the quadrangle the north-trending contact between the tuff of Goblin Knobs and the tuff of Northern Reveille Range previously interpreted as a set of left-lateral strike-slip faults and kinematically related thrust faults by Ekren et al. (1973) is here interpreted as

a caldera margin (Figs. 2 & 3). The data supporting this interpretation include: 1) a buttress unconformity of the tuff of Northern Reveille Range against tuff of Goblin Knobs (a minimum of 100 meters of relief is observed along this buttress), in addition, there is no evidence for brecciation or offset of geologic markers along this contact that would support the existence of a fault; 2) the tuff of Northern Reveille Range is intensely silicified along the contact against unsilicified tuff of Goblin Knobs. Silicification of intracaldera fill is often seen along caldera margins (Burbank, 1968; Lipman, 1984); and 3) buttressed against the caldera wall is a ~25-50 meter thick silicified pyroclastic surge deposit overlying and interbedded with the tuff of Northern Reveille Range. Interbedded with the surge deposit is a breccia sheet of tuff of Goblin Knobs containing up to 5-10 square meter blocks of shattered tuff of Goblin Knobs. This breccia sheet may have broken loose from the unstable caldera wall and slid into the active caldera of tuff of Northern Reveille Range.

These relations, including the overall thickness and coarseness of the tuff of northern Reveille Range, strongly suggest that a portion of the caldera wall for the tuff of Northern Reveille Range is exposed in the northern Reveille Range and maybe nested within the caldera of Goblin Knobs. These observations also clearly indicate the tuff of Northern Reveille Range is younger than the tuff of Goblin Knobs.

Tuff of Streuben Knob

The tuff of Streuben Knob is comprised of two cooling units (Ekren et al., 1973; this study). Both units contain large felsic igneous clasts (<50 cm) suggesting proximity to its caldera. Field relations suggest that the tuff of Streuben Knob may be the outflow sheet for the tuff of Northern Reveille Range which is interpreted as an intracaldera fill deposit. Field evidence that suggest this interpretation consist of: 1) similar modal phenocryst percent in both tuffs; 2) large granitic clasts in both tuffs; and 3) similar basal vitrophyres with distinctive glassy flattened pumice and granitic clasts.

Flow-banded rhyolite rests depositional on the tuff of Streuben Knob. This rhyolite, named rhyolite of Streuben Knob by Ekren et al. (1973), in places contains diagnostic orthoclase feldspar phenocrysts (0.5-4 cm.). West of Streuben Knob, orientations in the flow banding in the rhyolite change from subvertical to subhorizontal, presumably draping paleotopography. The overall composition and modal phenocryst percent of the this flow-banded rhyolite is similar to orthoclase porphyry rhyolite plugs and dikes found elsewhere in the Reveille quadrangle that Ekren et al. (1973) identified as quartz latites.

Rhyolite Porphyry Plugs and Dikes

Ekren et al. (1973) reported a K/Ar age of 18.7 Ma for porphyry plugs and dikes in the Reveille Range. These intrusions are spatially associated with the intracaldera tuff of Northern Reveille Range (Plate 1) and although lacking absolute age control, may be associated with the latter stages of the development of this caldera (i.e. resurgent doming). As suggested above, if the rhyolite of Streuben Knob, which rests depositionally on the tuff of Streuben Knob (outflow sheet(?) to the intracaldera tuff of northern Reveille Range), and the rhyolite porphyry dikes and plugs are equivalent then the rhyolite of Streuben Knob may also be genetically associated with late stage development of the caldera of Northern Reveille Range. This interpretation implies that the caldera of northern Reveille Range was active around 18.7 Ma.

Pliocene Basalt

Previous field, geochemical and geochronologic work on the Pliocene basalts in the northern Reveille Range by Naumann et al. (1991) determined that two episodes basaltic volcanism occurred in the area, 5.0-5.9 Ma and 3.0- 4.6 Ma. Each of these episodes of have isotopically different signatures (E.I. Smith, personal comm.).

An important goal of the present study was to determine if preexisting structure influenced the emplacement and eruption of basaltic volcanism in this area. Previous studies by Naumann et al. (1991) identified basaltic centers in the northern Reveille Range. An important conclusion drawn from the study by Naumann et al. (1991) and this study that pertains directly to

characterization of the Yucca Mountain site is that basaltic centers are found within the central portions of mountain ranges and not solely along the range margins and flanking alluvial basins as suggested by Crowe et al. (1991). This finding, if not already factored into probabilistic studies at Yucca Mountain by DOE scientists, needs to be considered as a variable in such studies.

An example of a basalt center positioned within the central part of the Reveille Range is the Dark Peak vent in the north-central part of the Reveille quadrangle, which rests on the topographic crest of the Reveille Range. This vent consists of scoria, cinder, and bombs, at least one vertical conical magma conduit (~2.0 meters in diameter), and basalt dikes that feed basaltic flows. Cumulative thickness of these flows, which flowed to the west, is ~50 meters. Erosion of the vent on Dark Peak allows scrutiny of ~25 meter vertical section of the plumbing architecture within the vent. Here, banded, vesicular siliceous veins cut basalt. The presence of these veins suggests that hydrothermal fluids (perhaps circulating ground water at the tuff of Northern Reveille Range caldera margin) were circulating after basalt eruption. This observation clearly suggests that hot fluids escaped through an existing vent. This observation may have important implications concerning the effect of basaltic magma emplacement on ground water circulation at the proposed repository site at Yucca Mountain.

Approximately 10% of all the vents in the Reveille Range and flanking alluvial basin rest within the central part of the Reveille Range (Fig. 4). It could be argued that these basaltic vents erupted prior to uplift of the Reveille Range. However, all the basaltic vents and their associated flows that occur within the range proper rest directly on Tertiary basement with no intervening alluvial sedimentary rocks or detritus. In addition, along the east flank of the Reveille Range, basaltic flows originated from vents at higher topographic levels within the range proper and flowed down steep vertical gradients (>30 degrees) into the flanking alluvial basin. These lavas clearly flowed over range bounding normal faults. These field relations support the observation that basalt lavas erupted onto a topography similar to present day topography.

Location of basalt vents in the Reville Range

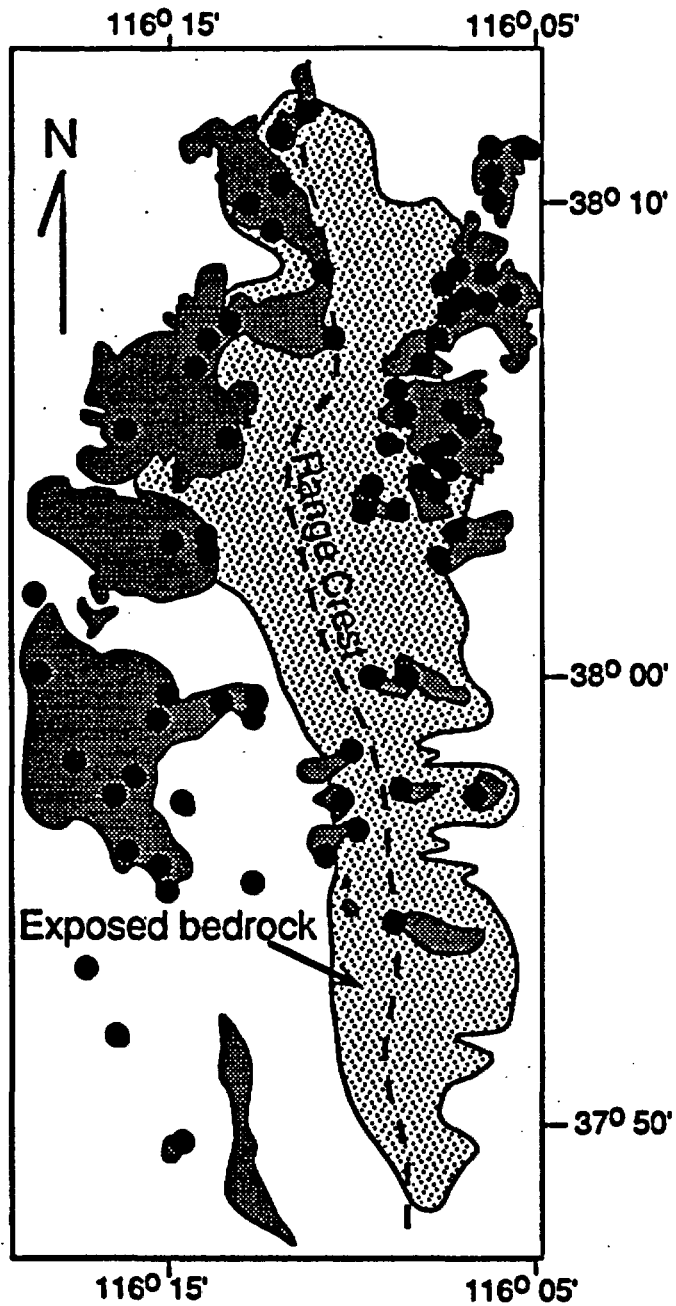


Figure 4

On the west flank of the northern Reveille Range, Ekren et al. (1973) show several north-trending normal faults cutting Pliocene basalt flows. The existence of these structures, is ambiguous. What is clear from the present level of exposure is that there is a zone of north-trending brecciation in pre-Pliocene Tertiary tuffs (presumably the result of a fault). However, because of the present level of exposure, it cannot be determined if the overlying basalts are themselves also faulted. These field relations permit the following alternative interpretations: 1) the basalts are not faulted, but, rather, flow over a pre-existing fault scarp; 2) the oldest basalt flows were faulted and younger lavas flowed over this fault scarp; and 3) the entire sequence of basalt flows is faulted as indicated by Ekren et al. (1973). Clearly, the present exposure in this area does not allow for a definitive interpretation. However, the field relations discussed in the previous paragraph would support the interpretation that the basalts are not faulted and flowed over existing fault scarps .

Basement Control of Pliocene Basalt Vents

The tuff of Goblin Knobs in the Reveille quadrangle contains a prominent north- to northwest-trending tectonic joint set (<1 meter spacing interval). In the east-central part of the Reveille quadrangle, two basaltic dikes (~1-1.5 meters thick) intruding the Monotony Tuff and feeding an overlying basalt flow have parallel trends to the north-trending joint set in the Monotony Tuff. Along strike these dikes temporarily jog parallel to the subordinate N30W-trending joint set and then jog back to parallelism with the dominant north-trending joint set. This observation suggests that some basaltic dikes that feed the Pliocene basalt flows in the northern Reveille Range use preexisting joint sets as conduits (perhaps only temporarily) in the shallow crust. However, it is also clear from field observation that basaltic dikes elsewhere ignore and intrude at high-angles to these older joint sets.

Along the inferred caldera wall of the tuff of Northern Reveille Range are at least two vents for the episode 1 Pliocene basalt flows (5.0-5.9 Ma, Naumann et al., 1991). The basalt vent on Dark Peak and probably the basalt vent ~1.0 mile north-northwest of Dark Peak (Fig. 2, Plate 1)

are situated along the range crest on or just inside the inferred caldera wall for the tuff of Northern Reveille Range. This relationship suggests that in this part of the Reveille Range, Pliocene basalt emplacement and eruption may have been directly aided by preexisting shallow crustal structural weaknesses typically found along caldera margins. Interestingly, though more speculative, several basalt vents lie close to the inferred trace of the northern wall of the caldera that erupted the tuff of Goblin Knobs (Fig. 2 & 3; Naumann et al., 1991; this study).

It should also be noted that in the Reveille quadrangle basalt centers are in areas where Tertiary basement apparently lacks structures at the present level of exposure. All the basalt vents that have basement exposures beneath them rest on Tertiary basement. There are no basalt centers that rest directly on Paleozoic marine sedimentary rocks in the Reveille Range. In general the Paleozoic sequence in the Reveille Range is undeformed. The faults that are exposed within the Paleozoic sequence are generally associated with silicification which probably sealed the faults to future fluid or magma migration. A majority of the Paleozoic rocks in the Reveille quadrangle occupy the highest topographic position along the range crest. It is possible that once the basaltic magma has migrated into the shallow crust it simply finds the easiest path to the surface. In the Reveille Range, the rise of basalt through the Paleozoic section was inhibited by topography, density of the Paleozoic rock, and the lack of open fractures.

CONCLUSIONS

The Reveille Range records a protracted history of Tertiary deformation and volcanism. Prior to deposition of the oldest volcanic unit, the Reveille Range experienced a period of normal faulting and associated sedimentation. This period of normal faulting together with previous Mesozoic contractile deformation probably led to the formation of east-trending paleovalleys that controlled the deposition of the oldest Tertiary volcanic rocks. The tuff of Goblin Knobs (24.5 Ma) erupted from a caldera in the northern Reveille Range. The northern margin of this caldera is located between the southern Pancake Range and the northern Reveille Range. The tuff of northern Reveille Range erupted from a younger caldera also located in the northern Reveille

Range, and likely nested within the older caldera. The tuff of Streuben Knob may be the outflow sheet correlative to the intracaldera tuff of northern Reveille Range. The rhyolite of Streuben Knob and rhyolite porphyry plugs and dikes may represent the latest stages of development of the caldera that erupted the tuff of northern Reveille Range.

Whereas previous interpretations of many of the Oligocene and Miocene lithologic contacts in the northern Reveille Range involved faults, this study finds that the field relations are most consistent with the interpretation that these contacts are depositional. Although many of these contacts are steep, field relations suggest that there was a significant amount of paleotopography during the deposition of many of the Tertiary units. Paleotopography in the Reveille Range appears to have been a function of Mesozoic contractile deformation, normal faulting prior to Tertiary volcanism, Miocene caldera formation, and range-bounding normal faulting. Prior to this study, the interpretations presented by Ekren et al. (1973) suggested that Pliocene basaltic volcanism in the Reveille Range might be strongly controlled by pre-existing basement faults. This study concludes that many of these faults do not exist, thereby decreasing the probability that such structures controlled subsequent Pliocene basaltic volcanism in this area.

Some, if not much of the Pliocene basaltic volcanism in the northern Reveille Range appears to have occurred after uplift of the range. Basaltic centers are located within the interior of the Reveille Range and not solely along the range margin or within the flanking alluvial basins. Pre-Pliocene basement structures within the range interior appear to influence the emplacement and eruption of several basalt centers. These structures consist of preexisting caldera margins and tectonic joints sets.

References Cited

- Best, M.G., Christiansen, E.H., Deino, A.L., Gromme, C.S., McKee, E.H., and Noble, D.C.,
1989, Eocene through Miocene volcanism in the Great basin of the western United States:
New Mexico Bureau of Mines and Mineral Resources Memoir 47, p. 91-133.

- Burbank, W.S., and Luedke, R.G., 1968, Geology and Ore deposits of the western San Juan Mountains, Colorado, in Ridge, J.D., ed., Ore deposits in the United States 1933/1967: New York, American Institute of Mining, Metallurgical and Petroleum Engineers (Graton-Sales Volume), P. 714-733.
- Crowe, B.M., Valentine, G., Morley, R., and Perry, F.V., 1991, Recent progress in volcanism studies: site characterization project: Report in U.S. Department of Energy (DOE) responses to State of Nevada comments on study plan 8.3.1.8.1.1, "Probability of magmatic disruption of a repository", 16 p.
- Ekren, E.B., Rogers, C.L., and Davis, G.L., 1973, Geologic and Bouguer Gravity map of the Reville Range quadrangle, Nye County, Nevada: U.S. Geological Survey Misc. Geologic Investigations Map I-806.
- Jones, G.L., and Bullock, K.C., 1985, Geology and ore deposits of the Reville mining district, Nye County, Nevada: Brigham Young University Geology Studies, v. 32, p. 63-84.
- Lipman, P.W., 1984, The roots of ash-flow calderas in western North America: windows into the tops of granitic batholiths: Journal of Geophysical Research, v. 89, p. 8801-8841.
- Naumann, T.R., Smith, E.I., Shafiqullah, M., and Damon, P.E., 1991, New K-Ar ages for Pliocene mafic to intermediate volcanic rocks in the Reville Range, Nevada: Isochron/West, n. 57, p. 12-16.

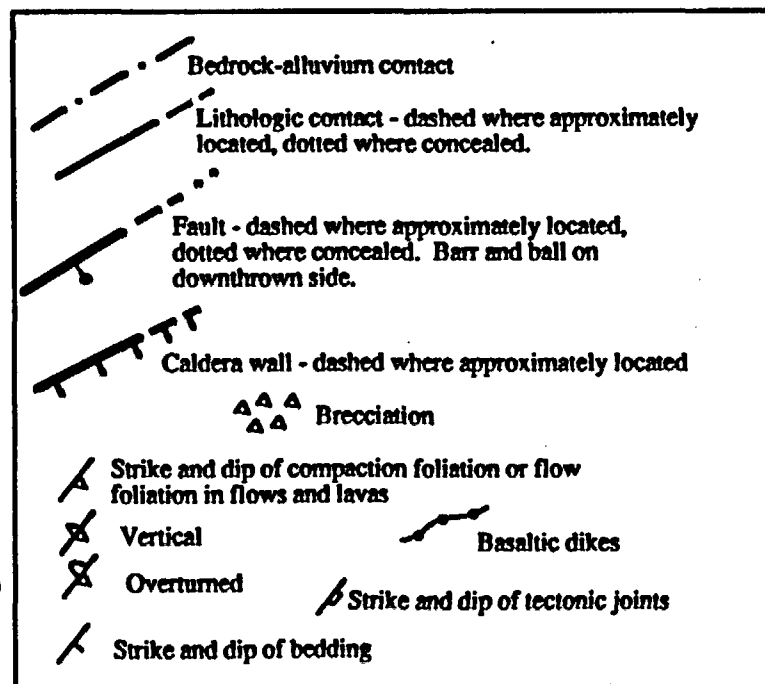
Explanation

(Mapping by Mark W. Martin, 1992)

Qal	Quaternary alluvium
TQal	Tertiary-Quaternary alluvium
Tb2	Pliocene basalt (5.0-5.9 Ma)
Tca	Pliocene alluvium
Tb1	Pliocene basalt (3.0-4.6 Ma)
Tt	Air-fall tuff
Tqv	Rhyolite vent breccia
Trp	Rhyolite porphyry plugs and dikes (18.7 Ma, Ekren et al, 1973)
Tns	Surge deposit of Northern Reveille range
Tn	Tuff of Northern Reveille Range (intracaldera)
Ta	Tuff of Arrowhead
Tg	Tuff of Goblin Knob (24.5 Ma, M.G. Best, personal comm.)
Tvc	Volcaniclastic sediment (conglomerate containing Paleozoic clasts and dacite, andesite and felsic tuff volcanic clasts)
Td	Dacite flow
Tad	Andesite
Tw	Windous Butte tuff(?) [31.3 Ma]
Tc	Fine to coarse grained clastic sediment (including paleozoic clast conglomerate, carbonate sandstone, siltstone and mudstone considered Pennsylvanian or Permian by Ekren et al. 1973)
~~~~~ Unconformity	
<b>MD</b>	Upper Devonian through Upper Mississippian (including Pilot Shale, Joana Limestone, and Diamond Peak Formation(?) (see Ekren et al., 1973))
<b>Dml</b>	Middle and Upper Devonian (includes limestone and dolomite of the Nevada Formation (see Ekren et al, 1973))
<b>DSd</b>	Silurian and Lower Devonian (dolomite (see Ekren et al. (1973))
<b>Omu</b>	Middle and Upper Ordovician (includes Eureka Quartzite and Ely Springs Dolomite)
<b>Oa</b>	Antelope Valley Limestone (Lower to Middle Ordovician)

<b>Tsr</b>	Rhyolite of Streuben Knob
<b>Tst</b>	Tuff of Streuben Knob (outflow sheet)
<b>Tbr</b>	Volcanic breccia

<b>Tor</b>	Tuff of Reveille Range
<b>Ts</b>	Unnamed moderately welded tuff (called Shingle Pass Tuff by Ekren et al. (1973), however, appears to rest topographically above tuff of Goblin Knobs).



## Summary of Work Completed by Tim Bradshaw

October 1992 to December 1992

### Introductory work

1. Background reading, including all of the relevant CVTS documents and a number of MSc theses, plus relevant reports concerning the general Yucca Mt. area and the waste repository project in particular (eg. USGS and DOE documents).
2. The 47th meeting of the USNRC Advisory Committee on Nuclear Waste was attended.
3. A Macintosh database was compiled for all of the available Crater Flat data. Comparisons were made to other published Crater Flat analyses (from Vaniman et al 1982), and geochemical modelling was started. A brief summary of some of the preliminary interpretations is given below.

### Field work

Introductory field work was conducted at Crater Flat with Gene Smith, and in the Reveille Range with Mark Martin. The Crater Flat area was subsequently visited on a number of occasions. Flow relationships were investigated to try and determine a relative chronology for the samples already analyzed. Nineteen further samples were collected from Red Cone and these are currently being prepared for analysis. Sample coverage of Red Cone is displayed in Figure 1. The new sampling was concentrated at the summit of Red Cone, to provide data for investigating the development of lava lakes, and on the southern flank of Red Cone where a large number of cinder cones are located. Here, a suite of intrusive bodies exposed in the eroded core of a cinder mound have been sampled. It is hoped that it will be possible to geochemically correlate these intrusions with lava flows in their close proximity, and thus further constrain both temporal relationships and the magmatic evolution of Red Cone.

Four local field trips were also made to examine other areas of late Cenozoic volcanism in southern Nevada. Parts of the McCullough Range, Sheep Mt. and the River Mountains were visited.

## Geochemistry

Some problems were identified with the current Crater Flat data set, concerning INAA analytical errors. Because the range of geochemical variation is rather limited for each cone, the errors on some trace elements (eg. Ta, Zr, Yb and Nd) are too great for the detailed investigation of intra-suite variations. The major and trace element data for Red Cone and Black Cone also display significant overlap (see Figure 2- note the near identical patterns for the Red Cone and Black Cone average data), although some of the youngest Red Cone lavas do have greater concentrations of the Light Rare Earth Elements (LREE). Thus, it is intended to re-analyze some of the more crucial samples, and also to obtain coverage of a wider set of trace elements by additional XRF analysis. However, the available data is still valuable for characterization of the Crater Flat samples relative to other magmatic provinces in the western USA.

## Geochemical modelling

All samples analyzed from Crater Flat can be classified as alkali basalts. Some of the general features of their geochemistry have previously been outlined in the CVTS yearly report for 1989, and by Vaniman et al (1982) The basalts have moderately high trace element concentrations (Fig. 2, see Sun and McDonough 1989) and most of the samples are diopside-olivine-hypersthene normative (Figure 3, after Thompson et al 1983).

Low concentrations of Cr, Co, Sc and MgO and low Mg#s (49-54) indicate that the basalts have undergone significant degrees of evolution from their primary magmas. Primary basalt magmas are typically thought to have Mg#s in the region of 68-76 (Mg#= 72, for primary magmas modelled in the western Great Basin, Ormerod et al 1991). Thus a back-correction to such values, from the Crater Flat data, would imply approximately 20-25wt% olivine fractionation.

Fractionation of olivine is also supported by its presence as the only abundant phenocryst phase in lavas from Crater Flat. However, covariation between Co, Sc and Cr within the spread of the Red Cone and Black Cone data suggests that orthopyroxene and clinopyroxene ( $\pm$ spinel) fractionation

may also have contributed to the magmatic evolution. Again, this is supported by the presence of these minerals as minor phenocryst phases in many of the samples.

The depth at which fractionation occurred is a critical factor in determining the probability of site disruption at Yucca Mt., although it is a figure that is difficult to constrain. However, estimates can be made from the normative mineral compositions of the magmas, and by consideration of the mineral phases that are thought to be involved in fractionation (see Figure 3). Magma apparently ponded in the upper portions of both Red Cone and Black Cone, although these events were probably short-lived. The individual units never exceed 80cm in thickness, and thus would have cooled fairly rapidly ( $\ll 1$ yr). On Figure 3 none of the Crater Flat samples fall near to the typical 1 atmosphere fractionation path, and instead plot closer to the higher pressure cotectic. This suggests that any magma residency in the upper crust/ near surface would only have been of limited duration, as equilibrium was not attained. Rather, fractionation is likely to have occurred at greater depths, possibly near the base of the crust; or even in the upper mantle below the plagioclase stability field, as this mineral is never observed as a phenocryst phase.

Fractionation at depth has also been recognized as a feature in other provinces of the western USA (for example: Bradshaw 1991; Glazner and Ussler 1988), and indeed this may be a pre-requisite for magmas to intrude further into the crust (Glazner and Ussler 1988).

The implied high degrees of fractionation obviously have a significant effect on the measured trace element abundances of the Crater Flat samples. However, most trace elements (with the exception of Ni, Cr, Co and Mn) are highly incompatible in olivine, and thus the relative concentrations of these elements are not drastically affected by olivine removal. In Figure 2 a range of trace element data are compared with average alkali basalt compositions from the Colorado River Trough (CRT) extensional corridor, to the south of Las Vegas. The patterns display a number of similarities, in that both areas have LREE (eg. La, Ce) and Large Ion Lithophile Element (Rb, Ba) abundances in excess of the Heavy REE (Yb, Lu) and High Field Strength Elements (eg. Ta, P, Hf, Ti). This results in a prominent 'trough' at Ta (and Nb), and peaks at Ba and La. These

features have been interpreted as the result of melting in the subcontinental lithospheric mantle in the CRT (Bradshaw 1991), and a similar interpretation may also be applicable to the magmatism at Crater Flat. However, isotopic evidence is not yet available to confirm this model, and so this is one of the main objectives of further work in 1993.

The degree of partial melting in the mantle is also difficult to constrain because of the extent of fractional crystallization. However, based on some preliminary trace element ratio modelling, the Crater Flat magmas may have been generated in mantle not dissimilar to the CRT source if the degree of partial melting were small, eg  $\leq 1\%$ .

#### **Other related work**

A paper entitled, "Basaltic Volcanism in the Southern Basin and Range: No Role for a Mantle Plume" [T.K.Bradshaw, C.J.Hawkesworth and K.Gallagher] was completed for publication. This paper was submitted in its final version, following favorable reviews, to the journal *Earth and Planetary Science Letters*. It is hoped that it will be published early in 1993.

Further collaborative papers with Chris Hawkesworth, concerning Cenozoic volcanism in the western USA, are also under consideration.

#### **References**

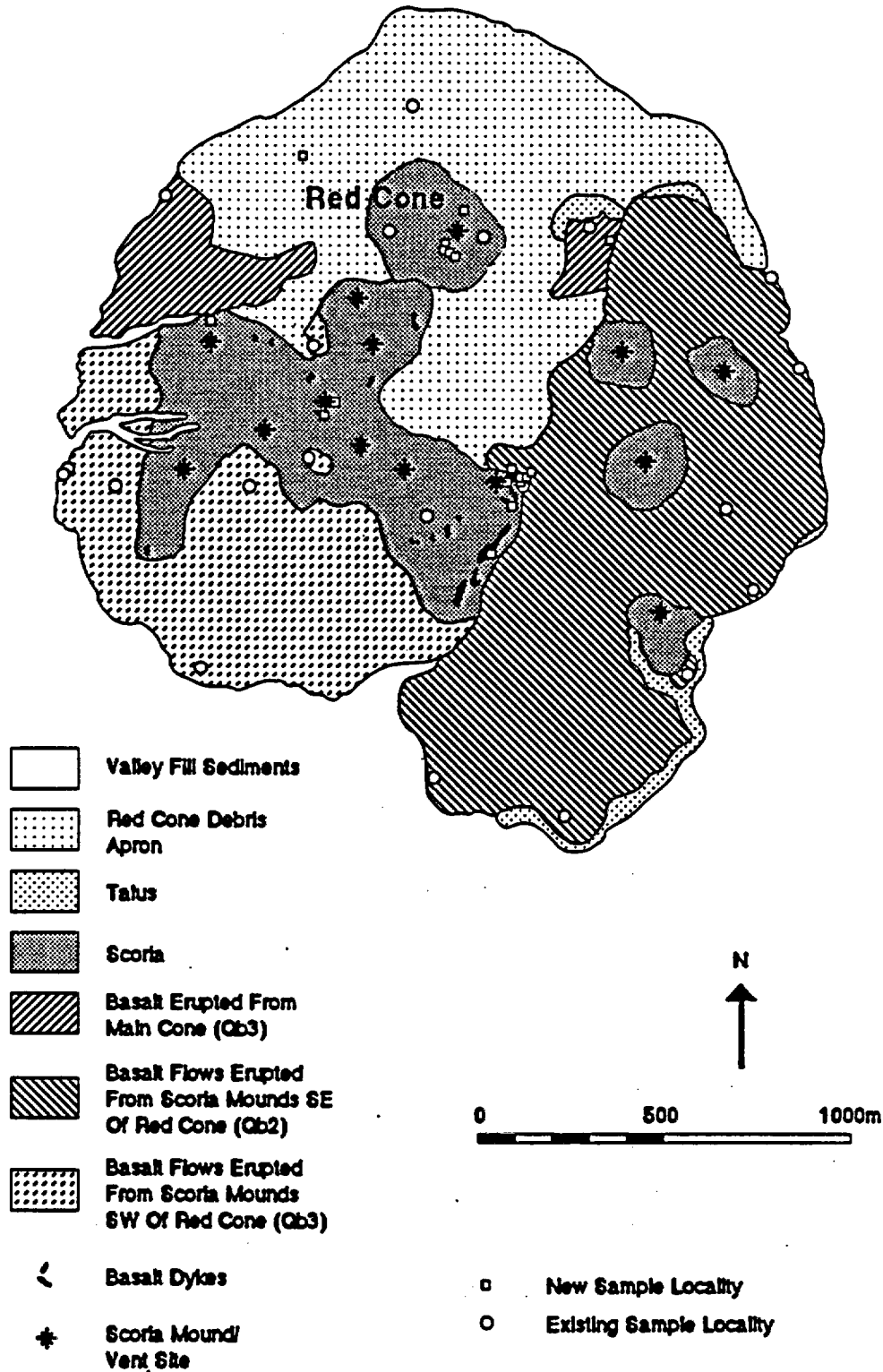
- Bradshaw T.K. (1991) *Tectonics and Magmatism in the Basin and Range Province of the western United States*. PhD. Thesis- The Open University, UK. 248pp.
- Glazner A.F. & Ussler W. III (1988) Crustal extension, crustal density, and the evolution of Cenozoic magmatism in the Basin and Range Province of the western United States. *J. Geophys. Res.* 94, 7952-7960.
- Ormerod D.S., Rogers N.W., and Hawkesworth C.J. (1991) Melting in the lithospheric mantle: Inverse modelling of alkali-olivine basalts from the Big Pine Volcanic Field, California. *Contrib. Mineral. Petrol.* 108, 305-317.

Sun S-s & Mc. Donough W.F. (1989) Chemical and isotopic systematics of oceanic basalts: implications for mantle compositions and processes. Geol. Soc. Am. Spec. Publ. 42, 313-345.

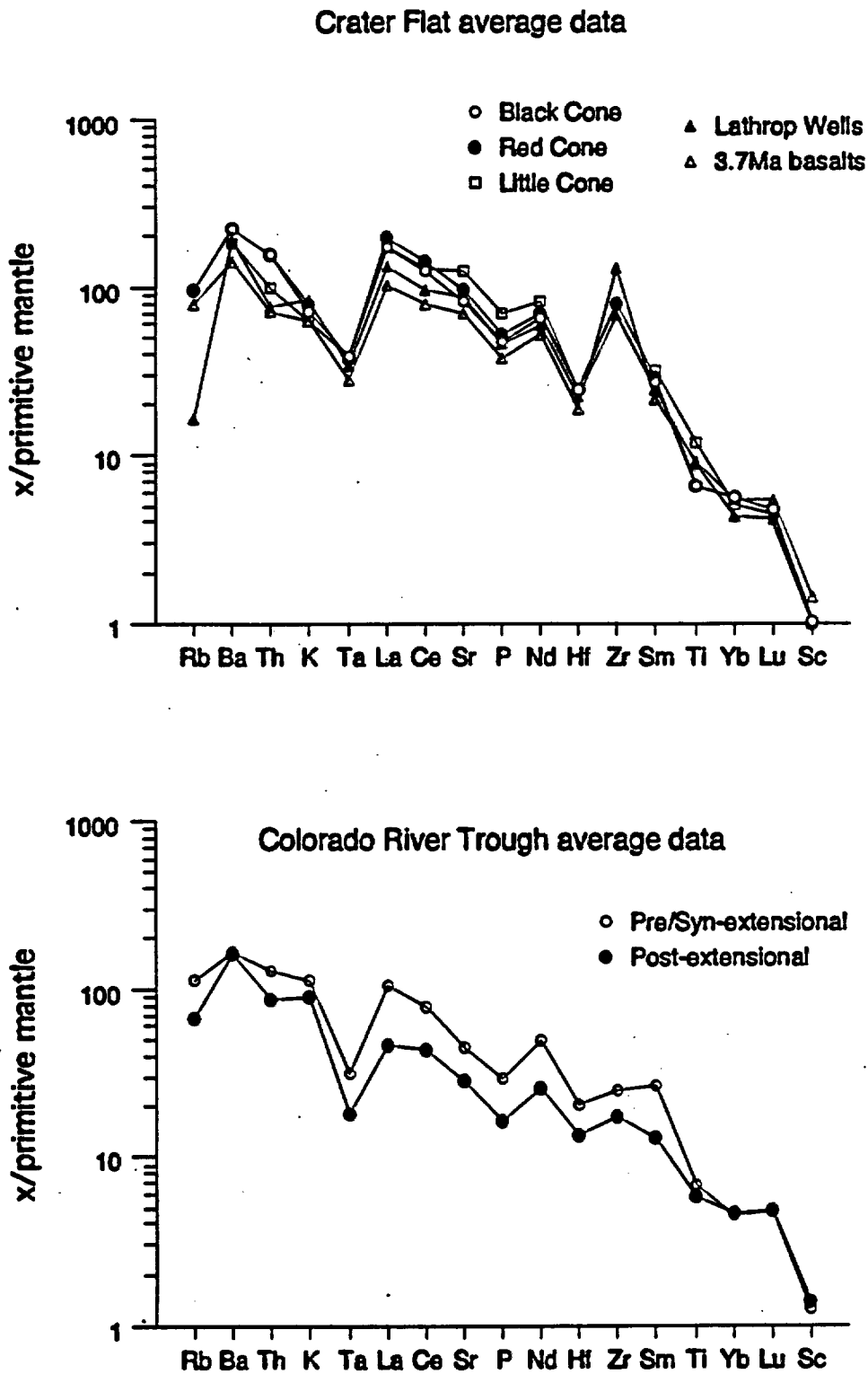
Thompson R.N., Morrison M.A., Dickin A.P. & Hendry G.L. (1983) Continental flood basalts, arachnids rule ok? in: Continental basalts and mantle xenoliths 158-185. Editors: Hawkesworth C.J. and Norry M.J.

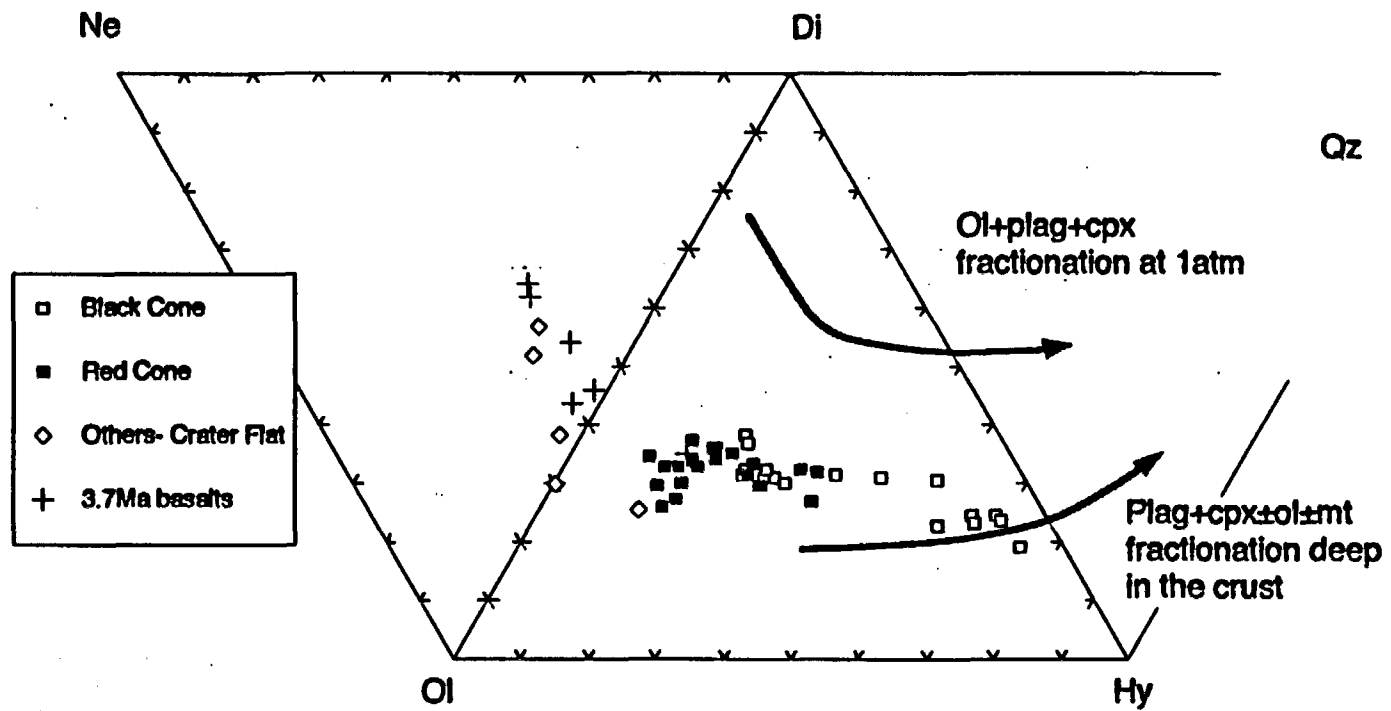
Vaniman D.T., Crowe B.M. and Gladney E.S. (1982) Petrology and geochemistry of Hawaiiite lavas from Crater Flat, Nevada. Contrib. Mineral. Petrol. 80, 341-357.

Figure 1. Schematic geology map of Red Cone, showing sample localities



**Figure 2. Comparison of averaged trace element data from Crater Flat and the Colorado River Trough extensional corridor, south of Las Vegas.**





**Figure 3.** After Thompson et al 1983. Normative mineral compositions for Crater Flat samples, projected from plagioclase. Typical fractionation paths are shown for evolution at high pressures, and at one atmosphere.

## **ABSTRACTS**

volcanic rocks ( $^{206}\text{Pb}/^{204}\text{Pb} = 18.11-18.24$  and  $^{207}\text{Pb}/^{204}\text{Pb} = 38.70-39.15$ ) but diverges from it in some samples.

The carbonate fraction of lead in both vein and calcrete samples resides dominantly in fine-grained, authigenic calcite. 1.5N HCl also attacks and removes lead from silicate phases, but a milder 0.5N  $\text{CH}_3\text{COOH}$  dissolution procedure identifies a significantly more uranogenic lead in most of the calcite ( $^{206}\text{Pb}/^{204}\text{Pb} = 18.11-20.21$  and  $^{207}\text{Pb}/^{204}\text{Pb} = 38.60-39.34$ ). Probably this radiogenic carbonate lead was transported into the vein system by the downward percolation of meteoric water that had previously interacted with surficial calcrete. Windblown particulate matter derived from Paleozoic and Late Proterozoic limestone in surrounding mountains may be the ultimate source of the calcite. Several samples, however, including two from a vein incorporating a thin zone of basaltic ash, contain carbonate lead that is only slightly different from their silicate lead. These isotopically more uniform samples suggest that volcanic rocks locally have contributed most of the lead to both fractions of the vein system.

The isotopically heterogeneous lead that characterizes the regional Paleozoic and Late Proterozoic sedimentary rocks and Middle Proterozoic crystalline rocks remains a candidate for at least some of the lead in the Trench 14 veins. An important finding of this study, however, is that the data do not require the more exotic origins that have been proposed for the veins. Instead, the similarity between lead isotopic properties of the veins and calcretes suggests a mutual origin related to pedogenic phenomena.

02:45 p.m. Harrington, Charles D.

No 16720

QUATERNARY EROSION RATES ON HILLSLOPES IN THE YUCCA MOUNTAIN REGION, NEVADA.

HARRINGTON, Charles D., Earth and Environmental Sciences Division, EES-1, MS D462, Box 1663, Los Alamos National Laboratory, Los Alamos, NM 87545 and WHITNEY, John W., U.S. Geological Survey, Federal Center, MS 913, Denver, CO 80225

Yucca Mountain is a series of eastward-thrust structural blocks. These blocks are composed of fine-grained, Tertiary volcanic rocks, primarily welded tuffs that are resistant to weathering in the present semiarid climate. In the Yucca Mountain region, Quaternary cycles of intense weathering on ridge crests and hillslopes during glacial (pluvial) episodes have resulted in a patchwork of thin colluvial deposits of variable ages.

Approximate long-term average erosion rates can be calculated for hillslopes that have dated colluvial boulder deposits. Twelve of these deposits were studied on seven different slopes that have gradients ranging from 15-32 degrees. Hillslope degradation marginal to these deposits ranges from 0.2-1.1 m. Maximum incision in active channels adjacent to colluvial deposits ranges from 0.3-2.8 m. Carbon-14 dating of rock varnish from surface boulders on these deposits yields age estimates from 170 ka to > 1 Ma. Long-term erosion rates calculated for hillslopes that have relict early to middle Quaternary deposits range from 0.2 to 7.3 mm/ka and average 1.2 mm/ka.

Erosion rates on Yucca Mountain are relatively low compared to rates for other semiarid regions. In California and New Mexico, published long-term erosion rates range from 10-43 mm/ka on hillslopes underlain by resistant lithologies. Erosion rates calculated for slopes on less resistant rock types and for shorter time periods, however, are as much as two orders of magnitude larger.

Hillslopes in the Yucca Mountain area record an exceptional history of geomorphic stability from the early Quaternary to the present. Several conditions contribute to these low long-term erosion rates: (1) bedrock outcrops as well as boulders in the hillslope deposits are erosionally-resistant welded tuffs, (2) rock varnish coatings on surface boulders inhibit weathering, (3) colluvial boulder deposits on hillslopes serve as a protective cap that inhibits removal of finer grained debris by slopewash, (4) hillslope channels isolate colluvial deposits by topographic inversion and remove them from active erosion by runoff, and (5) debris flows, although effective in removing bouldery colluvium from upper slopes, are generally restricted to active channels on middle and lower hillslopes and rarely strip debris from non-channelized areas.

03:00 p.m. Faulds, James E.

No 6918

NEW INSIGHTS ON STRUCTURAL CONTROLS AND ENPLACEMENT MECHANISMS OF PIOCENE/QUATERNARY BASALTIC DIKES, SOUTHERN NEVADA AND NORTHWESTERN ARIZONA

FAULDS, James E., Dept. of Geology, University of Iowa, Iowa City, IA 52242; FEUERBACH, Daniel L. and SMITH, Eugene I., Dept. of Geoscience, University of Nevada, Las Vegas, NV 89154

Five Quaternary basaltic volcanic centers lie within 20 km of the proposed high-level nuclear waste repository at Yucca Mountain. The basalts rose through the crust without contamination. Previous studies suggested that relatively thin (< 5 m) dikes fed the basaltic centers. The Quaternary dikes, scoria mounds, and cinder cones generally trend NNE. Potential NNE-striking near-surface channelways for the basalts include normal fault segments, layering in highly deformed Proterozoic and Paleozoic rocks, and joints. However, lack of dissection of these young volcanoes precludes direct observation of feeder dikes and controlling structures.

To elucidate the geometry of plumbing systems beneath Quaternary volcanoes near Yucca Mountain, highly-dissected Pliocene basaltic centers were studied in the Fortification Hill field of northwestern Arizona. The most highly dissected centers are located on the west flank of Malpais Mesa. Here, dikes within and directly beneath three centers range from 10-25 m in width and 100-225 m in length. Two centers are linked by a 1-2 m wide dike. Thus, dike widths increase by an order of magnitude directly beneath some centers. The NNE- to NW-striking dikes in the Fortification Hill field commonly parallel but are rarely intruded directly along preexisting structures. Some dikes cut directly across Miocene normal faults. All dikes have near vertical dips. These observations imply that dikes may have propagated upward through "self-generated" fractures produced by tensile stresses near the dike tip. The fractures probably developed perpendicular to the least principal stress.

In the Yucca Mountain region, the preexisting NNE-striking structures may have locally facilitated transport of magmas. In most cases, however, we suspect that magmas created their own pathways perpendicular to the N50W orientation of least principal stress. Hazard assessments of Yucca Mountain should consider the potential for dike intrusion along self-generated fractures not associated with preexisting faults and dike widths as great as 25 m.

03:15 p.m. Westling, J. R.

No 25537

SURFICIAL MAPPING IN MIDWAY VALLEY: IMPLICATIONS FOR FUTURE STUDIES TO ASSESS SURFACE FAULTING POTENTIAL AT PROSPECTIVE SURFACE FACILITIES FOR THE POTENTIAL YUCCA MOUNTAIN REPOSITORY, NEVADA

WESTLING, J.R., SWAN, F.H., BULLARD, T.F., ANGELL, M.M., and PERMAN, R.C., Geomatrix Consultants, Inc., One Market Plaza, Spear Street Tower, Suite 717, San Francisco, California 94105; GIBSON, J.D., Org. 6315, Sandia National Laboratories, P.O. Box 5800, Albuquerque, New Mexico 87185.

Preliminary Quaternary geologic mapping of Midway Valley reveals that some alluvial surfaces and associated deposits are of sufficient antiquity to satisfy DOE's guidelines for evaluating surface faulting potential at the site of prospective surface waste-handling facilities. Guidelines include identifying and evaluating faults that have had a slip rate > 0.001 mm/yr during the past 100 ka. Eight alluvial surfaces ( $Q_0-Q_7$ ) and associated deposits are recognized in Midway Valley based on geologic and geomorphic mapping. The oldest surface ( $Q_0$ ) is preserved as a single terrace remnant and may be Plio-Pleistocene in age. Younger surfaces, ranging in age from early or middle Pleistocene ( $Q_1$ ) to latest Pleistocene/early Holocene ( $Q_7$ ), are preserved as stream terraces and alluvial fan surfaces. Holocene units occur as low terraces and vegetated bars ( $Q_8$ ) along active washes ( $Q_9$ ). Colluvial units of at least three ages mantle hillslopes.

02:15 p.m. Marshall, Brian D.

No 7474

A MODEL FOR THE FORMATION OF PEDOGENIC CARBONATE BASED ON STRONTIUM ISOTOPE DATA FROM SOUTHWEST NEVADA

MARSHALL, Brian D. and MAHAN, Shannon, U.S. Geological Survey, MS 963, DFC Box 25046, Denver, CO 80225

Calcareous soils are ubiquitous in arid regions such as the southwestern United States. Models describing the formation of the calcium carbonate that cements loose, porous material in these soils usually require an allogenic component for the source of the large amounts of calcium in the calcite. The isotopic composition of strontium, a common trace constituent in carbonates, is an ideal tracer for the origin of the calcium. Analyses of strontium in calcretes, fault-filling veins, rhizoliths, surface coatings, and eolian sediment near Yucca Mountain, Nevada, provide important constraints on the origin of the alkaline earths incorporated in these various surficial materials.

Calcretes, fault-filling veins and rhizoliths contain carbonate-bound (=HCl leachable) strontium with  $^{87}\text{Sr}/^{86}\text{Sr}$  averaging 0.7124. This value is significantly different from the average of 0.7117 found for carbonate-bound strontium in the surface coatings and in eolian sediment. These results lead to two conclusions: (1) calcite surface coatings on bedrock derive their alkaline earths from the eolian carbonate component and (2) the alkaline earths in calcrete and fault-filling-vein calcite are not entirely derived from an eolian carbonate component.

The strontium-isotope data suggest that some of the alkaline earth content in the pedogenic carbonate is derived from the weathering of local detritus. To test this hypothesis, isotopic analyses of the silicate detritus are in progress.

Within the volcanic bedrock of Yucca Mountain, calcite occurs as coatings on open fractures. The  $^{87}\text{Sr}/^{86}\text{Sr}$  of these calcites varies from pedogenic-type values near the surface to lower values (0.7093) at and below the water table. Some of the alkaline earths in these fracture coatings may be partially or totally derived from the volcanic bedrock, which has widely varying isotopic compositions.

These data preclude the involvement of upwelling ground water in the genesis of surficial carbonate in the immediate vicinity of Yucca Mountain.

02:30 p.m. Stuckless, J. S.

No 19828

Isotopic Evidence for a *Par* *Basalticum* Origin for Hydrogenetic Veins in Faults near Yucca Mountain, Nevada

STUCKLESS, J.S., PETERMAN, E.E., WHELAN, J.F., and MOHS, D.R., US Geological Survey, MS 963, Denver Fed. Ctn., Denver CO 80225

Vein-like deposits of calcite and opaline silica that infill faults and fractures in the vicinity of Yucca Mountain have been the center of considerable debate because the deposits occur near a possible site for the Nation's first high-level nuclear waste repository. The various proposed modes of origin for the deposits, such as catastrophic upwelling of water or downward percolating fluids related to pedogenic processes, have differing implications for the performance of a geologic repository. Isotopic data for oxygen, carbon, strontium, and uranium in the carbonate minerals exposed at Trench 14 preclude deposition from upwelling waters from either of the regionally extensive aquifers known to exist beneath Yucca Mountain. Oxygen isotopes imply deposition of calcite at unreasonably to impossibly low temperatures; strontium is too radiogenic; and uranium activity ratios are too low. Data from calcites deposited by the adjacent Ash Meadows flow system further suggest that the isotopic compositions of ground water in southern Nevada have not changed markedly during the last 60 to 600 k.y. and that, therefore, conclusions based on present-day water compositions are probably valid for at least the last 600 k.y. Isotopic compositions of the Yucca Mountain calcites are similar to those observed in secondary soil carbonates and, in combination with existing geologic, mineralogic, and paleontologic data, show that the carbonate and opaline silica deposits must have formed from descending water related to a pedogenic process.

stem Aleutian crust between ~43 and 15 Ma. After 15 Ma, small volumes of andesite and dacite were erupted on Atsu Island and throughout the western Aleutians. These strongly calcalkaline rocks are geochemically related to magnesian andesites of Phip Volcano which is located immediately behind the western-most Aleutian ridge. Phip Volcano is a hydrothermally-active seamount that has formed on small dilatational structures within the regionally transpressive regime of the modern western Aleutians. This 'leaky transform' setting is inferred to have been established at approximately 15 Ma following trans-tensional rifting and voluminous tholeiitic magmatism. The switch from tholeiitic magmatism related to a trans-tensional regime to strongly calcalkaline magmatism related to a trans-compressional regime may have resulted from clogging of the Aleutian - Kamchatka junction with buoyant, subduction-related terranes. These terranes probably originated to the east and were transported by strike-slip motion along the western arc.

Booth 27 Higman, S. L.

No 17231

APPLICATIONS OF CHAOS THEORY TO ZONING MORPHOLOGY IN MAGMATIC PLAGIOCLASE

HIGMAN, S.L. and PEARCE, T.H., Department of Geological Sciences, Queen's University, Kingston, Ontario, Canada, K7L 3N6  
The thicknesses and morphology of oscillatory zones in magmatic plagioclase from Mt. St. Helens, Washington, and St. Kitts, Lesser Antilles show sequences of ordered planar zones separated by sequences of disordered convolute zones. This pattern suggests that during crystal growth, some factor controlling crystallization in the melt changed to cause apparent periodic and chaotic zonation patterns. As a result, the zonation patterns observed suggest that plagioclase crystallization is a nonlinear dynamic process. Determining the dimensionality and functional form of the nonlinear dynamical equations represents the first step in creating a predictive model for plagioclase crystal growth.

Reconstruction of the state space of the system from the relative time-series of zone-thickness measurements reveals two types of behaviour: a spiral geometry, and a limit cycle geometry. These are indicative of a non-chaotic Hopf bifurcation.

In low-dimensional chaotic systems, the same state space can be used for prediction of the time series of zone thicknesses. Poor correlation between time-series predictions and actual zone thicknesses suggests that plagioclase growth is not governed by a low-dimensional chaotic system of equations. However, this poor correlation is not inconsistent with the Hopf bifurcation hypothesis.

The correlation dimension can be used to constrain the dimensionality of the nonlinear system controlling crystal growth. Recent workers have concluded that the data requirements for this calculation are not as extreme as previously suggested. Using the method of Grassberger and Procaccia (1983), a definitive dimension cannot be obtained from the time-series of plagioclase crystals examined to date because of the limited number of zone thicknesses observed. Consequently, a different approach is required to calculate the correlation dimension in natural systems characterized by limited data.

Grassberger, P. and Procaccia, I. 1983. Measuring the strangeness of strange attractors. *Physica 9D*, pp. 189-208.

Booth 28 Herzig, Charles T.

No 6345

CALC-ALKALINE VOLCANISM OF THE EARLY CRETACEOUS SANTIAGO PEAK VOLCANICS, NORTHERN SANTA ANA MTS., CALIFORNIA: EARLY MAGMATISM OF THE PENINSULAR RANGES BATHOLITH.

HERZIG, Charles T., Dept. of Earth Sciences, University of California, Riverside, CA, 92521.  
The results of detailed mapping, geochemistry, and the first microprobe mineral analyses of the Early Cretaceous Santiago Peak Volcanics (SPV) at their "type" locality in the northern Santa Ana Mtns yield insights into the magmatic evolution of the Peninsular Ranges batholith (PRB) during its earliest stages of emplacement. Structurally intact sequences of subaerial flows, welded tuffs, volcanoclastic breccias, epiclastic rocks, and hypabyssal intrusions are the remnants of the volcanic arc built above the batholith. Flows are dominantly basaltic andesites and andesites, with lesser basalts, dacites and rhyodacites. Major element compositions of andesites, basaltic andesites and basalts are of a low-K, calc-alkaline series. Rocks of tholeiitic affinity are also present. Cpx with a compositional range of  $Wo_{35-46}En_{33-45}Fs_{9-22}$  plots within the non-alkali field on discrimination diagrams, straddling the calc-alkaline - tholeiitic line of Lettierier and others (1982). The compositions of cpx from the SPV overlap with those from gabbros of the PRB. Calcic amphiboles from the SPV are pargasite and edenite with rare magnesio-hornblende. These compositions show limited overlap with amphiboles from gabbros of the PRB. Plagioclase crystals are dominantly labradorite-bytownite (overall range is  $An_{50-59}$ ). Opx is completely altered to chlorite, part of a greenschist facies alteration assemblage present in all rocks. The field setting, abundance of andesitic compositions and calc-alkaline affinity of the rocks is consistent with an origin of the SPV as a volcanic arc constructed at or near the margin of North America.

Booth 29 Durant, Dolores G.

No 17194

CRYSTAL SIZE DISTRIBUTION STUDIES IN SPANISH PEAKS, COLORADO

DURANT, Dolores G. and CLIFFORD, Paul M., Dept. Geology, McMaster University, Hamilton, Ont. L8S 4M1  
The Spanish Peaks (SP) dual intrusions of southern Colorado, their surrounding radial dyke swarm and several related plugs form a spectacular volcanic complex in the Rio Grande Rift.

To shed light on the crystallization history of some Rio Grande magmas, petrographic relationships and crystal size distribution (CSD) have been examined for opaques, olivine, and augite from a gabbroic dyke of Huerfano Butte (HB) and feldspars and opaques from a "rhyolitic" dyke of the SP swarm.

CSD plots for HB augite and HB opaques yield straight lines with steep negative slopes. These are consistent with constant, continuous growth and nucleation during crystallization, as well as no crystal fractionation during emplacement and size independent growth.

Similar plots for HB olivine, SP feldspars, and SP opaques yield asymmetric bell curves indicating fines depletion. HB olivines show resorption features on all grain sizes. The resorbed material was possibly redeposited as HB augite; this may explain the higher slope values for HB augite compared to HB opaques. SP opaques also show loss of material due to resorption.

SP phenocrystic feldspars near the dyke boundary lack resorption features whereas SP xenocrystic feldspars show resorption throughout the dyke. The absence of fines for both populations could be due to sorting of the crystals in a magma chamber perhaps by neutral density buoyancy or by magma movement within the chamber. Decreasing CSD slopes across the SP dyke for both SP feldspars and SP opaques are probably due to thermal and chemical disequilibrium towards the centre of the dyke.

Booth 30 Cascadden, T. E.

No 25911

INTERMEDIATE AND MAFIC VOLCANIC ROCKS OF THE NORTHERN WHITE HILLS, ARIZONA: IMPLICATIONS FOR THE PRODUCTION OF INTERMEDIATE COMPOSITION VOLCANIC ROCKS DURING REGIONAL EXTENSION

CASCADDEN, T.E., Dept. of Geology, University of New Mexico, Albuquerque, NM 87131  
SMITH, E.L., Dept. of Geoscience, University of Nevada, Las Vegas, NV 89154

The generation of intermediate composition igneous rocks during regional extension is commonly ascribed to the commingling of mafic and felsic magmas on the basis of geochemical, petrographic and field evidence. In the Lake Mead area of the northern Colorado extensional corridor, magma commingling produced intermediate composition calc-alkaline lavas and associated phonons in the Black Mountains, Arizona and River Mountains, Nevada. However, in some areas of the Basin and Range, thick sections of mafic to intermediate volcanic rocks lack the petrographic, field and chemical evidence for commingling. An example of such an area is the northern White Hills (NWH), northwestern Arizona, the easternmost exposure of mid-Tertiary igneous rocks at the latitude of Las Vegas.

The NWH contains three mid-Miocene mafic to intermediate volcanic centers. Lavas are subalkalic to alkalic and vary in composition from basalt (46-52% SiO₂) to basaltic trachyandesite (52 to 57% SiO₂) to trachyandesite (57-61% SiO₂). Na₂O+K₂O varies from 4-8%; rocks have not been subjected to K-metasomatism. Each volcano is composed of chemically and petrographically distinct magmas. The three magma types are unrelated by fractionation, contamination or AFC. Incompatible trace elements (Hf, Th, LREE) show small but significant differences. However, compatible trace elements (Co, Cr, Sc, V) concentrations for the most primitive samples of each magma type are similar. All lavas contain olivine as an equilibrium phase. Variation within magma types is explained by fractionation of olivine or olivine-clinopyroxene-plagioclase.

These observations suggest that the intermediate volcanic suites in the White Hills were derived by partial melting of chemically different, but mineralogically similar sources. Because olivine is an equilibrium phase in the three magma types, it must have been on the liquidus in the source. We suggest that the most likely source for NWH magmas is spinel peridotite. High Sr contents (856-1300 ppm) argue against crustal contamination. This model is similar to that proposed by Barker and Thompson (1989) for the alkalic lavas of the Hamblin-Cicopatra volcano (to the northwest of the NWH) but contrasts with the magma commingling models proposed for the compositionally heterogeneous volcanic rocks of the River and Black Mountains. Therefore, in the Lake Mead area two independent processes (partial melting and magma commingling) were responsible for the production of intermediate composition igneous rocks during mid-Miocene extension.

Booth 31 Hoch, Anthony R.

No 23712

PETROGRAPHIC EVIDENCE FOR MIXING OF ALKALINE AND SUB-ALKALINE MAGMAS IN THE RATTLESNAKE HILLS INTRUSIVE COMPLEX, CENTRAL WYOMING.

HOCH, Anthony R.; MYERS, James D.; FROST, Carol D., Dept of Geology and Geophysics, University of Wyoming, Laramie, WY 82071.

The Rattlesnake Hills of central Wyoming host Eocene intrusions and extrusive bodies of quartz-normative rhyolite and quartz latite. These are spatially divided into two groups: the eastern felsic group (EFG) and the western felsic group (WFG). Nepheline-normative phonolites, trachytes and lamprophyres comprise the central alkalic group (CAG), which is located between the EFG and WFG.

Although the EFG and WFG rocks have similar bulk-rock chemical compositions, they are petrographically different. The EFG rocks (plag+hb+ap+mt+/-qtz) are coarsely porphyritic (phenocrysts up to 7 mm) with unzoned oligoclase

Booth 85 Wild, Steve

No 24719

## REMEDICATION OF PETROLEUM HYDROCARBON-CONTAMINATED GROUND WATER AND SOIL USING IN-SITU AIR SPARGING AND ACTIVE SOIL WASH EXTRACTION AT LUST SITES IN NEW MEXICO.

WILD, Steve, New Mexico Environment Dept., 1190 St. Francis Dr., Santa Fe, NM 87503; BILLINGS, Jeffrey F., Billings & Assoc., Inc., 3816 Academy Pkwy N-NE, Albuquerque, NM 87109; BROWN, William J., Albuquerque Environmental Health Dept., P.O. Box 1293, Albuquerque, NM 87103; ARDITO, Cynthia F., Inters, Inc., 8100 Mtn. Rd. NE, Albuquerque, NM 87110

As part of the New Mexico Environment Department's (NMED's) efforts to locate and evaluate cost-effective and efficient remediation technologies for leaking underground storage tank (LUST) sites, NMED has been closely tracking the development of an in-situ remediation technology called the Surface Volatilization and Ventilation System (SVVS, patent pending, 1989).

The SVVS consists of a series of well nests which are installed within the areas of soil and ground-water contamination at LUST sites. Each well nest consists of a vapor extraction well screened within the vadose zone and an air-injection well screened below the water table.

The SVVS utilizes three remediation processes: vadose zone vapor extraction (in-situ ventilation); air sparging of the saturated zone (in-situ air stripping); and enhanced microbial biodegradation.

The SVVS has proven very effective in the remediation of LUST sites in New Mexico where a shallow water table exists. Significant reductions in benzene, toluene, ethylbenzene, and xylenes (BTEX) have been observed over relatively short time spans. SVVS treatment has been demonstrated to be an extremely efficient remediation technology when compared to conventional pump and treat systems.

Booth 96 Wyatt, D. E.

No 28605

## SOIL GAS GEOCHEMICAL SAMPLING AS A METHOD OF GROUNDWATER FLOW DETECTION AT THE CHEMICALS, METALS AND PESTICIDES PITS (CMP PITS) AT THE SAVANNAH RIVER SITE.

WYATT, D. E., BLOUNT, G. C., PRICE, V., Westinghouse Savannah River Company, P. O. Box 616, Aiken, SC 29801; PIRKLE, R. J., MicroSeeps Ltd., 220 William Pitt Way, Pittsburgh, PA 15238.

The CMP Pits consisted of two parallel trenches used for disposal of oil, organic solvents, pesticides and metals during the years 1971 through 1979. The disposal area is centrally located within the Savannah River Site on a topographic high. In 1984, the waste was removed, the contaminated soil excavated and 20 groundwater monitoring wells were installed in an effort to monitor, remediate and close the site. Minor organic plumes are known to exist in the shallow aquifers.

Recent soil gas surveys, in support of a RCRA/CERCLA integrated investigation identified elevated concentrations of organics in areas away from the disposal site and different from the presumed groundwater flow directions. Groundwater flow directions at the site are to the north for the shallow aquifer and towards the disposal area from the north, south and east for the deeper aquifer. Geological data from monitoring wells suggests that a carbonate zone underlying the disposal area may affect localized groundwater flow.

Soil gas survey data identified contaminated groundwater plumes emanating from the site but not predicted by monitoring wells. Data indicates that soil gas surveys may be utilized to refine groundwater flow directions in areas where complex shallow aquifers are contaminated with volatile organics.

The information in this abstract was developed during the course of work under contract DE-AC09-89SR18035 with the U.S. Department of Energy.

SESSION 98, 1:30 p.m.

TUESDAY, OCTOBER 22, 1991

## T 25: CENOZOIC EXTENSION IN THE CORDILLERA: GEOMETRY, TIMING, MECHANISMS, AND REGIONAL CONTROLS (PART II)

SDCC: Room 16AB

01:30 p.m. Metcalf, Rodney V.

No 26750

## HORNBLENDE GEOBAROMETRY FROM MID-MIOCENE PLUTONS: IMPLICATIONS REGARDING UPLIFT AND BLOCK ROTATION DURING BASIN AND RANGE EXTENSION.

METCALF, Rodney V., and SMITH, Eugene L., Department of Geoscience, University of Nevada, Las Vegas, Nevada 89154

Al₂O₃-hornblende geobarometry was used to determine the depth of crystallization for two Miocene age plutons, Wilson Ridge (WRP) and Mt. Parkins (MPP), from the northern Colorado River extensional corridor. The WRP exhibits a hypabyssal cap to the north and extends 30 km to the south where it intrudes Precambrian gneisses. North trending faults and dikes indicate the WRP has experienced east-west extension. The MPP intrudes Precambrian gneiss with a hypabyssal cap to the west and extends 1.5 km east where it is cut by the low-angle Mockingbird Mine fault (Faulds, 1957). North trending dikes suggest some east-west extension of the MPP. Paleomagnetic data suggest no tilt for WRP and 50° west tilt for MPP (Faulds, 1957). Both plutons range in composition from monzodiorite to quartz monzonite. Evidence of magma commingling and large angular blocks of older hornblende diorite occur in both plutons. Hornblende zoning profiles reveal complex growth histories. For this reason individual analyses rather than averages were used in geobarometry calculations. Small anhedral interstitial grains yield anomalously low Al contents and pressures and represent grains isolated from coexisting phases required by the geobarometer. Some rims of larger euhedral grains also exhibited low Al contents and were avoided. Analyses used in calculations were taken from areas of relatively uniform composition within about 50 microns of grain edges. Using multiple grains in each, three samples of quartz monzodiorite and one bi-modal diorite from the southern end of WRP yield similar results with Al₂O₃-total (based on 23 oxygens) of 1.15 to 1.3. This yields pressures ranging from 1.49 to 2 kbars and depths of 4.9 to 6.7 kms. Averaging these results (n=10) yields P=1.6 ± 0.3 kbars and a depth of 5.3 ± 0.9 kms. A single sample of WRP monzodiorite from 10 kms south of the hypabyssal cap yields Al₂O₃-total=1.82; P=6.85; and a depth of 2.8 kms. Assuming rotation about a horizontal east-west axis these results are consistent with 15° ± 3° of northward tilt. Rotation of WRP must have occurred as temperatures cooled from the solidus to the Currie point. Multiple grains from two samples of quartz monzodiorite from the eastern end of the MPP yield Al₂O₃-total of 1.81 to 1.3; pressures of 6.31 to 1.3 kbars; and depths of 2.7 to 4.4 kms. Averaging these results (n=4) yields P=1.1 ± 0.3 kbars and a depth of 3.6 ± 0.7 kms. This result is consistent with a westward tilt of 35° ± 9° provided that the Precambrian-Late Tertiary unconformity, 3 km west of the apex of MPP, was the surface at the time of intrusion. We infer that some or all of the rotation of the MPP occurred below the Currie temperature.

01:45 p.m. Anderson, R. E.

No 16613

## RELATIONSHIP BETWEEN MIOCENE PLUTONISM, UPLIFT, AND EXTENSION, LAKE MEAD AREA, NORTHWESTERNMOST ARIZONA AND ADJACENT NEVADA

ANDERSON, R.E., and BARNHARD, T.P., U.S. Geological Survey, Box 25046, MS 966, DFC, Denver, CO, 80225

The Lake Mead area can be added to the growing list of areas in the Cordillera that expose evidence for a close association between Cenozoic plutonism and extension. The Wilson Ridge pluton in the northern Black Mountains is a north-broadening, triangular, composite, epizonal mass, about 20 km on each edge, that was emplaced into Proterozoic crystalline rock and Paleozoic and Cenozoic cover rocks during late Miocene time. Petrogenetic studies by Larson and Smith (1990, JGR, v. 95, p.17693) indicate that it formed by commingling of a large volume of mafic magma with a smaller volume of felsic magma. The pluton is tilted about 5 degrees north, exposing its hypabyssal zone and roof in the north and its deeper parts in the south.

The extent of preintrusion Cenozoic deformation is best evaluated in the north, where the pluton intrudes Miocene sedimentary and volcanic rocks. Those rocks show a mild to moderate degree of preintrusion tilting that increases southward. The pluton there consists of thousands of dikes that record 8-15 km of synemplacement extension-related tilting in an approximately east-west direction. This tilting by dike-on-dike emplacement was accompanied by a southward-increasing degree of synemplacement extension-related tilting. In the northernmost part of the pluton, dikes are mostly vertical and preintrusive strata dip gently. By contrast, directly south of Lake Mead, preintrusive volcanic strata are subvertical, main-phase dikes dip at moderate angles, and late dikes are subvertical, indicating protracted pre- and syn-intrusion extension-related tilting events that ended with plutonism. The country rocks and pluton were tilted away from and downfaulted toward the axis of the pluton in these events, suggesting extensional collapse of the growing, rising pluton and of the rising Black Mountains structural block. Contrary to current models of extensional deformation in the area, we find no evidence that the northern Black Mountains served as a source terrane for west-transported extensional allochthons.

T  
U  
E

pm

E. I.  
Smith



**Tercera Reunión Nacional  
"Volcán de Colima"  
Segunda Reunión Internacional  
de Vulcanología**

---

**"Volcán de Colima"  
Third National Reunion  
Second International Reunion  
on Volcanology**

*Resúmenes / Abstracts*

---

## Volcanic risk assessment studies for the proposed high-level radioactive waste repository at Yucca Mountain, Nevada, U.S.A.

---

*Eugene I. Smith, Daniel L. Feuerbach, Terry R. Naumann,¹ Ho, Chih-Hsiang²*

Volcanic hazard studies by the Center for Volcanic and Tectonic Studies related to the proposed high-level radioactive waste repository at Yucca Mountain, Nevada have concentrated on producing a synthesis of Late Miocene to Quaternary basaltic volcanism in the southern Great Basin. To obtain a regional perspective of basaltic volcanism, detailed mapping and sampling of analog systems as well as volcanic centers within 50 km of the proposed repository have been completed. Important advances from these studies include the documentation of detailed chronostratigraphy within volcanic fields and development of geochemical models for the genesis of alkalic mafic magmas within continental rift environments. These data in combination with studies of the structural controls on the emplacement of mafic magmas have led to the determination of an area of most recent volcanism (AMRV) near Yucca Mountain. Data from volcanic centers within the AMRV are being used to estimate recurrence rates and conditional probability of future volcanism for risk assessment. The AMRV includes ten eruptive centers and encompasses all post-4 Ma volcanic complexes within

50 km of the proposed repository. High-risk rectangles were constructed at each cluster of Quaternary centers within the AMRV. The size, shape and orientation of these high-risk zones is based on structural and volcanic studies in the AMRV as well as in analog volcanic fields. The proposed waste repository lies within one of the risk rectangles associated with the Lathrop Wells volcano.

The possible recurrence of volcanic activity in the AMRV was evaluated by estimating the instantaneous recurrence rate using a nonhomogeneous Poisson process with Weibull intensity and by using a homogeneous Poisson process to predict future eruptions. Based on data from Quaternary data, the estimated instantaneous recurrence rate for volcanism is about  $5.5 \times 10^{-4}$ /year. We conclude that the estimated probability of at least one eruption occurring in the AMRV in the next 10 000 years is about 5 percent.

---

1. Center for Volcanic and Tectonic Studies, Department of Geoscience, University of Nevada, Las Vegas, Nv 89154, USA.  
2. Department of Mathematical Sciences, University of Nevada, Las Vegas, Nv 89154, USA.

Available U-Pb zircon ages and our new Sm-Nd whole-rock isochrons indicate that metamorphism in the Adirondacks occurred between 1155 and 1100 Ma. The rocks were subsequently metamorphosed to granulite facies between 1100 and 1050 Ma. The duration of about 100 million years between the inception of plutonism and cessation of metamorphic overprint constitutes the Adirondack Crustal Accretion-Differentiation Superevent (CADS). The Adirondack CADS represents just one of the many crustal accretion and mantle differentiation events during the middle Proterozoic (1.1-1.6 Ga) that may have increased the Sm/Nd ratio of the Earth's depleted mantle reservoir by about 10 percent.

04:00 p.m. Owens, B. E.

**THE LABRIEVILLE MASSIF, QUEBEC: A HIGHLY "EVOLVED", ~1.8 GA, POST-OROTHOSITIC ANORTHOSITE-LEUCOGABBRIO-JOTUNITE SUITE.**  
OWENS, B.E., TUCKER, R.D., BRANNON, J.C., PODOSEK, F.A. and DYMEK, R.F., Dept. of Earth and Planet. Sci., Washington Univ., St. Louis, MO 63130

Despite the fact that the Labrieville anorthositic complex (LBV) is found in the central high-grade granulite terrane of the Grenville Structural Province, it is an unmetamorphosed and unaltered plutonic body. LBV consists of four main units: [1] a domal core zone of coarse pink anorthosite (plag + opx + ilm), containing minor leucocratic and a small ilmenite-bearing gabbroic sheet, typically at the boundary between 1 and 2 (see *Canad. Mineral.* 30, 163-190); and [4] fine-grained, green jotunite (=pyroxenodiorite, but enriched in ilm, mgst, apatite and zircon) found as an extensive dike in core anorthosite, and at the SW margin of the complex. Despite these differences in color, texture and mineralogy, several features suggest that these units are cogenetic and possibly comagmatic. For example, they contain highly alkalic plagioclase (e.g.,  $-\text{An}_{30}\text{Or}_{12}$  in anorthosite; mesoperthite in jotunite), and there is a progression in mineral compositions (decreasing An in plag and En in pyrox) from anorthosite to leucogabbro to jotunite. In addition, all units have extreme levels of Sr and Ba (e.g., ~2000 and ~1000 ppm Sr, and ~1000 and ~2700 ppm Ba, in anorthosite and jotunite, respectively).

U-Pb ( $^{207}\text{Pb}/^{206}\text{Pb}$ ) zircon ages confirm the near contemporaneity of leucogabbro (1008 ± 2 Ma) and jotunite (1010 ± 2 Ma). In contrast, metamorphic zircon in pyroxene-amphibolite from adjacent country rock gneiss yields an older age of 1016 ± 2 Ma, which may date the timing of regional Grenvillian metamorphism or the effects of contact metamorphism related to an early phase of anorthositic intrusion. At any rate, these dates clearly indicate that LBV is one of the youngest massifs in the Grenville Province, and confirm that it was emplaced late relative to Grenville orogenic events. We suggest that there may be a correlation between the post-orogenic nature of LBV and its "evolved" character, perhaps as a result of the doubling of crustal thickness during the Grenville.

Sm-Nd isotopic data also support a comagmatic relationship between leucogabbro ( $t_{\text{DCHUR}} = 1010 \text{ Ma} \pm 1.9 \pm 0.3$  on a plag megacryst) and jotunite ( $t_{\text{DCHUR}} = +1.7 \pm 0.3$ ). Core anorthosite ( $t_{\text{DCHUR}} = +0.8 \pm 0.3$ ), however, cannot be strictly comagmatic with the other units, although it could have been derived from an isotopically equivalent source if it is as old as ~1070 Ma. At present, it is unclear whether these differences in Nd isotopic compositions reflect different ages, sources or contamination effects.

04:15 p.m. Rockow, Michael W.

**FINE-GRAINED ENCLAVES IN JOTUNITE AND MANGERITE, MORIN COMPLEX, QUEBEC: NEW CLUES FOR MASSIF ANORTHOSITE PETROGENESIS?**

ROCKOW, Michael W. and DYMEK, Robert F., Department of Earth and Planetary Sciences, Washington University, St. Louis, MO 63130

Fine-grained "macromafic" enclaves (FGE), although common in granites worldwide, appear to have never before been recognized in granulite rocks associated with massif anorthosite. However, at the Morin Complex, FGE are widespread in the jotunite and mangerite units (pyroxene monzonite and pyroxene quartz monzonite, respectively), where they comprise up to a few % of individual outcrops. FGE are small (~3 x 5 cm), have elliptical to rounded cross-sections, are homogeneous with a distinctive "ink and pepper" appearance, and exhibit sharp contacts against their hosts. Eight FGE-host pairs (four from each unit) have been studied petrographically. FGE exhibit fine-grained polygonal inquisitorial textures - very different from their hosts, which are coarse-grained, foliated rocks characterized by elliptical feldspathic domains separated by stress-lined mafic aggregates. The mineralogy of hosts and FGE is the same (plag + opx + cpx + hbl + ilm + mgst + Kf + qtz + ap + cr ± bio ± gr). Mineral compositions (determined by microprobe analysis) vary widely in the sample suite (plag:  $\text{An}_{45}\text{Ab}_{55}$  in jotunite vs.  $\text{An}_{35}\text{Ab}_{65}$  in mangerite; opx:  $\text{En}_{57}\text{Fs}_{43}$  vs.  $\text{En}_{51}\text{Fs}_{49}$ ; cpx:  $\text{Ca}_{17}\text{Mg}_{27}\text{Fe}_{25}$  vs.  $\text{Ca}_{16}\text{Mg}_{23}\text{Fe}_{21}$  vs.  $\text{Ca}_{15}\text{Mg}_{21}\text{Fe}_{19}$ ), but variations in each sample are small (of mole%). Most importantly, mineral compositions are essentially the same in each host-FGE pair. Major and trace element compositions have been determined for two host-FGE pairs (one from each unit) by XRF and ICP methods. The FGE in the jotunite has a basaltic composition (52.4 wt%  $\text{SiO}_2$ , 6.5 wt%  $\text{MgO}$ ) and is more siliceous than its host (46.8 wt%). The FGE in the mangerite contains 58 wt%  $\text{SiO}_2$  and is less siliceous than its host (63.9 wt%). The concentrations of many trace elements (Rb, Sr, Zr, Hf, Nb, Ta, Ba, Pb, Th and U) in FGE and host are similar. For example, Rb contents of the jotunite host-FGE pair are low (1.8 ppm and <2.6 ppm, respectively), while those in the mangerite host-FGE pair are high (90 ppm and 94 ppm). The jotunite FGE has low REE abundances (~15X chondrites), a flat pattern ( $\text{La}_N/\text{La}_N = 1.5$ ) and a positive Eu anomaly ( $\text{Eu}/\text{Eu}^* = 1.8$ ), while its host has higher concentrations ( $\text{La}_N = 60X$ ), a fractionated pattern ( $\text{La}_N/\text{La}_N = 3$ ) and no Eu anomaly. The mangerite and its FGE both have high REE concentrations ( $\text{La}_N = 200X$ ) and fractionated patterns ( $\text{La}_N/\text{La}_N = 6$ ); both also have negative Eu anomalies ( $\text{Eu}/\text{Eu}^* = -0.9$  &  $-0.6$ ). We suggest that the FGE represent disaggregated globules of mafic liquid introduced into the magma chamber that was evolving to produce the jotunites and mangerites. This mafic liquid was progressively modified by liquid-liquid interaction during crystallization-differentiation of the host, resulting in the variable compositions of the FGE and the close agreement of trace element abundances between FGE and host. FGE may represent samples of the elusive mafic component invoked as being important to the petrogenesis of anorthosites.

04:30 p.m. Seaman, S. J.

**MAGMA MINGLING AND MIXING IN THE ROOTS OF A PROTEROZOIC ISLAND ARC: THE MINNEHAHA MAGMATIC COMPLEX, CENTRAL ARIZONA**

SEAMAN, S.J., and WILLIAMS, M.L., Dept. of Geology and Geography, Univ. of Massachusetts, Amherst, MA 01003; HEKRON, P.M.; O'BRIEN, J.A.; and COLLIER, S.A., Geology Dept., Colgate Univ., 13 Oak Dr., Hamilton, NY 13346

The Minnehaaha magmatic complex is a ~1720 Ma composite intrusive terrane which preserves evidence for large-scale mingling of granitic and basaltic magmas, and the in-situ synthesis of intermediate composition magma. The complex is bounded on the north by the Crooks Canyon granodiorite, on the east by a septum of ~1740-1720 Ma metasedimentary rocks, on the south by the ~1682 Ma (Chamberlain and Bowring, pers. comm.) Horse Mountain pluton, and on the west by an unnamed very coarse-grained granite. Four main lithologies are represented in the complex: a K-spar megacrystic granite (megacrysts to ~5 cm long), a hornblende basalt, a hornblende diorite, a coarse-grained, spotted rock with plagioclase-dominated matrix hosting spherical accumulations of hornblende crystals. The diorites lie compositionally on mixing lines between the granite and the basaltic end members. The spotted rocks are enriched in Ca, Mg, and Cr relative to the basalts and may be cumulates separated early from basaltic magma. In addition to these four lithologies, a variety of fine-grained hybrids representing mixing of large proportions of basalt and small proportions of granite are common.

Textures preserved in the complex provide abundant evidence that the K-spar megacrystic granitic magma and the basaltic magma were contemporaneously partially liquid. Thick accumulations of deformed, mushroom-shaped droplets of basalt (to 1m diameter), surrounded by megacrystic granite, probably represent droplets of basaltic magma injected into the granitic magma chamber. K-spar megacrysts in the granite are progressively resorbed and digested with increasing proximity to basaltic droplets.

The Minnehaaha complex is one of several magmatic centers in the Big Bug block of the Yavapai province. The block may have been a Proterozoic compressional, subduction-related complex. The textures and compositions of the complex suggest that granite/basalt hybridization contributed heavily to the production of intermediate magmas in the arc complex. The basalt may represent a hydrous partial mantle melt which provided heat for anatexis of crustal material to generate felsic orogenic plutons.

04:45 p.m. Metcalf, R. V.

**THE MT. PERKINS PLUTON: SHALLOW-LEVEL MAGMA MIXING AND MINGLING DURING MIOCENE EXTENSION**

METCALF, R.V., SMITH, E.L., NALL, K.E., and REED, R.C., Department of Geoscience, University of Nevada-Las Vegas, Las Vegas, NV 89154

Generation of intermediate magmas during crustal extension is an important question. The Miocene Mt. Perkins Pluton, AZ, within the Colorado River Extensional Corridor is a complex, compositionally expanded body and provides an ideal laboratory for such a study. The pluton was formed by multiple dike-on-dike emplacement events which are divided into four phases (P1-P4): the oldest, P1, is a coarse-grained hbl gabbro (49 wt%  $\text{SiO}_2$ ); P2 is a medium-grained, hbl-d and biotite-bearing qtz monzonite (53-61 wt%  $\text{SiO}_2$ ); P3 is a fine-grained biot (hbl) granodiorite (63-73 wt%  $\text{SiO}_2$ ); and P4 is a suite of aphanitic plagioclase dikes (widths of cm to 3 meters) of mafic, intermediate, and felsic compositions. Al-in-hbl geobarometry on samples from P2 and P3 give similar results,  $P = 6.3 \pm 0.25$  kbars, yielding a crystallization depth of 2.3 ± 0.96 km.

Hbl-d qtz diorite (51-63 wt%  $\text{SiO}_2$ ) mafic microgranitoid enclaves (MME), ranging in size from a few cm to several meters, are abundant in P2 and P3 rocks and in some intermediate dikes of P4. MME microstructures (ovoid pillow-like shapes with crystalline margins that are finer grained than interiors) and microstructures (lath-shaped plagioclase with complex internal subhedral zoning; minute subhedral plagioclase grains poikilolitically enclosed in dendritic apatite in fine-grained margins; acicular apatite grains) indicate that MME formed as globules of hotter mafic magma quenched within cooler, more felsic magma. Linear trends on major element Harker variation diagrams and hyperbolic trends on major-trace element ratio plots indicates a magma mixing origin for intermediate rocks of P2 and P3. P3 granodiorite host served as the felsic mixing end member. P1 gabbro falls off the mixing trends and is not the mafic end member for mixing; modeling suggests the MME are not related to the gabbro by fractional crystallization. In both P2 and P3 MME, embayed plagioclase and cpx are poikilolitically enclosed in larger feldspar grains, and hbl grains are mantled by biotite. These features indicate that the MME is not the mafic mixing end member but is also a hybrid formed by magma mixing. Features indicative of advanced mechanical mixing (mafic schlieren, disrupted mafic dikes, magmatic flow structures) are absent at the current exposure indicating that mixing (hybridism) occurred at depth. Studies at Mt. Perkins indicate that compositionally expanded suites formed during Miocene extension are the result of magma mixing.

1538h

Footwall Uplift Recorded in a Supra-detachment Basin: The Miocene Shadow Valley Basin.

John Engdram and Douglas W Burbank (Dept. of Earth Sciences, Univ. of So. Cal., Los Angeles, CA 90089-3070 213-740-6119)

Temporary models for sedimentation in extensional basins do not accurately reflect the depositional and tectonic evolution of basins of highly extended terrain. Traditional models describing a half-graben fault geometry, usually with a steeply dipping bounding fault, hanging-wall sourced sedimentation, and a depocenter along the main basin extension, are appropriate for continental rifts such as the East African Rift, East Africa, and modern Death Valley. In contrast, ongoing research in the Miocene Shadow Valley Basin, which formed above the low-angle Halloran Range detachment, describes a very different tectonic package. Basin sedimentation there was controlled (1) by a depocenter at least 30 km from the active normal breakaway, and (2) by footwall-sourced sedimentation. These features seem present in other supra-detachment basins, e.g. Sacramento Mtns. and Yerington.

Key differences between the stratigraphic holoypes can be attributed to active uplift of the detachment footwall during extension. This active uplift operates in addition to and is distinct from passive isostatic uplift due to tectonic unloading. Active uplift enlarges the footwall catchment, facilitates active transport of footwall sourced sediments, and defines the depocenter from the breakaway. Additional features, such as large (> 30 m) intrabasin paleocanyons, overbank bypassing, abundant rock avalanche deposits, and debris-bearing alluvial fans > 40 km from their source may be a product of active footwall uplift. Such uplift could be driven by rotation above a lower detachment, thermal anomalies, magma and heat advection, or isostatic uplift of an unroofed root. For the Shadow Valley system, magma/heat advection and rotation above a lower structure appear to be most likely.

1545h

Sharp Change in Tectonic Style Along the Northeastern Front of the Sierra Nevada Uplift at Constantia, CA

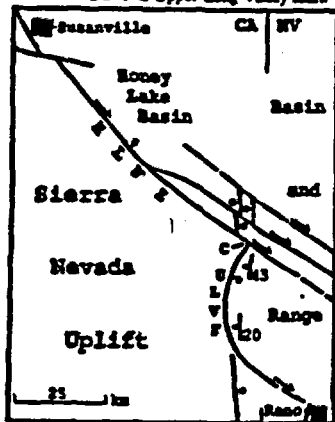
L.T. Grosse (Dept. of Geology and Geological Engineering, Colorado School of Mines, Golden, CO; 303-273-3806)

Three km SE of Constantia, CA along Hwy. 395, 30 km W of Reno, occurs a simple and local (as opposed to messy or smeared out) 90° intersection of the NW-trending Honey Lake right-slip fault and the NE-trending Upper Long Valley normal fault. This tectonic junction accommodates a profound and remarkably abrupt change in the two tectonic styles that characterize the NE and E front of the Sierra Nevada Uplift in NE California.

To the N of the Constantia junction faults of the Honey Lake fault zone (part of the Walker Lane) are associated with the small pull-apart depression of Lower Long Valley of normal faults dipping steeply to the W into the deep Honey Lake basin. To the S of the Constantia junction is the very different tectonic domain of Upper Long Valley.

The Valley is underlain by a two-km-thick section of siltstone, sandstone, boulder conglomerate, and diatomite of the Upper Miocene Hallelujah Formation. The formation dips moderately W into the 45° E-dipping Upper Long Valley fault, a listric normal fault breakaway that characterizes the Sierra Nevada front in this area. The internal structure of the fault zone is extraordinarily well exposed revealing large massed, up to 1-km thick, of variously embayed and sized granitic rocks.

Figure below: C is Constantia tectonic junction. Lines are strike with relative displacement indicated. HLZF is Honey Lake fault zone. ULVF is Upper Long Valley fault.



732F-10 1628h

Plutonism and the Origin of Metamorphic Core Complexes

G.S. Lister (Victorian Institute of Earth and Planetary Sciences, Department of Earth Sciences, Monash University, Melbourne, Victoria, 3168 Australia) S.L. Baldwin (Department of Geosciences, University of Arizona, Tucson, Arizona 85721)

Phases of ductile deformation have taken place in mylonites of the lower plates of many core complexes during short lived thermal events caused by the heat input from intruded plutons, sills or dikes. Fast cooling inferred from argon thermochronology is not the result of rapid erosional or tectonic denudation, but rather due to rapid cooling in the thermal aureoles of sills intruded at shallow crustal levels. Isothermal decompression paths inferred from thermobarometric data may actually link trajectories of P-T points set by transient mineral growth in thermal aureoles formed during periods of igneous activity. The upper levels of many core complexes may have been at relatively shallow crustal levels before the onset of magmatism triggered ductile behavior. The implications of these observations are numerous. Intrusion may be the underlying reason for footwall uplift, rather than isostasy as described by Spencer (1994), and Wernicke and Axen (1988). The mylonite front may be a transient phenomenon. Plutonism may be linked to the formation of detachment faults, and the ductile-to-brittle transition observed in many core complexes may be the result of cooling in a ductile shear zone above a pluton, and is not necessarily a depth dependent transition.

732F-11 1615h

Extent of the Rio Grande Rift in West Texas

Julia L. Whitclaw, Michael Whitclaw, G. R. Keller (Department of Geological Sciences, The University of Texas at El Paso, El Paso, TX 79968)

The Rio Grande rift is a Cenozoic feature which extends southward from Colorado through New Mexico and into West Texas and northern Mexico. The southern extent of the rift in West Texas and northern Mexico is currently being studied using gravity and drill hole data. The sources of many low gravity anomalies in the area, which trend NW-SE and N-S are generally attributed to rift basins with substantial amounts of low density alluvial fill. Gravity models and drilling results across the Hueco Bolson reveal three structurally complex, asymmetric sub-basins containing approximately 3 km of late Cenozoic fill. Similar studies of the Salt Flat Graben and the Presidio Bolson also indicate complex rift basins with varying amounts of fill.

This paper presents the results of geophysical studies of Eagle Flat, a NW-SE trending alluvial valley approximately 125 km southwest of El Paso, Texas. Models from gravity and drill hole data suggest that the predominant source of a linear negative gravity anomaly results from thickened sections of Miocene sedimentary rocks, rather than a major Tertiary basin as previously suggested. There is a small Tertiary basin associated with Eagle Flat and the gravity models and drill hole data indicate that it deepens to the southwest. Paleomagnetic studies of cores drilled to Cretaceous bedrock in the Eagle Flat basin indicate that sedimentation was initiated in the NW portion of the basin 4.5-3.0 myr ago. As the longest core studied was only 250 feet in length, this implies a low average sedimentation rates and a relatively quiescent late Tertiary tectonic history for the basin. Regional gravity anomalies indicate a broad N-S trending block which may have resisted Rio Grande rift Basin and Range tectonics.

732F-12 1638h

Evidence from monoliths for recent thermal reactivation of the southern Rio Grande rift

Mark R. Reid (Dept. Earth & Space Sci., UCLA, CA 90024-1567)

The southern Rio Grande rift is characterized by thinned crust, intermediate to high heat flow (> 80 mW/m²), and anomalous upper mantle Pn velocities (< 7.3 km/s) reflecting relatively recent crustal extension and advective heat transport. P-T conditions recorded by monoliths from El Boqueron Hole, southern New Mexico, define a geotherm that exhibits a thermal bulge between depths of at least 20 and 30 km. Mafic intrusion of the lower crust and upper mantle during mid-Tertiary (30-20 Ma) extension can account for both the present geophysical characteristics of the rift and the apparent geotherm if the granulite temperatures reflect conditions frozen in during thermal relaxation of the lower crust (Bissel and Williams, 1991).

Temperatures for the granulite monoliths determined using each of the ternary feldspar endmembers are often remarkably concordant (ΔT < 15°C) between 800 - 900°C, requiring high temperatures of feldspar equilibration and subsequent quenching at rates like those inferred for volcanic rocks. Sr and Nd mineral isochrons for these lithologies representing Proterozoic crust are generally < 2.5 Ma and give a weighted average of ~4 Ma; minerals separated from a strong isochron gradient yield the only apparent exception (t = 34 Ma). Consequently, the granulite monoliths record conditions associated with thermal reactivation of the lower crust by Phanerozoic crustal extension.

The inverse correlation between isochron age and diffusion rate of the slowest diffusing species that is expected of cooling through closure temperatures of ~900°C is not observed. Rather, the late Tertiary ages of the mineral isochrons can be explained by radioactive decay concomitant with contemporary diffusional exchange in the lower

crust. Together with evidence for quenching at nearly 1 between ternary feldspar components, current temperatures in excess of 800°C are indicated for the lower crust. Relatively recent intrusion of the lower crust, perhaps associated with increased regional volcanism in the past 5 Ma, is suggested.

732F-13 1645h

Geochemical Fingerprinting of Progressive Extension in the Colorado River Extensional Corridor, USA: A Preliminary Report

D.L. Fouch (University of Iowa, Iowa City, IA 52242); E.I. Smith (University of Nevada, Las Vegas, NV 89154); J.E. Faulds and M.K. Reagan (University of Iowa, Iowa City, IA 52242); J.D. Walker (University of Kansas, Lawrence, KS 66045)

As part of an ongoing study in the Colorado River extensional corridor (CREC), southwestern USA, we are investigating the role of lithospheric and asthenospheric mantle in Tertiary magmatism and the relationship between mantle processes and extension. The CREC is ideally suited for studying the link between extension and mantle processes because coeval magmatism and extension swept northward across the region during Miocene time.

Our initial focus has been on the northernmost part of the corridor in the Lake Mead area, where the left-lateral Lake Mead fault system (LMFS) separates the highly extended CREC to the south from the relatively unextended part of a broad magmatic zone to the north. Isotopic data indicate that between 11 and 6 Ma, during and just following peak extension, the CREC/magmatic zone boundary evolved into a mantle domain boundary. All mafic lavas in the magmatic zone were generated from lithospheric mantle (LM) (εNd = -3 to -9; 87Sr/86Sr = 0.706-0.707). In the northern CREC, lavas erupted before 6 Ma have a similar LM signature, whereas those erupted after 6 Ma have a hybrid asthenospheric mantle (AM), HIMU and minor LM component (εNd = 0 to +4; 87Sr/86Sr = 0.703-0.705). An exception to this is a 9.4 Ma basalt that erupted in the Gold Butte area, east of Lake Mead that contains an AM signature. Peak extension in this area occurred ca. 15 Ma compared to 12-9 Ma in the Lake Mead area. LM may have been thinned and replaced by AM earlier in the eastern part of the northern CREC than to the west. This suggests there may be a spatial and temporal correlation between upper crustal extension and the thinning of the lithospheric mantle in the northern CREC. During extension in the northern CREC, the LM in the magmatic zone remained intact. The LMFS may represent the crustal manifestation of differential thinning of the AM or the rejuvenation of an older lithospheric structure.

Preliminary major and trace element data from mafic lavas erupted between 13 and 14 Ma further south in the CREC suggest that their source contains a mixture of AM and LM which is compatible with the northward younging of extension. When compared to OIB, alkalic lavas are moderately depleted in Nb and moderately enriched in Ba. These trends are similar to AM derived lavas in the northern CREC erupted from 6 to 4.7 Ma. Together with geochronology studies, we hope to delineate geochemical trends and isolate the role of the mantle both orthogonal and parallel to the extension direction across the entire CREC. This region includes two major rift-block domains that may be floored by oppositely dipping detachment systems. These data may therefore elucidate the kinematic evolution of rifted continental crust with large magmatic budgets.

732F-14 1780h

Fault-Valve Action along Bending Strain Faults in a Metamorphic Carapace: the Origin of the Otago Schist Gold-Quartz Lodes?

R.H. Sibson (Department of Geology, University of Otago, P.O. Box 56, Dunedin, New Zealand)

Quartz vein systems, hosted on low-displacement faults cross-cutting the generally flat-lying foliation of the Otago Schists in southern New Zealand, are the source of the >240 tonnes of gold mined (mostly from placers) from the schist belt. The predominantly quartz-feldspathic schists were metamorphosed under greenschist facies conditions during the late Jurassic to early Cretaceous Rangitikei Orogeny and outcrop in a NW-SE belt, about 100 km wide, flanked by lower grade metamorphic assemblages to the NE and SW. The belt extends inland for over 200 km from the east coast of the South Island. The dominant strike of the Au-quartz lodes is NW-SE, parallel to the axis of greatest post-metamorphic uplift, defined by higher grade assemblages along the centre of the schist belt. Some of the lodes developed along steep normal faults, implying NE-SW extension. Others, in apparent contraction, formed along low-angle thrusts during NE-SW contraction. Fluid inclusion studies suggest a metamorphic origin for the mineralising fluids. However, while some of the lodes developed in a mesothermal environment at considerable depth (e.g. ~10 km for the thrust-hosted Macraes deposits), others appear to have formed very close to the surface (e.g. <1 km for the normal fault lodes at Methuon). Timing of mineralisation is poorly constrained but postdates the main Rangitikei metamorphism, and probably initiated during early Cretaceous unroofing of the schist belt (120-100 Ma?).

These structural characteristics are consistent with a model involving progressive arching and exhumation of the cooling metamorphic belt about a NW-SE axis. Tangential longitudinal strains and faulting become concentrated in regions of maximum curvature within an

## Eruptive probability calculation for the Yucca Mountain site, USA: statistical estimation of recurrence rates*

Chih-Hsiang Ho¹, Eugene I Smith², Daniel L Feuerbach², Terry R Naumann²

¹ Department of Mathematical Sciences and ² Center for Volcanic and Tectonic Studies, Department of Geoscience, University of Nevada, Las Vegas, NV 89154, USA

Received July 23, 1990/Accepted June 5, 1991

**Abstract.** Investigations are currently underway to evaluate the impact of potentially adverse conditions (e.g. volcanism, faulting, seismicity) on the waste-isolation capability of the proposed nuclear waste repository at Yucca Mountain, Nevada, USA. This paper is the first in a series that will examine the probability of disruption of the Yucca Mountain site by volcanic eruption. In it, we discuss three estimating techniques for determining the recurrence rate of volcanic eruption ( $\lambda$ ), an important parameter in the Poisson probability model. The first method is based on the number of events occurring over a certain observation period, the second is based on repose times, and the final is based on magma volume. All three require knowledge of the total number of eruptions in the Yucca Mountain area during the observation period ( $E$ ). Following this discussion we then propose an estimate of  $E$  which takes into account the possibility of polygenetic and polycyclic volcanism at all the volcanic centers near the Yucca Mountain site.

### Introduction

The Yucca Mountain region is located within the Great Basin portion of the Basin and Range physiographic province, a large area of the western USA characterized by alternating linear mountain ranges and alluvial valleys. Crowe and Perry (1989, Figure 1) divide the Cenozoic volcanism of the Yucca Mountain region into three episodes that include (1) an older episode of large volume basaltic volcanism (12 to 8.5 Ma) that coincides in time with the termination of silicic volcanic activity; (2) the formation of five clusters of small volume basalt scoria cones and lava flows (9 to 6.5 Ma), all located north and east of the Yucca Mountain site; and (3) the

formation of three clusters of small volume basalt centers (3.7 to 0.01 Ma), all located south and west of the Yucca Mountain site. The two youngest episodes form northwest-trending zones that parallel the trend of structures in the Spotted Range-Mine Mountain section of the Walker Lane belt. Crowe and Perry (1989) suggest a southwest migration of basaltic volcanism in the Yucca Mountain area based on this structural parallelism, a pattern that may reflect an earlier southwest migration of silicic volcanism in the Great Basin. Smith et al. (1990a) suggest that there is no preferred migration trends for post-6-Ma volcanism in the Yucca Mountain region.

Concern that future volcanism might disrupt the proposed Yucca Mountain repository site motivated the assessment of the volcanic risk to the Yucca Mountain area, located within the Nevada Test Site (NTS). Crowe and Carr (1980) calculate the probability of volcanic disruption of a repository at Yucca Mountain, Nevada using a method developed largely by Crowe (1980). Crowe et al. (1982) refine the volcanic probability calculations for the Yucca Mountain area using the following mathematical model:

$$Pr [\text{disruptive event before time } t] = 1 - e^{-\lambda t p},$$

where  $\lambda$  is the recurrence rate of volcanic events and  $p$  is the probability of a repository disruption, given an event. The parameter  $p$  is estimated as  $a/A$ , where  $a$  is the area of the repository and  $A$  is some minimal area that encloses the repository and the area of the volcanic events. Crowe et al. (1982) develop a computer program to find either the minimum area circle or minimum area ellipse (defined as  $A$ ) that contains the volcanic centers of interest and the repository site.  $A$  is defined to accommodate tectonic controls for the localization of volcanic centers and to constrain  $\lambda$  to be uniform within the area of either the circle or ellipse. The rate of volcanic activity is calculated by determination of the annual rate of magma production for the NTS region and by cone counts using refined age data. Resulting probability values using the refined mathematical model are calculated for periods of 1 year and 100,000 years. Two

* Paper financed by the Nuclear Waste Project Office, State of Nevada, USA

Offprint requests to: C-H Ho

procedures (explained below) are used for the rate calculations (Crowe et al. 1982). As calculated by Crowe et al. (1982), the probability of volcanic disruption of a waste repository located at Yucca Mountain falls in the range of  $3.3 \times 10^{-10}$  to  $4.7 \times 10^{-8}$  during the first year, which increases approximately linearly with isolation time.

#### Issues that arise in connection with the work of Crowe et al. (1982)

Although the procedure outlined in Crowe et al. (1982) represents a more formal approach to this problem than ever attempted previously, flaws exist. The method must be modified because the existing data base is inadequate to reasonably constrain  $\lambda$ . Despite the fact that there are well-recognized means of gathering data in the NTS region (field mapping; determinations of the eruptive history of basaltic centers; petrology; geochemistry; geochronology, including magnetic polarity determinations; tectonic setting; and geophysical studies) many considerations are still unknown, e.g., age of volcanism and vent counts.

Present understanding of eruptive mechanisms is not yet advanced enough to allow deterministic predictions of future activity. The only attempts at long-term forecasting have been made on statistical grounds, using historical records to examine eruption frequencies, types, patterns, risk, and probabilities. Reliable historical data make possible the construction of activity patterns for several volcanoes (Wickman 1966, 1976; Klein 1982, 1984; Mulargia et al. 1987; Condit et al. 1989; Ho 1990). Unfortunately, detailed geologic mapping of volcanic centers is in its infancy in the Yucca Mountain area. A formal structure, with conclusions depending on the model assumptions, needs to be developed to evaluate volcanic risk for the NTS.

This paper investigates important parameters required to calculate the probability of site disruption and provides estimates for the unknown parameter(s) that are meaningful both statistically and geologically, taking into account the limited availability of precise ages in the NTS region.

#### The Poisson model

The application of statistical methods to volcanic eruptions is put onto a sound analytical footing by Wickman (1966, 1976) in a series of papers that discuss the applicability of the methods and the evaluation of recurrence rates for a number of volcanoes. Wickman observes that, for some volcanoes, the recurrence rates are independent of time. Volcanoes of this type are called "Simple Poissonian Volcanoes." Theoretically, the probability formula (Crowe et al. 1982) is derived for this type of volcanic activity from the following assumptions:

1. Volcanic eruptions in successive time periods of length  $t$  for each period are independent and should

follow a Poisson distribution with a constant mean (average rate)  $\lambda t$ , i.e. a simple Poissonian volcano.

2. Every eruption has the same probability of repository disruption  $p$ . That is, there is no heterogeneity with respect to disruptiveness.

3. The disruptiveness of the eruptions are independent of one another.

This very brief description is purely mathematical and has no direct interpretation in geologic terms. Since the Poisson model is both the state-of-the-volcanological-art (e.g. Wickman 1966, 1976) and used in actual risk assessment (e.g. Gardner and Knopoff 1974; McGuire and Barnhard 1981), we do not question the above assumptions in this article. Therefore, the following statistical development is based on the assumptions of a simple Poisson model. Of course, exploring alternative models derived from different assumptions based on detailed geologic data and statistical analysis would be valuable as well (e.g. see Ho 1991).

#### Probability formula

The probability model of Crowe et al. (1982) is based on the following relationship:

$$Pr [\text{disruptive event before time } t] = 1 - e^{-\lambda tp}$$

The power series expansion for  $\exp^{-\lambda tp}$  (Ellis and Gullick 1986, p. 545) is:

$$e^{-\lambda tp} = \sum_{k=0}^{\infty} \frac{(-\lambda tp)^k}{k!} = 1 - \lambda tp + \frac{(\lambda tp)^2}{2!} - \frac{(\lambda tp)^3}{3!} + \dots$$

Therefore, the final probability calculation can be simplified as:

$$Pr [\text{disruptive event before time } t]$$

$$= \lambda tp - \frac{(\lambda tp)^2}{2!} + \frac{(\lambda tp)^3}{3!} - \dots$$

$$\approx \lambda tp, \text{ for small } \lambda \text{ and } p \text{ relative to } t.$$

The approximation is reasonable and is true for virtually all of the calculations in Crowe et al. (1982) since all of their estimated values of both  $\lambda$  ( $< 10^{-5}$ ) and  $p$  ( $< 10^{-3}$ ) are small. Therefore, the accuracy of estimating the unknown parameters  $\lambda$  and  $p$  directly influences the significance of values for the probability of repository disruption.

#### Recurrence rate

The Poisson process is used to describe a wide variety of stochastic phenomena that share certain characteristics and phenomena in which some "happening" takes place sporadically over a period of time in a manner that is commonly thought of as "at random." We will refer to a "happening" as an event. If events in a Poisson process occur at a mean rate of  $\lambda$  per unit time (1 year,  $10^5$  year, etc.), then the expected number (long-run average) of occurrences in an interval of time in  $t$  units is  $\lambda t$ . In quantifying volcanism at Yucca Moun-

tain, we define a volcanic eruption as an event. Therefore, the collection of data is directly or indirectly based on the number of eruptions.

Crowe et al. (1982) try three methods to calculate  $\lambda$  in their probability calculations. These are: (1) evaluation of intervals of volcanic activity for evidence of periodicity; (2) counts of volcanic events in Quaternary time; and (3) evaluation of the ratio of magma production rate and mean magma volume. Based on method 1, they conclude that the data suggest no distinct patterns or periodicity of basaltic volcanism in late Cenozoic time. Therefore, the data are insufficient to analyze interval patterns and thus cannot be used to calculate future rates of volcanic activity (Crowe et al. 1982). We believe, however, that according to the Poisson model assumptions, intervals of volcanic activity should follow an exponential distribution and thus  $\lambda$  can be estimated statistically. We shall demonstrate such statistical sampling and estimation techniques in the following section.

Based on method 2, Crowe et al. (1982) calculate  $\lambda$  as  $N/T$  where  $N$  is the number of scoria cones and  $T$  is the period of time represented by the age of the cones or some other specified time period. Thus  $\lambda$  is the average number of eruptions per unit time. In their calculation of  $N/T$ , they define no statistical sampling technique that is associated with the assumed model. Moreover, they do not provide evidence that counting cones is equivalent to counting eruptive events. Crowe et al. (1989) and Wells et al. (1990) now recognize and classify the Lathrop Wells volcanic center as a polygenetic volcano and suggest that some cones may have erupted more than once. Note that the Lathrop Wells volcanic center is only 12 miles away from the proposed Yucca Mountain repository site. We shall introduce a statistical estimation procedure to interpret the estimator.

Based on method 3, Crowe et al. (1982) determine the rate of magma production for the NTS region by fitting a linear regression line to a data set of four points collected from four volcanic centers. Each value thus represents magmatic volume of a single eruption at a corresponding volcanic center. The mean magma volume for 4 m.y. is calculated by taking the average of these four values. The ratio (rate/mean) is then calculated as an estimate for the annual recurrence rate  $\lambda$ . Similarly, the annual recurrence rate for Quaternary time is obtained using only the two Quaternary data points. We consider this approach questionable, since a simple Poisson model requires a constant rate of occurrence, which is not the same as steady-state magma production in a volume-predictable model (e.g. see Wickman 1966, 1976; Wadge 1982). We shall show that such calculations based on magma volume duplicate those of method 2, if the rate of magma volume is constant. Moreover, we shall also point out that, in this case, they apparently assume only four (two) eruptions in the NTS region during the last 4 m.y. (Quaternary time). This apparent assumption explains why their final probabilities based on magma volume are consistently smaller than those based on cone counts (Crowe et al. 1982, tables IV and V).

The rate of volcanic eruption,  $\lambda$  is a critical parameter for the probability calculation. We shall now examine various statistical methods for calculating  $\lambda$ , how the geologic record of volcanism in the Yucca Mountain can be used to estimate values of  $\lambda$ , and the limitations in calculating  $\lambda$ .

#### Estimation based on Poisson count data

In dealing with distributions, repeating a random experiment several times to obtain information about the unknown parameter(s) is useful. The collection of resulting observations, denoted  $x_1, x_2, \dots, x_n$ , is a sample from the associated distribution. Often these observations are collected so that they are independent of each other. That is, one observation must not influence the others. If this type of independence exists, it follows that  $x_1, x_2, \dots, x_n$  are observations of a random sample of size  $n$ . The distribution from which the sample arises is the population. The observed sample values,  $x_1, x_2, \dots, x_n$ , are used to determine information about the unknown population (or distribution).

Assuming that  $x_1, x_2, \dots, x_n$  represent a random sample from a Poisson population with parameter  $\lambda$ , the likelihood function is:

$$L(\lambda) = \prod_{i=1}^n f(x_i; \lambda) = e^{-n\lambda} \lambda^{\sum_{i=1}^n x_i} / \prod_{i=1}^n x_i!$$

Many good statistical procedures employ values for the population parameters that "best" explain the observed data. One meaning of "best" is to select the parameter values that maximize the likelihood function. This technique is called "maximum likelihood estimation," and the maximizing parameter values are called "maximum likelihood estimates," also denoted MLE, or  $\hat{\lambda}$ . Note that any value of  $\lambda$  that maximizes  $L(\lambda)$  will also maximize the log-likelihood,  $\ln L(\lambda)$ . Thus, for computational convenience, the alternate form of the maximum likelihood equation,

$$\frac{d}{d\lambda} \ln L(\lambda) = 0$$

will often be used, and the log-likelihood for a random sample from a Poisson distribution is:

$$\ln L(\lambda) = -n\lambda + \sum_{i=1}^n x_i \ln \lambda - \ln \left( \prod_{i=1}^n x_i! \right).$$

The maximum likelihood equation is:

$$\frac{d}{d\lambda} \ln L(\lambda) = -n + \sum_{i=1}^n \frac{x_i}{\lambda} = 0,$$

which has the solution  $\hat{\lambda} = \sum_{i=1}^n \frac{x_i}{n} = \bar{x}$ . This is indeed a maximum because the second derivative:

$$\frac{d^2}{d\lambda^2} \ln L(\lambda) = - \sum_{i=1}^n \frac{x_i}{\lambda^2},$$

is negative when evaluated at  $\bar{x}$ .

Let us demonstrate this estimation technique. Let  $X$  denote the number of volcanic eruptions for a  $10^5$ -year period for the NTS region from this assumed Poisson process. Then  $X$  follows a Poisson distribution with average recurrence rate  $\mu$ , with  $\mu = \lambda t = 10^5 \lambda$ . If we wish to estimate  $\lambda$  for the Quaternary using the Poisson count data for the NTS region, the successive number of eruptions from the last 16 consecutive intervals of length  $10^5$  years ( $16 \times 10^5 = 1.6 \times 10^6 =$  Quaternary period) must be estimated. The number of observed eruptions per interval are denoted as  $x_1, x_2, \dots, x_{16}$ . Thus, these 16 values represent a sample of size 16 from a Poisson random variable with average recurrence rate  $\mu$ . Estimating the mean of the Poisson variable from these count data gives:

$$\hat{\mu} = \bar{x} = \sum_{i=1}^{16} x_i / 16,$$

and

$$\hat{\lambda} = \hat{\mu} / 10^5 = \sum_{i=1}^{16} x_i / (1.6 \times 10^6)$$

This shows that the estimated annual recurrence rate,  $\hat{\lambda}$ , is the average number of eruptions during the observation period (in years). Based on this estimation technique,  $\hat{\lambda}$  can be defined as:

$$\hat{\lambda} = E/T, \quad (1)$$

where  $E$  = total number of eruption during the observation period,  
and  $T$  = observation period.

Note that for the estimation of  $\lambda$  in this model, an individual observation  $x_i$  is not required. However, the distribution of  $x_i$ 's can provide information for model selection, for model-adequacy checking, and for parameter estimation in general.

#### Estimation based on repose times

With any Poisson process there is an associated sequence of continuous waiting times for successive occurrences. If events occur according to a Poisson process with parameter  $\lambda$ , then the waiting time until the first occurrence,  $T_1$ , follows an exponential distribution,  $T_1 \sim \text{Exp}(\theta)$  with  $\theta = 1/\lambda$ . Furthermore, the waiting times between consecutive occurrences are independent exponential variables with the same mean time between occurrences,  $1/\lambda$  (Parzen 1962, p. 135). Several simplifying assumptions must be made in treating eruptions as events in time. Although the onset date of an eruption is generally well-defined as the time when lava first breaks the surface, the duration is harder to determine because of such problems as slowly cooling flows or lava lakes, and the gradual decline of activity. We adopt the same definition for repose time as used by Klein (1982). Therefore, we ignore eruption duration, we choose the onset date as the most physically meaningful parameter, and we measure repose times from one onset date to the next. Thus, our definition of "repose time" differs from the classic one as a noneruptive

period. This procedure seems justified because most eruption durations are much shorter than typical repose intervals. The mean time between two events (eruptions),  $\theta$ , is inversely related to the volcanic recurrence rate  $\lambda$ . Assumptions of the Poisson process are rather restrictive, but at least a very tractable and easily analyzed model can be proposed. The maximum likelihood estimator for  $\theta$  (Hogg and Tanis 1988, p. 336) is:

$$\hat{\theta} = \bar{t} = \sum_{i=1}^m t_i / m, \text{ and } \hat{\lambda} = \hat{\theta}^{-1} = \bar{t}^{-1},$$

where  $t_1, \dots, t_m$  represent values of a random sample of size  $m$  from an exponential population with parameter  $\theta$ . For the NTS region, the exact values of  $t_i$ 's (repose times) are difficult to obtain because the precise date of each eruption is not known. However, based on the definition of repose times we can calculate:

$$\sum_{i=1}^m t_i = \text{time between the first and last eruptions during the observation period,}$$

and

$m$  = total number of repose times =  $E - 1$ , which gives

$$\hat{\lambda} = (E - 1) / (T_0 - T_y), \quad (2)$$

where

$E$  = Total number of eruptions between  $T_0$  and  $T_y$ , inclusive,

with

$T_0$  = age of the oldest eruption,

$T_y$  = age of the youngest eruption.

Note that the numerical values of  $E$  in both Eqs. 1 and 2 are identical for the same observation period of length  $T$ . In practice, however, the observation period for the exponential model (Eq. 2) must be trimmed to a period between  $T_0$  and  $T_y$ , inclusive, to reflect that exactly  $m$  ( $= E - 1$ ) repose times ( $t_1$  through  $t_m$ ) are obtained. Theoretically, the two estimates obtained for  $\lambda$  (Eqs. 1 and 2) should be consistent, but not identical.

#### Estimation based on magma volume

Let  $V$  be the total volume of basaltic magma erupted at the surface in the NTS region during the observation period of length  $T$ . From Eq. 1, we obtain:

$$\hat{\lambda} = E/T = EV/TV = (V/T)/(V/E) = r/\bar{v} \quad (3)$$

where

$r = V/T$ , the annual rate of magma production,

and

$\bar{v} = V/E$ , the mean volume of magma during the observation period of length  $T$ .

Equation 3 is valid, but it also requires an accurate estimate of  $E$  for  $\bar{v}$ . If  $E$  (or  $r$ ) is underestimated, so is  $\lambda$ . The most efficient way to calculate  $r$  is  $V/T$ . Crowe and Perry (1989) present a refined method to calculate  $r$ .

They evaluate  $r$  as the slope of the curve of cumulative magma volume plotted versus time. It is essentially identical to  $V/T$ , assuming a constant rate of magma volume (an assumption that Crowe et al. (1982) and Crowe and Perry (1989) have been striving to prove). In this case, the degree of erosional modification of volcanic landforms should be studied to estimate volumes of missing volcanic deposits. The overall error, which is multiplicative, is compounded in the values of Crowe and Perry (1989) for  $r$ . Moreover,  $E$  must be estimated when calculating  $\bar{v}$ , the mean volume of magma. Therefore, we see no economy in Eq. 3 and consider it to duplicate Eq. 1. We derive Eq. 3 merely to demonstrate that the estimation procedures used by Crowe et al. (1982) and Crowe and Perry (1989) are flawed and therefore must be modified.

#### Estimation of $E$

All of the statistical estimation methods considered for  $\lambda$  (Eqs. 1-3) require knowing the value of  $E$  (total number of eruptions during the observation period). An accurate count of  $E$  is possible for volcanoes with a complete historical record. Identifying  $E$ , however, depends strictly on a clear understanding of eruptive processes and reliable dating techniques for the NTS region, since no historical record is available. Scientists differ in their opinions of volcanism at the NTS area. The following is the view of Crowe et al. (1983):

"Basalt centers are composed of multiple vents, each marked by a scoria cone. In the NTS region the cones are divided into two categories: large central cones, referred to as the main cones, and satellite cones. The average number of cones at a single center, based on cone counts of seven Quaternary basalt centers in the NTS region, is about two to three cones. Thus, field data suggest a general eruption pattern where the initial breakthrough of magma to the surface is marked by the development of an eruptive fissure with two or three loci of effusion. Each of these vents becomes the site of small scoria cones. As the eruption proceeds, activity shifts or concentrates at a single vent that becomes the site of the main scoria cone."

The above description indicates that a main scoria cone is the final stage of a single eruption, and a single eruption could have several small vents to accompany the main cone. However, the possibility of polycyclic volcanism at all the volcanic centers needs to be evaluated.  $\lambda$  would be underestimated if nearby vents have distinguishable ages. We, therefore, estimate  $E$  as follows:

Let  $I$  denote the number of volcanic centers under investigation, and let  $J_i$  be the number of main cones in the  $i$ th volcanic center, where  $i = 1, \dots, I$ . The proposed estimate of  $E$  is:

$$\hat{E} = \sum_{i=1}^I \sum_{j=1}^{J_i} (m_{ij} + e_{ij}), \quad (4)$$

where  $m_{ij}$  = number of multiple, time-separate eruptions of the  $j$ th main cone in the  $i$ th volcanic center,

and  $e_{ij}$  = number of vents that are separate in space and time (with distinguishable age measurements) from the  $j$ th main cone in the  $i$ th volcanic center.

The rationale for this estimate is that significant information has emerged that some of the volcanic centers are polygenetic volcanoes (e.g. Lathrop Wells center (Wells et al. 1990)). This estimation for parameter  $E$  (total number of eruptions) given by Eq. 4 takes into account such a possibility for the NTS area. Studies are in progress to attempt to evaluate the values of  $m_{ij}$ 's and  $e_{ij}$ 's for the Quaternary volcanic centers of the Yucca Mountain.

#### Empirical results

Specifying the observation period ( $T$ ) is important in modeling the volcanism at NTS. Most of the volcanic risk assessment studies in the Yucca Mountain area are centered around the post-6-Ma (Pliocene and younger) and Quaternary (<1.6 Ma) volcanism (Crowe et al. 1982, Smith et al. 1990a, and Wells et al. 1990). We shall use a preliminary data set based on the Quaternary volcanism to demonstrate the estimation techniques of the recurrence rate.

According to Crowe and Perry (1989), the younger zone of basaltic activity in the vicinity of Yucca Mountain is characterized by basaltic centers occurring as clusters of scoria cones and lava flows. There are seven Quaternary volcanic centers: the sequence of four 1.2-Ma centers in Central Crater Flat, two centers of the 0.28-Ma Sleeping Butte site, and the Lathrop Wells center. The age of the Lathrop Wells center has been refined from the original 0.27 Ma (Crowe et al. 1982) to 0.01 Ma (Crowe and Perry 1989). This date (0.01 Ma) is in the range of 0 to 0.02 Ma, the period of the most recent volcanic activity of the Lathrop Wells Cone as reported by Wells et al. (1990). The sequence of four 1.2 Ma centers in central Crater Flat includes Red Cone, Northern Cone, Black Cone, and two Little Cones (Fig. 1). Smith et al. (1990a) concentrate on this group of five cinder cone complexes in the central part of Crater Flat in Fig. 1. Based on their discussion, the cones form a 12-km-long arcuate chain. Details of vent alignment are best observed on Black Cone and Red Cone in the central part of the chain. In the Black Cone complex, the cinder cone is the most prominent topographic feature (about 100 m high and 500 m in diameter), but it may only account for a small volume of flows. A larger volume of basalt erupted from at least ten vents located north, south and east of Black Cone. These vents are commonly represented by scoria mounds composed of cinder, ash, and large bombs. Vents are aligned along two sub-parallel zones that strike approximately N35° E. One zone includes Black Cone and four scoria mounds; the other zone lies 300 m to the southeast of Black Cone and contains at least seven mounds. Dikes exposed in eroded mounds strike northeast and parallel the trend of the vent zones. The Red Cone complex contains three vent zones; two trend approximately N45° E and a third zone strikes N50° W (Fig. 2). This

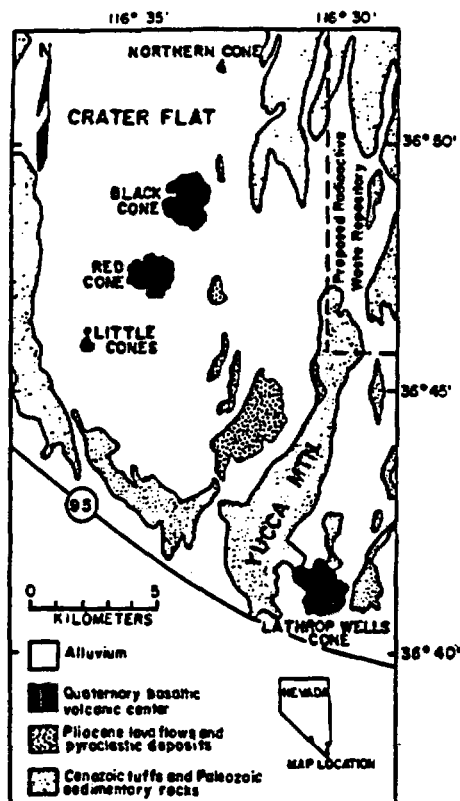


Fig. 1. Generalized geologic map of Crater Flat volcanic field area and boundary of proposed radioactive waste repository; inset map shows location of the Crater Flat volcanic field. (Source: Wells et al. 1990, figure 1)

provides substantive justification of our treatment of the total number of eruptions ( $E$ ), and demonstrates that data for the Yucca Mountain region are incomplete at this preliminary stage of the site characterization studies.

Another key issue in the volcanic risk assessment studies is the disagreement over age-dating of the rocks. For example, the K-Ar dates for Red Cone presented by Smith et al (1990b, table 4) are:  $0.98 \pm 0.10$  Ma for dike,  $1.01 \pm 0.06$  Ma for amphibole-bearing unit, and  $0.95 \pm 0.08$  for basalt on top of Red Cone. Until more reliable dating techniques are available, we have no way to distinguish the ages of the cones within each cluster of volcanic centers. Notice that, although an individual observation ( $x_i$  or  $t_i$ ) is not required for the estimation of  $E$  developed in this article, the limited availability of precise ages would affect the counts of both  $m_{ij}$  and  $e_{ij}$  in Eq. 4.

Consistent with the notations used in the previous sections, the Quaternary volcanism yields:

$$T = 1.6 \text{ Ma}, E = 8, T_0 = 1.2 \text{ Ma}, \text{ and } T_1 = 0.01 \text{ Ma.}$$

Therefore, based on Eq. 1,

$$\hat{\lambda} = E/T = 8/(1.6 \times 10^6) = 5 \times 10^{-6}/\text{yr}$$

Based on Eq. 2,

$$\hat{\lambda} = (E - 1)/(T_0 - T_1) = (8 - 1)/(1.2 \times 10^6 - 0.01 \times 10^6) = 5.9 \times 10^{-6}/\text{yr}$$

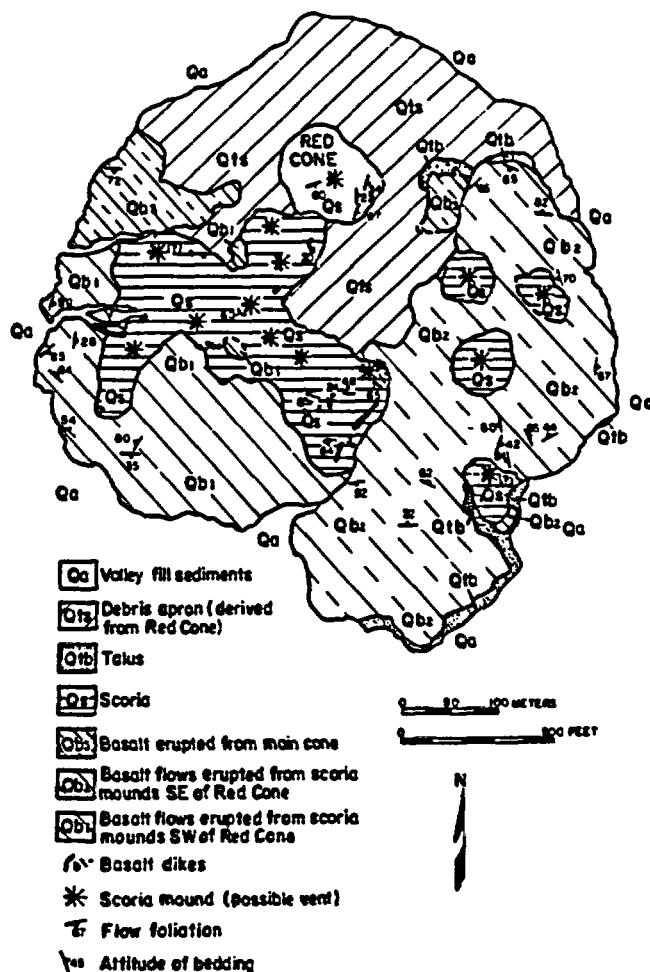


Fig. 2. Geologic map of Red Cone, Crater Flat, Nevada

Of course, the estimated rate based on Eq. 3 is  $5 \times 10^{-6}/\text{yr}$  regardless of the value of  $V$ , since the magma volume is really never needed in this calculation.

### Discussion and conclusion

The statistical estimation of recurrence rate  $\lambda$  requires a reliable count of distinguishable vents. This approach is based on the geologic record of volcanism at the NTS region. The methods of the approach are supported by sound statistical sampling theory. Crowe and Perry (1989), however, object that vent counts record only the recognition of a volcanic event, not its magnitude, and so they refine the parameter estimation by concentrating on the cumulative magma volume, which is a continuous variable. Nonetheless, their model assumptions and development are still based on a discrete simple Poisson model, which treats each eruption equally in order to calculate the final probability.

We now conclude this section with a few comments and point to some further work.

1. Their recommended method for estimating  $\lambda$  is to construct a curve of cumulative magma volume versus time, which is also affected by the counts of vents ( $\hat{E}$ ) in

the observation period ( $T$ ). Their ignorance of the critical factor  $E$  in Eq. 3 leads them to believe that estimation based on magma volume is the most acceptable method (Crowe and Perry 1989); this questionable belief, in turn, handicaps their estimates for  $\bar{v}$  and thus for  $\lambda$ .

2. All of the published results that demonstrate statistical sampling techniques for volcanic activity require a representative sample and a sufficiently large sample size to calculate a reliable long-run average with precision at a desired level (flipping a coin twice does not tell the whole story of the fairness of the coin).

3. Their recognition of the fact that short periods of eruptive activity are bounded by long periods of inactivity at NTS indicates that their choice of a simple Poisson model should be adequately checked based on more detailed geologic data. So far, the problems of model assumptions and parameter estimations have been treated only separately by Crowe et al. (1982) and Crowe and Perry (1989), despite the fact that the model (simple Poisson, or Volume-predictable model) assumptions and parameter (occurrence rate, or magma effusion rate) estimation methods virtually always depend on each other in volcanic hazard and risk calculations.

Yucca Mountain is remote from human habitation. There is no historical record of volcanism near Yucca Mountain. Therefore, the volcanic record must be developed by detailed field, geomorphic, and geochronologic studies. Precise ages are critical for volcanic rate calculations, but traditional K-Ar dating commonly has a large error in the age range recorded by the volcanoes near Yucca Mountain (1.1 Ma to 20 Ka). Until more precise techniques are developed, there will be uncertainties with regard to the age and duration of volcanism. Since predictions are needed, one possible improvement would be to reconfirm all of the crucial assumptions using data that are the only basis we have for making necessary plans, calculations, and model selections. We have no choice but to form our notion of governing laws on the basis of data and to act accordingly. This is particularly true in volcanic studies, where data are rare and expensive ( $\approx$  \$300-\$600 per age of a vent at Yucca Mountain). Our efforts for future studies will be devoted to considerably more detailed data collection and statistical modeling. At this preliminary stage of our work, all we can conclude is that the probabilistic results of Crowe et al. (1982) are based on idealized model assumptions, a premature data base, and inadequate estimates of the required parameters. For the reasons discussed, we think that Crowe et al. underestimate the risk of volcanism at the proposed Yucca Mountain repository site.

*Acknowledgements.* We wish to thank Dr. Donald A. Swanson for his useful and thoughtful suggestions to this work. We also thank Nate Stout for drafting the figures.

## References

Condit CD, Crumpler LS, Aubele JC, Elston WE (1989) Patterns of volcanism along the southern margin of the Colorado plateau: the Springerville Field. *J Geophys Res* 94:1975-1986

- Crowe BM (1980) Disruptive event analysis: volcanism and igneous intrusion. Battelle Pacific Northwest Laboratory Rep PNL - 2882
- Crowe BM, Carr WJ (1980) Preliminary assessment of the risk of volcanism at a proposed nuclear waste repository in the Southern Great Basin. US Geol Survey Open-File Rep 80-375, 15p
- Crowe BM, Johnson ME, Beckman RJ (1982) Calculation of the probability of volcanic disruption of a high-level radioactive waste repository within Southern Nevada, USA. *Radioactive Waste Management* 3:167-190
- Crowe BM, Self S, Vaniman D, Amos R, Perry F (1983) Aspects of potential magmatic disruption of a high-level radioactive waste repository in Southern Nevada. *J Geol* 91:259-276
- Crowe BM, Harrington C, Turrin B, Champion D, Wells S, Perry F, McFadden L, Renault C (1989) Volcanic hazard studies for the Yucca Mountain Project. *Waste Management* 89, Vol 1. High Level Waste and General Interest, pp 485-491
- Crowe BM, Perry FV (1989) Volcanic probability calculations for the Yucca Mountain site: estimation of volcanic rates. Focus '89, Nuclear waste isolation in the unsaturated zone, September, 1989, hosted by the Nevada section of the American Nuclear Society, pp 326-334
- Ellis R, Gulick D (1986) *Calculus* (3rd) Harcourt Brace Jovanovich, New York
- Gardner JK, Knopoff L (1974) Is the sequence of earthquakes in Southern California, with aftershocks removed, Poissonian? *Bull Seismol Soc Am* 64:1363-1367
- Ho CH (1990) Bayesian analysis of volcanic eruptions. *J Volcanol Geotherm Res* 43:91-98
- Ho CH (1991) Time trend analysis of basaltic volcanism for the Yucca Mountain site. *J Volcanol Geotherm Res* 46:61-72
- Hogg RV, Tanis EA (1988) *Probability and statistical inference*, 3rd edn. Macmillan, New York
- Klein FW (1982) Patterns of historical eruptions at Hawaii volcanoes. *J Volcanol Geotherm Res* 12:1-35
- Klein FW (1984) Eruption forecasting at Kilauea volcano, Hawaii. *J Geophys Res* 89:3059-3073
- McGuire RK, Barnhard P (1981) Effects of temporal variations in seismicity on seismic hazard. *Bull Seismol Soc Am* 71:321-334
- Mulargia F, Gasperini PI, Tinti S (1987) Identifying different regimes in eruptive activity: an application to Etna volcano. *J Volcanol Geotherm Res* 34:89-106
- Parzen E (1962) *Stochastic processes*. Holden-Day, San Francisco
- Smith EI, Feuerbach DL, Naumann TR, Faulds JE (1990a) The area of most recent volcanism near Yucca Mountain, Nevada: Implications for volcanic risk assessment. *Proceedings of the International Topical Meeting, High-Level Radioactive Waste Management: American Nuclear Society/American Society of Civil Engineers, Vol 1*, pp 81-90
- Smith EI, Feuerbach DL, Naumann TR, Faulds JE (1990b) Annual Report of the Center for Volcanic and Tectonic Studies for the period 10-1-89 to 9-30-90. The Nuclear Waste Project Office, Report No 41
- Wadge G (1982) Steady state volcanism: evidence from eruption histories of polygenetic volcanoes. *J Geophys Res* 87:4035-4049
- Wells SG, McFadden LD, Renault CE, Crowe BM (1990) Geomorphic assessment of late Quaternary volcanism in the Yucca Mountain area, southern Nevada: implications for the proposed high-level radioactive waste repository. *Geology* 18:549-553
- Wickman FE (1966) Repose-period patterns of volcanoes. *Ark Mineral Geol* 4:291-367
- Wickman FE (1976) Markov models of repose-period patterns of volcanoes. In: Merriam DF (ed) *Random processes in geology*. Springer, New York Berlin Heidelberg, pp 135-161

Editorial responsibility: Y. Kastui